Uncovering triggers of colonization

in brain metastasis

Doctoral thesis

In partial fulfillment of the requirements for the degree

"Doctor rerum naturalium (Dr. rer. nat.)"

in the Molecular Medicine Study Program

at the Georg-August University Göttingen

submitted by

Raquel Blazquez

born in Madrid

Göttingen 2016

Members of the thesis committee:

Supervisor:

Prof. Dr. Tobias Pukrop

Department of Internal Medicine III

University Hospital Regensburg

Second member of the thesis committee:

Prof. Dr. Heidi Hahn

Department of Molecular Developmental Genetics

Institute of Human Genetics, University of Göttingen

Third member of the thesis committee:

Prof. Dr. Peter Burfeind

Department of Molecular Developmental Genetics

Institute of Human Genetics, University of Göttingen

Date of Disputation: 24th January 2017

AFFIDAVIT

I hereby declare that I wrote my doctoral thesis entitled "Uncovering triggers of colonization in brain metastasis" independently and with no other sources and aids than quoted.

Göttingen, November 2016

_____

(Signature)

List of publications

<u>Original articles:</u>

Schwartz, H., Blacher, E., Amer, M., Livneh, N., Abramovitz, L., Klein, A., Ben-Shushan, D., Soffer, S., **Blazquez, R.**, Barrantes-Freer, A., Müller, M., Müller-Decker, K., Stein, R., Tsarfaty, G., Satchi-Fainaro, R., Umansky, V., Pukrop, T., Erez, N. Incipient melanoma brain metastases instigate astrogliosis and neuroinflammation (2016), Cancer Research 76(15):4359-71.

Siam, L., Bleckmann, A., Chaung, HN., Mohr, A., Klemm, F., Barrantes-Freer, A., **Blazquez, R.**, Wolff, HA., Lüke, F., Rohde, V., Stadelmann, C., Pukrop, T. The metastatic infiltration at the metastasis/brain parenchyma-interface is very heterogeneous and has a significant impact on survival in a prospective study (2015), Oncotarget 6(30):29254-67.

<u>Book chapters:</u>

Blazquez, R., Pukrop, T. 3D co-culture model of the brain parenchyma/metastasis interface of brain metastasis. 3D Cell Culture: Methods and Protocols, Methods in Molecular Biology, Springer, *accepted*.

List of Contents

Acknowledgements

También me gustaría agradecer a mi familia su incondicional apoyo durante toda mi vida, pero especialmente durante esta excitante etapa. Particularmente me gustaría agradecer a mis padres el haberme dado la posibilidad de llevar a cabo mi gran sueño. Gracias Mamá, gracias Papá por estar siempre a mi lado. Gracias por apoyarme en cada una de mis decisiones por muy difíciles que puedan resultaros a vosotros. Gracias simplemente por estar orgullosos de mí.

Zuletzt, aber zutiefst möchte ich mich besonders bei meinem Mann, Marcus, bedanken. Danke mein Schatz, dass Du meine Karriere unterstützest und jeden Schritt ermöglichst. Danke dass Du immer bei mir bist, in den guten und schlechten Zeiten. Danke dass Du meine Erfolge mitfeierst und bei meinen Niederlagen mitleidest. Danke einfach dass Du mich liebst und stolz auf mich bist.

Abstract

Brain metastases (BM) are frequent in cancer patients and are associated with poor prognosis. The incidence of BM is increasing mainly due to an improved control of primary tumors and an increased median survival of the patients. However, only limited treatment strategies are available nowadays. From a biological point of view, metastases are highly inefficient. Recent studies point out the colonization as the bottleneck of this process. Moreover, the colonization of the target organ seems to be the only targetable event to stop brain metastasis. However, although much effort has been made during recent years to understand the first steps of the metastatic cascade, the colonization of the target organ remains unexplored. Therefore, we aimed to investigate the mechanisms underlying this process and looked for triggers of colonization during brain metastasis.

By means of a new quantification tool, the Colonization Index, the breast cancer cells 4T1 were found to have a higher colonization potential than the parental 410.4 in our brain colonization in vivo models. The expression of the mesenchymal marker vimentin seemed to confer certain plasticity to the cellular architecture, which in turn promoted a better colonization of the brain parenchyma by the tumor cells without the loss of their fundamental epithelial phenotype. Therefore, we propose the acquisition of mesenchymal features by the tumor cells as a feasible trigger of colonization during brain metastasis.

Moreover, the present work underlies once again the importance of the tumor microenvironment in supporting metastasis formation, and proposes the PI3-kinase as a feasible therapeutic target for the treatment of this devastating illness. Here, we demonstrate that BKM120 can effectively block the PI3K/Akt signaling pathway, and consequently blunts the innate pro-tumorigenic activity of tumor-associated macrophages into a tumor-suppressing phenotype. This phenotypic change is driven by the modulation of the myeloid transcription factor PU.1 in the metastatic tissue, and results in prolonged overall survival. We propose that such macrophage-re-educating agents in combination with immunotherapy may constitute a promising therapeutic option for patients suffering from BM.

In conclusion, our data emphasize once again the complexity of metastasis. In this work, both the acquisition of metastatic traits by tumor cells, as well as the tumor promoting role of the surrounding stromal cells were identified as feasible triggers of brain colonization.

List of Figures

List of Tables

Abbreviations

5-FU	fluorouracil
AKT	protein kinase B
APS	ammonium persulfate
AS	astrocytes
BBB	blood brain barrier
BCR	B cell receptor
BKM	BKM120
BM	brain metastases
BSA	bovine serum albumin
CAM	chorioallantoic membrane
cDNA	complementary DNA
CI	cell index, colonization index
CMV	cytomegalovirus
CNS	central nervous system
CSC	cancer stem cell
CSF	cerebrospinal fluid
CTC	circulating tumor cells
CTL	control
CTLA-4	cytotoxic T lymphocyte-associated protein 4
DEG	differentially expressed gene
DMEM	Dulbecco's modified eagle medium
DMSO	dimethyl sulfoxide
DNA	deoxyribonucleic acid
ECM	extracellular matrix
EDTA	ethylenediaminetetraacetic acid
EGF	epidermal growth factor
eGFP	enhanced green fluorescent protein
EGFR	epidermal growth factor receptor
EMT	epithelial to mesenchymal transition
ER	estrogen receptor
FCS	fetal calf serum
FITC	fluorescein isothiocyanate

GEMM	genetically engineered mouse models
GSK3β	glycogen synthase kinase 3 beta
GTR	gross total resection
H&E	hematoxylin and eosin
HBSS	Hank's balanced salt solution
Her2	human epidermal growth factor receptor 2
HK	house-keeping
HRP	horseradish peroxidase
HSP90	heat shock protein 90
IHC	immunohistochemistry
IL	interleukin
INPP4B	inositol polyphosphate-4-phosphatase type II
ITAM	immune-receptor tyrosine-based activation motif
KW	kilo weight
LPS	lipopolysaccharide
M-CSF	macrophage colony-stimulating factor
MDM	monocyte-derived macrophages
MEM	minimum essential medium
Met	metastasis
MET	mesenchymal to epithelial transition
MG	microglia
MMP	milk powder
MMTV-PyMT	mouse mammary tumor virus - polyoma middle T
MØ	macrophage
mRNA	messenger RNA
MRP	multidrug resistance-related protein
MTT	3-(4,5-dimethylthiazol-2-yl)-2,5-diphenyltetrazolium bromide
n.s.	non-significant
NGS	normal goat serum
NHS	normal horse serum
NSCLC	non-small cell lung cancer
OS	overall survival
P/S	penicillin/streptomycin
PAGE	polyacrylamide gel electrophoresis
PBS	phosphate buffered saline

PD-1	programmed cell death 1
PDK1	phosphoinositide-dependent kinase 1
PD-L1	programmed cell death 1 ligand 1
PFA	paraformaldehyde
PI3K	phosphatidylinositol 3-kinase
PIP2	phosphatidylinositol 4,5-bisphosphate
PIP3	phosphatidylinositol 3,4,5-bisphosphate
PR	progesterone receptor
PTEN	phosphatase and tensin homolog
qRT-PCR	quantitative real-time polymerase chain reation
RNA	ribonucleic acid
RTK	receptor tyrosine kinases
S6K	S6 kinase
SD	standard deviation
SDS	sodium dodecyl sulfate
SEM	standard error of the mean
TAM	tumor-associated macrophages
TBST	tris-buffered saline with Tween 20
TCR	T cell receptor
TEM	transendothelial migration
TIL	tumor infiltrating lymphocytes
TKI	tyrosine kinase inhibitors
TME	tumor microenvironment
UV	ultraviolet
WB	western blot
WBRT	whole brain radiation therapy
WT	wild type

Measurement units:

% (v/v)	% volume per volume
% (w/v)	% weight per volume
bp	base pairs
°C	degree Celsius
g	gram (for weight specifications), g-force (for centrifugation protocols)
l	liter
m	meter
M	Molar
V	Volt
W	Watt

Metric prefixes:

k	kilo (10^3)
c	centi (10^{-2})
m	milli (10^{-3})
μ	micro (10^{-6})
n	nano (10^{-9})

1   Introduction

1.1   Brain metastasis

Brain metastasis is commonly defined as the spread of cancer cells from a primary tumor to the brain. Among tumor types, lung cancer accounts for the highest number of brain metastases, followed by breast cancer, melanoma and colon cancer. The exact incidence of brain metastases is not known. Studies suggest that brain metastases occur in 20%-40% of cancer patients; which represents an estimated 100000 to 200000 new cases per year in the United States (Nussbaum, Djalilian, Cho, & Hall, 1996). Furthermore, metastases, rather than primary tumors, are responsible for most cancer related deaths. Patients dying from metastasis are about 20% of all cancer patients, and this rate is exponentially rising, mainly due to the increased median overall survival of patients suffering from primary tumors.

Advances in primary cancer treatments, new imaging techniques for early detection, and vigilant surveillance protocols for monitoring recurrence have contributed to a longer survival of cancer patients. However, brain metastases still occur months or even years after the first cancer treatment with fatal consequences in the vast majority of cases. The reason for that is the reduced treatment response of brain metastases to the majority of systemic cancer treatments. Moreover, despite its high mortality, the mechanisms of metastatic disease remain almost unknown. Thus, specific, new approaches to combat brain metastases are urgently needed.

1.1.1 Current therapeutical strategies

Standard therapeutical approaches for brain metastasis include local treatments with surgical resection and radiation therapy (whole brain radiation, and stereotactic radiation therapy), and systemic treatments with chemotherapy or targeted therapies. Systemic treatments are however, less effective in the case of brain metastases compared to metastases in the periphery, due to the lower drug concentrations that reach the brain (Lockman et al., 2010).

a)   Local treatments
Surgical resection is a current approach for brain metastases, for example, with mass effect in non-eloquent regions, and involves the macroscopic removal of metastasis until reaching the glial pseudo-capsule, a method that is known as gross total resection (GTR). Whole brain radiation

therapy (WBRT) was a mainstream therapy for brain metastasis; however, currently the indications for WBRT are more and more under debate and not all types of cancer are sensitive to this treatment. Stereotactic radiosurgery is a more preferred treatment modality for radio-resistant lesions. However, patients treated with these therapies have local recurrence after a few months mainly due to remaining infiltrating metastatic cells at the metastasis/brain parenchyma interface, and suffer from memory deficits (Bindal, Sawaya, Leavens, & Lee, 1993; Minniti et al., 2011; Siam et al., 2015; Soffietti, Trevisan, & Ruda, 2012).

b)   Systemic treatments

Additionally, a variety of chemotherapeutic agents have been used to treat brain metastasis, including fluorouracil (5-FU), cyclophosphamide, etoposide, cisplatin, irinotecan, ifosfamide, temozolomide, etc.. In most cases, several agents are used in combination and in conjunction with whole brain radiation therapy (WBRT) to improve response rates. However, the outcome of patients that receive chemotherapy, alone or in combination, is not promising. Reasons are that some of the drugs are substrates of the Multidrug Resistance-Related Protein (MRP) or doesn't even cross the blood brain barrier at all.

The arrival of small-molecule tyrosine kinase inhibitors (TKI) and monoclonal antibodies on the market offered promising new tools in the management of brain metastasis. Gefitinib, erlotinib and osimertinib, epidermal growth factor receptor (EGFR) inhibitors, have demonstrated promising results in non-small cell lung (NSCL) cancers that metastasize to the brain, especially if they are EGFR-mutated (Park et al., 2012). The use of lapatinib in combination with capecitabine is effective in treating HER2-positive brain metastasis; similarly, vemurafenib is effective in patients with BRAF V600E-positive melanoma brain metastasis (Soffietti et al., 2012). Monoclonal antibodies such as trastuzumab have been used in treating metastatic breast cancer. However, most of these antibodies are not effective enough in crossing the blood brain barrier or the drug concentrations that reach the metastatic lesion are not sufficient, and this results in relapse within the central nervous system.

That means that, to date, there are less effective treatments against this live-threatening and fatal disease for the majority of the brain metastasis patients. Furthermore, the mechanisms underlying the successful colonization of the brain by the disseminated cancer cells are not fully understood. For this reason, new therapeutic options and research tools are needed to try to shed some light on the progress of brain metastasis.

1.1.2 The metastatic cascade: a branched evolution process

The process of cancer metastasis consists of a large series of sequential, interrelated steps (see Figure 1). Each of these can be rate limiting, as any uncompleted or unsuccessful step can stop the entire process (Poste & Fidler, 1980). To metastasize, tumor cells have to get into the circulation, survive in the blood stream, extravasate into the target organ, and re-establish themselves at the secondary site. This process requires the tumor cells to detach from the tumor mass, disperse, and cross the epithelial/endothelial frontier. Tumor cells accomplish this by secreting proteolytic enzymes, particularly metalloproteinases and cathepsins, which help them to break down the basal matrix. Furthermore, they have to survive in the circulation and avoid the immune reconnaissance during this journey. Tumor cells achieve that by coating themselves with coagulating elements such as fibrin and platelets in the blood. These metastatic emboli also produce adherens to slow themselves down in the blood stream and re-attach onto the vascular wall where they gain access to the host tissue by disrupting the endothelial barrier. Once in the target organ, disseminated tumor cells must survive in the foreign microenvironment and colonize it in order to form distant metastases (G. F. Weber, 2008).
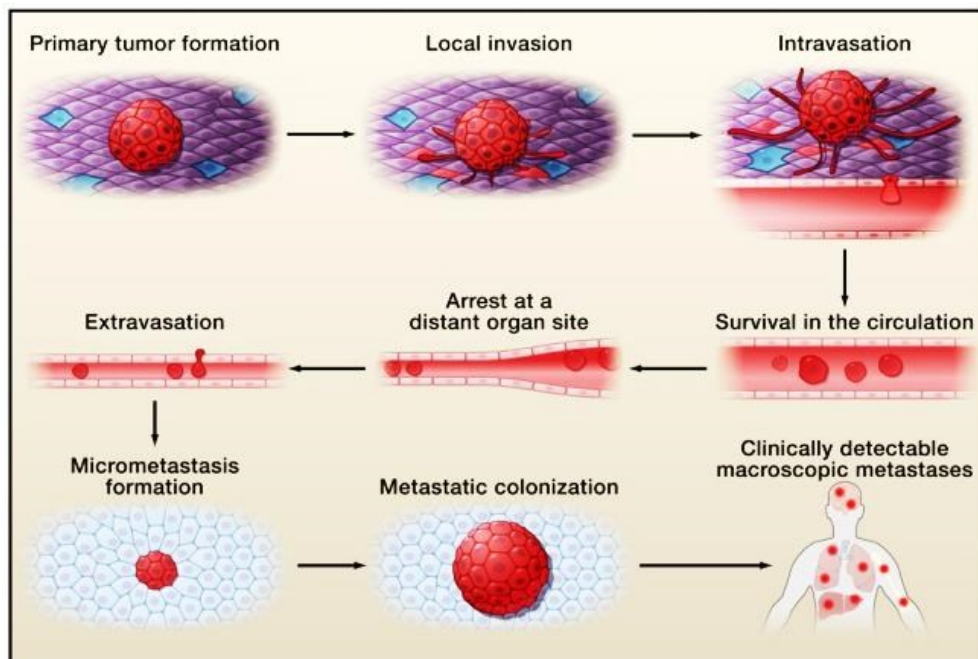
Figure 1: The metastatic cascade

The metastatic cascade involves multiple steps, including: invasion, entry into the circulation, survival in the bloodstream, systemic dissemination, arrest and extravasation in secondary organs, settlement into latency, re-activation and metastatic outgrowth. Taken from (Faltas, 2012) with permission from Frontiers Journal Series.

Interestingly, the metastatic cascade is not a developmental program but a branched evolutionary process, in which, at early time points, the tumor cells spread to the target organ and evolve there independently of the primary tumor (see Figure 2). Studies conducted by Fidler et al. in the 70's, prompted the question of whether the development of metastases are the consequence of the accidental survival and growth of very few malignant cells in a distant organ, or whether it represents the selective growth of unique subpopulations in the tumor mass with special metastatic traits. Subsequent studies clearly showed that primary tumors are biologically heterogeneous and that the process of metastasis is rather selective (Fidler, 2002). Although no metastasis-specific driver mutations have been demonstrated so far, metastatic cell clones clearly do not represent the whole primary tumor population, but only parts of it (Campbell et al., 2010). Recently, Brastianos et al. demonstrated that clonally related primary tumor and brain metastasis samples share a common ancestor, but they continue to evolve separately during the metastatic cascade (Brastianos et al., 2015). These observations highlight the Darwinian selection or branched evolutionary pattern of brain metastasis.
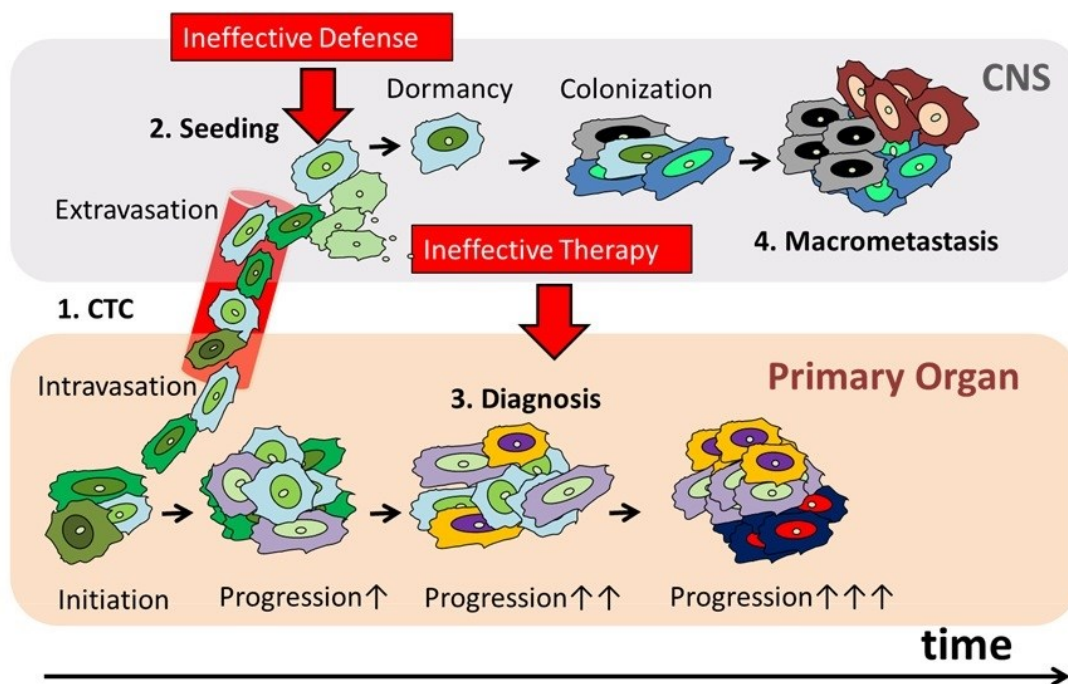
Figure 2: Metastasis - a branched evolutionary process
Metastasis is a complex process which comprises several rate-limiting steps. Tumor cells intravasate and get into the circulation, where they must survive until they reach the target organ. Once there, they extravasate and get into dormancy or re-establish themselves to colonize the secondary site, after failure of the local defense. The metastatic cascade represents a branched evolutionary process, in which tumor cells spread to the target organs at early time points, even months before the diagnosis, and evolve genetically independently of the primary tumor.

1.1.2.1   The colonization: a very inefficient process

From a biological point of view, metastasis is a highly inefficient process. The last steps of the metastatic cascade (the colonization) are considered the bottleneck of the entire process since from the thousands tumor cells that enter the circulation every day, less than 0.1% of them survive, and only less than 0.01% of the circulating tumor cells succeed in the establishment of a metastatic lesion (Fidler, 1970).

Colonization includes several steps: survival upon entry into the secondary tissue, formation of micro-metastasis, adoption of latency/dormancy states (which can last up to decades), re-activation of growth in the latent micro-metastases, and the conquest of the host tissue (Vanharanta & Massague, 2013).

The colonization of the brain, though being the most ineffective step of the whole metastatic cascade, is also the most decisive and threatening one. Once metastases are established, current treatments frequently fail to provide durable responses. To date, there are few effective therapeutical agents that really penetrate the blood brain barrier, or the drug concentrations that reach the metastatic lesion are not sufficient. On the other hand, the cells that get into the brain have already undergone a series of selection steps and a genetically branched evolution, which make them more aggressive and resistant to therapy (see 1.1.2). For this reason, therapeutical agents against the primary tumor are usually ineffective or can even have a boomerang effect when applied for the respective metastatic lesions. Additionally, the dissemination of tumor cells from the primary tumor is a very early process. Usually circulating tumor cells (CTC) have already arrived at the target organ before the primary tumor is diagnosed (see Figure 2). This could be an explanation why most cancer patients have local recurrence after a few months and develop distant metastases in spite of long cycles of therapy.

All this indicates that colonization is the only feasible and meaningful targetable step of the metastatic cascade since all other steps (dissemination, extravasation, etc.) have already taken place before the first diagnosis is done. For this reason, agents that specifically target the colonization of the secondary organ by the tumor cells are needed in order to prevent the development of fatal metastases.

How cancer cells undergo Darwinian selection processes in the course of the disease and acquire the necessary and distinctive skills to colonize distant organs remains a central question in cancer biology. More remarkably, the mechanisms that prevent the colonization of the target organ are still

an unresolved mystery. Nevertheless, uncovering these biological dark horses of colonization may provide the scientific community with the ultimate weapon to combat brain metastases.

1.1.3 Uncovering brain metastasis: experimental models

Much effort has been made in understanding the molecular mechanisms of cell invasion and migration that lead cancer cells to enter the circulation and reach distant organs (Kessenbrock, Plaks, & Werb, 2010; Roussos, Condeelis, & Patsialou, 2011). However, leaving the primary tumor is rather trivial. As has already been mentioned, the main bottlenecks for metastasis formation seem to occur during the colonization of distant organs, since most of disseminated cancer cells die at distant sites. Why this happens is currently unknown, but this massive death represents a major barrier to metastatic cancer progression. Clinically, the colonization of the distant organ is also the most relevant obstacle, because dissemination from primary tumors occurred months before the diagnosis (see Figure 2) (Vanharanta & Massague, 2013). However, despite the importance of the colonization and its relevance for the successful and meaningful management of brain metastases, very few study the mechanisms underlying this bottleneck step.

1.1.3.1   In vitro and ex vivo models

In vitro models to study brain metastasis generally consist of cocultures of tumor cells and brain-derived cells. These models represent a feasible alternative to in vivo models, since they avoid the use of a large number of animals and allow the study of specific stages of brain metastasis progression. However, in vitro and ex vivo models lack the interactions of the tumor cells with the microenvironment in a living animal and they can only model single steps of the metastatic process.

The most used approaches include: transendothelial cell migration assays and chorioallantoic membrane (CAM) assays. Additionally, we established a brain slice coculture system, which will be described afterwards.

a)   Methods to study cell invasion, transendothelial migration and angiogenesis
The chorioallantoic membrane (CAM) assay is widely employed for the study of angiogenesis. Since the lymphoid system is not fully developed until late stages of incubation, the chick embryo serves as a naturally immune-deficient host capable of sustaining xenograft tissues. Implantation of cancer cells into the CAM allows the live monitoring and also pharmacological manipulation of cell migration, cell invasion and angiogenesis (Lokman, Elder, Ricciardelli, & Oehler, 2012). This assay has

provided useful information regarding the establishment of primary tumors; however, it is rather useless for the study of the colonization.

Another experimental approach, transendothelial cell migration assays, measure cell motility and invasiveness of tumor cells. This procedure models the dissemination of circulating tumor cells into the endothelium. It consists of a Boyden Chamber system in which endothelial cells are cultured on top of a porous membrane coated with extracellular matrix (ECM). Tumor cells are added above the endothelial monolayer. The invasion of tumor cells across the endothelium is determined by measuring the number of cells that migrate into the lower chamber (Reymond, d'Agua, & Ridley, 2013). This method provides reliable quantification of transendothelial migration (TEM); however, it dismisses the study of other (more decisive) steps of the metastatic cascade.

b)   Investigating the interactions with the brain parenchyma

Organotypic ex vivo cocultures are especially interesting for the study of the colonization. Our lab developed such a model in which we coculture a 3D tumor cell plug embedded in extracellular matrix (ECM) with an organotypic brain slice (Chuang, Lohaus, et al., 2013; Pukrop et al., 2010). This model especially mimics the interactions of cancer cells and glial cells at the interface of the brain parenchyma and the metastatic tissue. This coculture method allows us to visualize and/or manipulate the interactions at this very important zone. Furthermore, it also permits the use of brain tissue from genetically engineered mice and/or genetically modified tumor cells to investigate genes of interest in the microenvironment or in cancer cells. However, due to the lack of innate immune cells in the brain slice, some important aspects of the colonization are missed in this model system.

1.1.3.2   In vivo models

In vivo brain metastasis models are those approaches where tumor cells from the mice (syngeneic models) or from human origin (xenograph models) are injected into a mouse and successfully form distant metastases in the brain of the animal. Tumor cells can be injected orthotopically, ectopically (through the tail vein, the left ventricle of the heart, or the internal carotid artery), or stereotactically into the mouse brain.

Orthotopic injection means that the tumor cells are injected in the same organ as they originated from. Spontaneous metastases are normally observed after a certain time when tumor cell lines or tissues are transplanted into orthotopic sites. However, to increase the success rate of this

technique, tumor cells are frequently injected into immunocompromised mice, missing the role of the adaptive immune system in metastasis formation.

Tail vein injection is used to mimic the hematogenous dissemination of the tumor cells. This technique is easy to perform, but has a big disadvantage when brain metastases are wanted. Most tumor cells injected into the tail vein are rapidly trapped in the lungs, as they are the first organ encountered with an extensive capillary bed. With this approach, reliable brain metastases are rarely developed, partially due to the fact that animals with lung metastases get sick very quickly and usually die before brain metastases can emerge.

On the other hand, tumor cells injected into the left ventricle of the heart or into the internal carotid artery find the brain as the first capillary bed. Direct injection of tumor cells into the left cardiac ventricle is technically easy to perform, but controlling the exact number of injected tumor cells can be problematic (C. Zhang & Yu, 2011). Intra-carotid artery injection is a very controversial system. First, injected tumor cells colonize several organs (and not only the brain) with a huge biological variability. Moreover, almost always, only micro-metastases and no macro-metastasis arise, and mostly outside of the CNS. These disadvantages make this system unattractive for the study of brain colonization.

Finally, the stereotactic implantation of tumor cells into the brain (Merkler, Ernsting, Kerschensteiner, Bruck, & Stadelmann, 2006) is a colonization method that reflects the final steps of the metastatic process. That the stereotactic injection of tumor cells may cause trauma to the brain affecting the tumor growth has been largely criticized. However, this approach has several benefits: the experimental setting is reproducible, it mimics the crucial step of the whole metastatic cascade of the human disease, and treatment effects are measurable. Taking into account the great importance of the colonization step in the development of brain metastasis, this method could shed some light on the mechanisms responsible for this process.

According to the origin of the cells being implanted into the mouse, in vivo models can be classified into syngeneic models and human xenotransplantation models.

1.1.3.2.1 Syngeneic mouse models

Syngeneic mouse models, also known as allograft mouse tumor systems, consist of the transplantation of tumor cells into a mouse with the same genetic background. These models

represent an effective approach for studying how tumor cells metastasize in the presence of a functional immune system and, more importantly, they are particularly relevant for studies of immunologically-based targeted therapies, either used alone or in combination with other drugs that modulate the immune system's ability to recognize and destroy cancer cells. On the other hand, they may not fully represent the complexity of human tumors in clinical situations as they work exclusively with murine material. Syngeneic mouse models can be classified into three groups: spontaneous, induced, and genetically engineered models.

a)   Spontaneous models

The spontaneous metastasis model recapitulates all the important steps of metastatic cascade. Spontaneous primary tumors may occur in mice; however, spontaneous metastases don't take place at all. Because of this, researchers had to select and establish metastatic murine cell lines from spontaneous primary tumors, by several rounds of selection of the tumor cells in the living animal. This fact may cause unexplainable traits in the metastatic cells that hinder the study of the colonization in itself. Some examples of spontaneous metastatic mouse models are the B16-B10 melanoma cell line (Nicolson, Brunson, & Fidler, 1978), the 4T1 breast cancer cell line (Aslakson & Miller, 1992) and the KHT mouse sarcoma (Conley, 1979).

b)   Induced models

Murine metastasis models can also be obtained after the induction of a malignant lesion by chemical agents or by exposure of healthy animals to ultraviolet (UV) radiation. Some examples are the K-1735 murine melanoma cell line (Kripke, 1979) and the highly metastatic UV-2237 MM cells with brain tropism (Raz, Hanna, & Fidler, 1981). Induced models are widely used to study metastatic progression. However, genetic alterations that lead to transformation of the cells (induction of oncogenes) have not been completely delineated. It is therefore not clear if these models actually reflect the human disease.

c)   Transgenic models

Genetically engineered mouse models (GEMMs), also known as transgenic mouse models, appeared in the 90s. They make use of different genetic techniques for genomic deletion of tumor suppressor genes and/or transgenic insertion of oncogenes in murine somatic cells. These genetic manipulations result in the development of primary malignancies, followed by metastasis to other organs, including the brain. Inducible expression of oncogenes, as well as conditional, tissue specific deletion systems have provided important insights into the mechanisms of cancer initiation and early steps of metastatic progression (Politi & Pao, 2011). A major problem with GEMM-induced tumors is the low

incidence of metastatic spread (Bos, Nguyen, & Massague, 2010), which in part may be explained by a rapid development of the primary lesions. One of the best known transgenic mouse with secondary spreading to the brain is the MMTV-PyMT mouse, a widely used model of breast cancer metastasis (Guy et al., 1992).

1.1.3.2.2 Human xenotransplantation models

In human-rodent xenotransplantation models, human cancer tissues or cell lines from human origin are transplanted into immunocompromised mice. A clear advantage of these models is that they make use of real human material and may be thus more representative of the properties and mutations of human cancer. On the other hand, because of the unavoidable need to employ immunocompromised mice, the role of the microenvironment on the metastasis formation remains unexplored. Ongoing studies to "humanize" the host mice may overcome some of the challenges of xenograft strategies.

Some of the best known xenograph models with secondary spreading to the brain are: the brain metastasing cell line, MDA-MB-231BR, obtained after repeated injections of the original triple negative MDA-MB-231 cells in nude mice (Heyn et al., 2006; Lorger & Felding-Habermann, 2010; R. D. Zhang, Fidler, & Price, 1991); the MCF-7 breast carcinoma cell line (ER$^-$ PR$^-$ Her2$^+$), originally established in 1973 from a pleural effusion in a patient with metastatic breast carcinoma (Soule, Vazguez, Long, Albert, & Brennan, 1973), and the A549 cell line, an orthotopic model of human non-small cell lung carcinomas (NSCLC) obtained by injecting the cells into the left lung of nude mice (Mathieu et al., 2004).

All pre-clinical models mentioned above (syngeneic and xenograph models) have limitations and none of these approaches fully reflect the tumor development and brain metastasis formation pattern seen in patients with metastatic disease. The most important restriction is the lack of validation against clinical brain metastases from patients, to ensure that the pathways identified in the model are also present in the human situation. The various model systems used, however, have provided important insight into specific mechanisms of the metastatic process. By combining the knowledge obtained from different animal models, new important information on the molecular mechanisms behind metastasis will be obtained, leading to the future development of new therapeutic strategies.

1.2 The seed and soil theory

The concept that different tumors metastasize preferentially to different target organs is not new. It was first proposed in 1889 by the English surgeon Stephen Paget in his "Seed and Soil" hypothesis. It comprises the idea that different cancer cells (the "seed") have an affinity for certain organs (the "soil") because they offer a compatible and hospitable microenvironment which allows tumor growth and metastatic progression (Paget, 1889). In 1929 Paget's theory was challenged. Stevens and Ewing proposed that metastatic dissemination occurs by purely mechanical factors that are a result of the anatomical structure of the vascular system (Stevens & Ewing, 1928). In the 1970s, a detailed analysis of experimental metastasis in syngeneic mice indicated that mechanical arrest of tumor cells in the capillary bed of distant organs could indeed occur, but that subsequent proliferation and growth into secondary lesions were influenced by specific organ cells (Hart & Fidler, 1980b).

In the last decades, this theory has been repeatedly proved by the routine use of animal models. An interesting example was the demonstration of organ specific metastasis by Fidler et al. after the injection of two different mouse melanoma cells into the internal carotid artery of immunocompetent mice. On the one hand, the K-1735 melanoma cell line showed a marked tropism for the brain parenchyma, whereas the B16 cells produced only meningeal metastasis (Schackert & Fidler, 1988). Such a difference in the tumor growth within the same target organ may be based on interactions between the metastatic cells and the organ environment and proves once more the seed and soil theory.

This idea has not only been proved in animal models but also in humans, however, not directly because of obvious ethical considerations. Human ovarian cancer cells can grow in the peritoneal cavity; however, they never metastasize to other visceral organs. One explanation for the lack of visceral metastases could be that the tumor cells could not gain entrance into the systemic circulation. Tarin et al. studied metastasis in ovarian cancer patients whose ascites were drained with peritoneovenous shunts into the venous circulation. The autopsy findings corroborated the clinical observations that the shunts did not significantly increase the risk of metastasis to organs outside the peritoneal cavity. In fact, despite continuous entry of millions of tumor cells into the circulation, metastases to the lung or other organs were rare (Tarin et al., 1984).

All these examples support the idea that the trafficking of cancer cells to their target organ is not entirely random and may be guided by factors produced by the stromal cells of their host organ.

As has already been mentioned (see 1.1.2.1), the main bottlenecks for metastasis formation seem to occur during the colonization of distant organs, since most disseminated cancer cells die at distant sites. Why this happens is currently unknown, but this massive death represents a major barrier to metastatic cancer progression (Vanharanta & Massague, 2013). In this context, understanding the natural mechanisms that eliminate disseminated cancer cells at distant sites may facilitate the development of new therapeutic strategies to prevent metastasis.

1.2.1 The tumor microenvironment (the "soil")

The tumor microenvironment (TME) is composed of immune cells, fibroblasts, bone marrow-derived inflammatory cells, lymphocytes, surrounding blood vessels, signaling molecules and the extracellular matrix (ECM) (Spill, Reynolds, Kamm, & Zaman, 2016). The stromal cells of the tumor microenvironment influence each of the rate-limiting steps of the metastatic cascade and may definitely play a role in eliminating disseminated cancer cells at the target organ.

As already mentioned, the colonization of the brain is highly inefficient. That means that, in most cases, the tumor microenvironment may effectively block the colonization of the target organ by exerting inhibitory effects on malignant cells. However, tumor cells can also evade these inhibitory signals and misuse the surrounding stromal cells to promote tumor progression and ultimately metastasis (Chuang, van Rossum, et al., 2013; Pukrop et al., 2010). In this context, for a successful colonization to take place, a failure of the local defense is required, since it is the first line of defense in the secondary organ (see Figure 2). Interestingly, all the major target organs of metastasis possess tissue-specific macrophage populations: Kupffer cells in the liver, alveolar macrophages in the lung, osteoclasts in the bone or Langerhans cells in the skin. All these tissue-specific macrophages have been shown to participate in the establishment of metastases (Gjoen, Seljelid, & Kolset, 1989; Hanisch & Kettenmann, 2007; Kaplan et al., 2005).

In the central nervous system (CNS), microglia represent the first line of defense. These tissue-resident macrophages arise from primitive hematopoietic progenitors present in the yolk sac during embryonic development (Yona et al., 2013). Microglial cells are supported by the astrocytes in their defense role. However, once this first line of defense in the CNS is overcome, microglial cells actively participate in the colonization of the brain by malignant cells (Chuang, van Rossum, et al., 2013; Pukrop et al., 2010). In fact, our group has already shown that human brain metastases are usually infiltrated by activated microglia/macrophages and surrounded by astrocytes, which build a protective capsule around the metastatic tissue (see Figure 3).
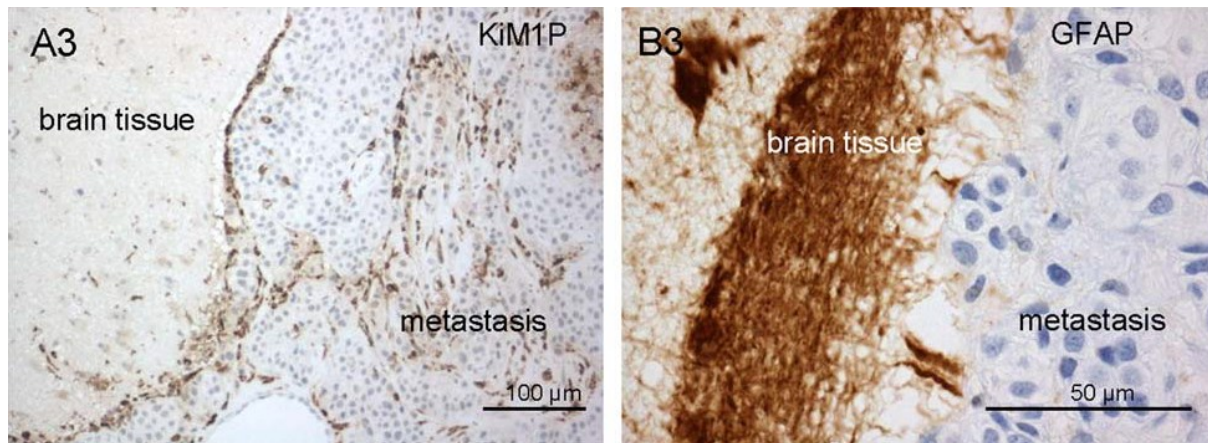
Figure 3: Distribution of microglia/macrophages and astrocytes in human brain metastases
A) Activated microglia/macrophages (Ki-M1P) are found at the interface of the metastasis and the brain tissue and inside the metastasis. **B)** Activated astrocytes (GFAP) accumulate in the adjacent brain tissue and form a barrier at the interface to the metastatic tissue. Taken from (Chuang, van Rossum, et al., 2013) under a Creative Commons Deed Attribution 2.5 License.

Until now, it was thought that the brain was an "immuno-privileged" organ, in which the only gateways into the CNS were the blood vessels. However, recently Louveau and colleges shed new light on the composition of the CNS drainage system. They discovered functional lymphatic vessels lining the dural sinuses which are able to carry immune cells (like T cells and monocytes) from the cerebrospinal fluid (CSF) into the brain (Louveau et al., 2015). Although immune cell infiltrates were first considered a failed attempt of the body to combat malignant foreign cells, it is now known that tumor cells can specifically attract and manipulate these cells to assist them in tumor progression (Joyce & Pollard, 2009) and metastasis formation (Chuang, van Rossum, et al., 2013; Pukrop et al., 2010). That means that not only the resident macrophages of the CNS (microglia) but also macrophages coming from the bone marrow could support the tumor cells during metastasis formation.

1.2.1.1 Tumor-associated macrophages (TAM)

Tumor-associated macrophages (TAM) are an essential cellular component of the innate immune system and key players in the tumor microenvironment. They are derived from myeloid progenitor cells in the bone marrow compartment and characterized by poor antigen-presenting capability, suppression of T cell proliferation and activity, and promotion of angiogenesis. This tumor promoting phenotype has been classically designated as polarized type II (alternatively activated) or M2. Tumor promoting macrophages (M2) contrast markedly with classically activated type I or M1 macrophages. M1 macrophages own a tumor suppressing phenotype characterized by an efficient immune effector

capacity and the ability to kill microorganisms as well as tumor cells, present antigens, and produce high levels of T cell stimulatory cytokines (Mantovani, Sozzani, Locati, Allavena, & Sica, 2002) (see Figure 4).
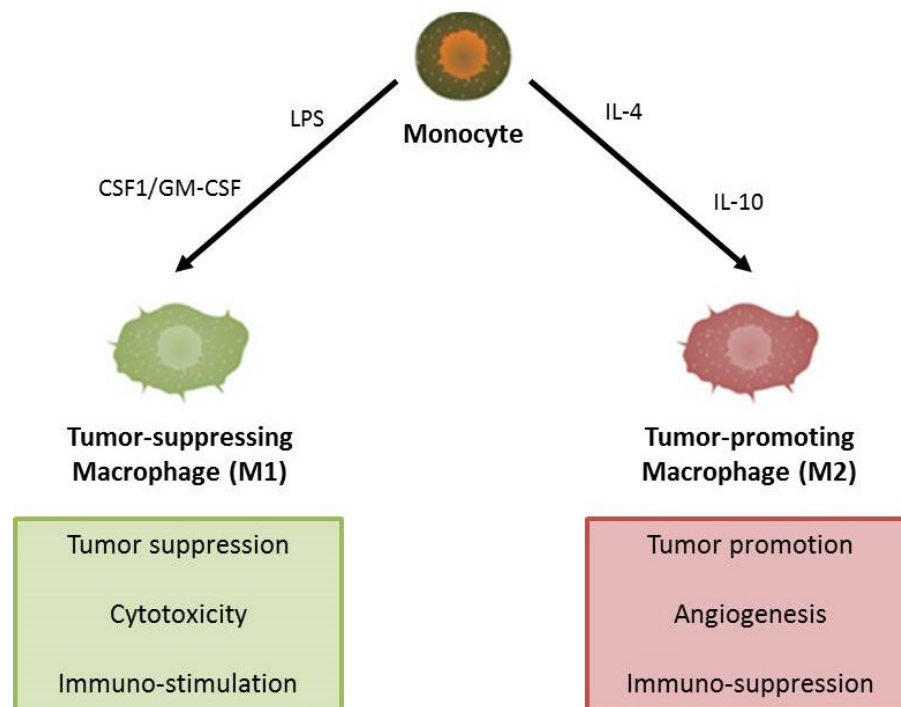
Figure 4: Classification of macrophages – M1 and M2 phenotypes

Macrophages can be classified in tumor suppressing (M1) and tumor promoting (M2) macrophages. Tumor suppressing macrophages are activated under LPS or GM-CSF stimuli and display cytotoxic and immuno-stimulating functions. Tumor promoting macrophages are activated by IL-4 or IL-10 and promote angiogenesis and immuno-suppression in the tumor microenvironment.

Macrophages are inherently plastic cells, and this adaptability may be abused by the tumor to carry out important functions at different stages during the metastatic cascade. In the primary tumor, TAM can stimulate angiogenesis and enhance tumor cell invasion by secreting epidermal growth factor (EGF) and remodeling the ECM (B. Z. Qian & Pollard, 2010). TAM also display an immuno-suppressive role, preventing tumor cells being attacked by natural killer and T cells during tumor progression, by secreting immunosuppressive factors like IL-10 (C. E. Weber & Kuo, 2012). In fact, infiltrating macrophages have been detected at the invasive front of mammary tumors in human samples as well as in mouse models (Pukrop et al., 2006; B. Qian et al., 2009; Wyckoff et al., 2007). Furthermore, macrophage infiltration in primary tumors usually correlates with poor patient prognosis and is associated with development of metastasis (Bingle, Brown, & Lewis, 2002; Robinson et al., 2009; Rohan et al., 2014; Talmadge, Donkor, & Scholar, 2007).

During metastasis, TAM have been shown to prime the pre-metastatic niche, recruit and retain circulating tumor cells at the metastatic site, and foster their growth, in a process driven by the CCL2-

induced chemokine cascade (Kitamura et al., 2015). However, the role of TAM during the colonization of the target organ by tumor cells is unknown. Metastases have been seen to be infiltrated by macrophage populations (Joyce & Pollard, 2009). But, in the special case of the CNS, it is still unclear whether this infiltrative pool is composed of the tissue-specific macrophages alone (microglia), or whether macrophages coming from the bone marrow also take part of the colonization process.

1.2.1.1.1 CSF1R signaling in the colonization of the CNS

One of the communication mechanisms between macrophages and tumor cells in the primary tumor involves a paracrine signaling loop in which cancer cells express the colony-stimulating factor 1 (CSF1), which acts as a potent chemoattractant and activator for CSF1R-expressing TAM; and macrophages in turn produce the epidermal growth factor (EGF) which increases the invasiveness and migration of neighboring tumor cells that express the EGF receptor (EGFR) (Joyce & Pollard, 2009). Thus the activating signaling loop between cancer cells and the surrounding stromal cells (especially tumor-associated macrophages) may be implicated in processes like enhancing the dissemination of cancer cells and promoting metastasis formation (see Figure 5).
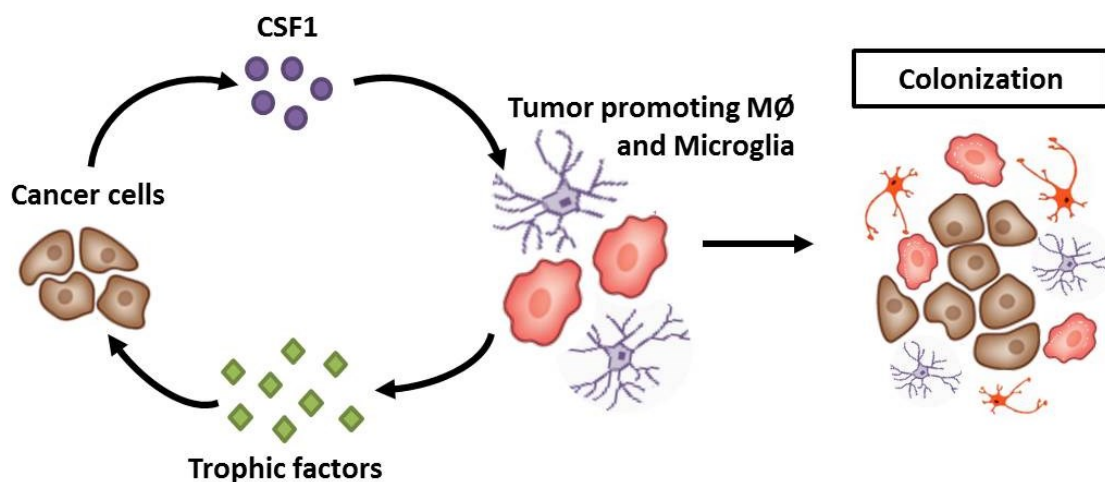
Figure 5: Activation loop between macrophages/microglia and tumor cells promotes colonization
Tumor progression is controlled through a paracrine loop involving colony-stimulating factor 1 (CSF1), and tropic factors (like EGF) and their receptors, which are differentially expressed on carcinoma cells and macrophages, resulting in a malignant switch of the macrophages/microglia in the CNS that promotes brain colonization and metastasis.

In view of the importance of the CSF1 paracrine loop in the metastatic cascade, CSF1 has become a remarkably feasible therapeutic target against cancer metastases. Several studies to block CSF1 have been performed, like for example, selective depletion of macrophages by the knockdown of

macrophage colony-stimulating factor (MCSF/CSF1) or pharmacological depletion with clodronate-liposome treatment or anti-CSF1 (Hiraoka et al., 2008; Lin, Nguyen, Russell, & Pollard, 2001). These studies showed a substantial decrease in macrophage infiltration into the primary tumor, which led to the inhibition of tumor angiogenesis, tumor growth and metastasis in different animal models. These experiments have been crucial in demonstrating the pro-tumorigenic functions for macrophages in the primary tumors. However, most of these strategies have both local and systemic effects, which make it difficult to determine whether the therapeutic effects take place on the macrophage lineage and/or directly affect the recruitment and survival of TAM in the tumor. Moreover, the effects of the resident macrophages in the target organs for distant metastasis are only barely understood or not investigated at all. For these reasons, broadly depleting all macrophage populations should be avoided in the context of cancer therapies.

An alternative to this general depletion is to ablate subpopulations or individual factors produced by macrophages. In fact, many studies have shown that the microenvironment is capable of normalizing tumor cells, suggesting that re-education of stromal cells, rather than targeted ablation per se, may be an effective strategy for treating cancer metastasis (Quail & Joyce, 2013). In other words, the idea is to blunt the innate pro-tumorigenic activity of the tumor-associated macrophages and reprogram the tumor microenvironment toward more effective dendritic cell activation and immune effector cell cytotoxicity in order to stop the colonization of the brain (see Figure 6).
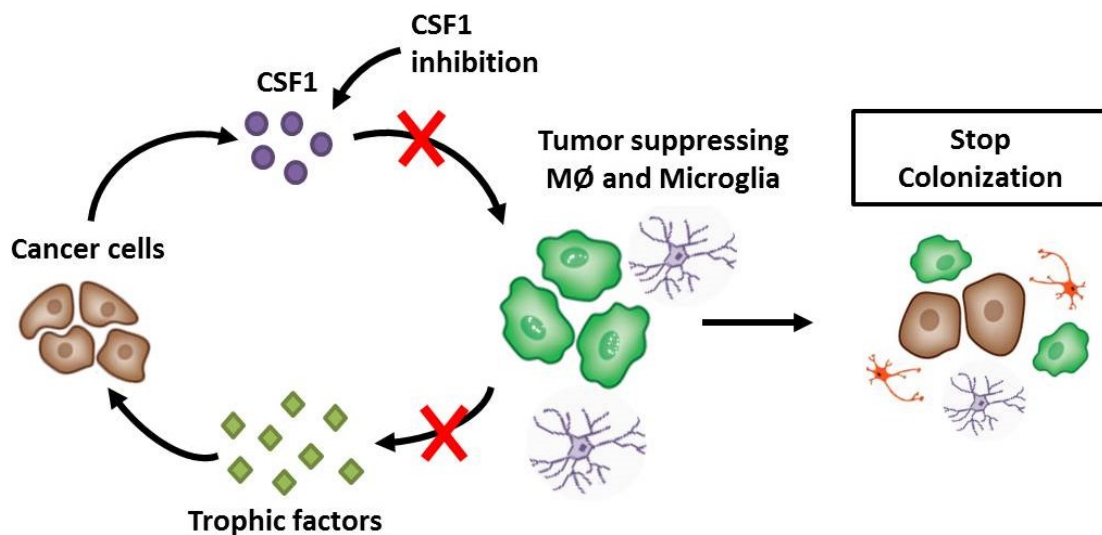
Figure 6: Therapeutical re-education of macrophages to abolish brain colonization
Treatment of stromal cells with agents that block the CSF1-signaling loop between tumor cells and macrophages/microglia, may lead to the re-education of macrophages into a tumor-suppressing phenotype and could be an effective strategy for treating cancer metastasis.

Previous work of our group showed, however, that in the special case of the CNS, the organ specific macrophages (microglia) cannot be successfully treated with anti-CSF1 agents (see Figure 7). This observation could be due to the fact that the resident microglia are significantly different from TAM. They not only differ in their origins (yolk sac vs bone marrow) but they also behave differently to anti-macrophage therapies based on inhibition of the CSF1 signaling. It could be due to the fact that, in the particular case of the CNS, the presence of an alternative ligand for the CSF1 receptor (CSF1R), interleukin 34 (IL34), may interfere with the anti-CSF1 treatment effects (Rietkotter et al., 2015).
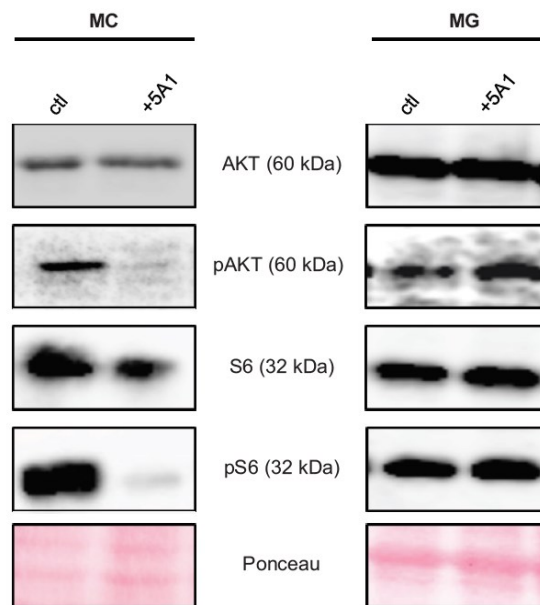
Figure 7: Microglia cannot be successfully targeted with anti-CSF1

CSF1R downstream signaling can only be effectively blocked in bone marrow-derived macrophages (MC) but not in the CNS-resident macrophages microglia (MG) after treatment with anti-CSF1 (5A1). Taken from (Rietkotter et al., 2015) with permission from Impact Journals, LLC.

According to this observation, anti-CSF1 agents seem to be unsuitable for the treatment of CNS-metastases, and therefore other targets should be regarded.

1.2.1.1.2 The PI3K/Akt signaling pathway

The phosphatidylinositol 3-kinase (PI3K) has been proposed as one of the targets of CSF1 in myeloid cells (Rommel, Camps, & Ji, 2007) (see Figure 8). In fact, some studies have shown that the binding of the PI3K to CSF1R in TAM stimulates their tumor promoting functions (Sampaio et al., 2011). According to that, PI3K seem to be a feasible therapeutic target against macrophage-associated tumor progression in the CNS.
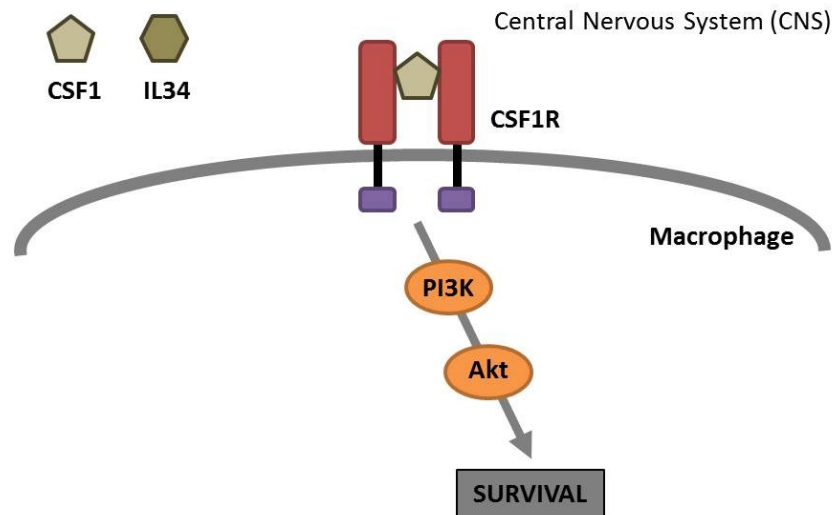
Figure 8: The PI3-kinase, a downstream effector in the CSF1R signaling pathway
After activation of the CSF1R in macrophages, downstream effectors like PI3K transmit the signal to the nucleus, leading to activation of cellular processes like migration, proliferation and survival.

The PI3K is the central molecule of the PI3K/Akt/mTOR signaling pathway. This pathway plays a key role in cell growth, survival, metabolism and metastasis. There are three classes of PI3-kinases according to their structure and function. Class IA PI3-kinases are the most relevant in human cancer and consist of a regulatory subunit (p85) and a catalytic subunit with three isoforms (p110α, p110β and p110δ). These kinases can be activated by growth factor stimulation through receptor tyrosine kinases (RTK) that bind the regulatory subunit p85 (Carpenter et al., 1993); by activated Ras, which directly binds p110 (Shaw & Cantley, 2006); or by G-protein coupled receptors that bind the p110β catalytic subunit (Katso et al., 2001). Upon activation, PI3K converts phosphatidylinositol 4,5-bisphosphate (PIP2) to phosphatidylinositol 3,4,5-bisphosphate (PIP3), which in turn activates a downstream signaling cascade involving two serine/threonine kinases, the phosphoinositide-dependent kinase 1 (PDK1) and the protein kinase B (AKT). PDK1 activates AKT by phosphorylating AKT at threonine 308 (Alessi et al., 1997; Currie et al., 1999). PI3K-AKT signaling promotes cell growth and survival by several mechanisms like, for example, the Akt-mediated inhibition of the pro-apoptotic Bcl-2 family members BAD and BAX (Engelman, Luo, & Cantley, 2006). Akt can also phosphorylate Mdm2 which antagonizes p53-mediated apoptosis, thereby reducing production of cell death-promoting proteins. The protein complex mTORC1 can be activated by AKT though the Rheb GTPase, which results in increased protein synthesis by the phosphorylation of eukaryotic initiation factor 4E and the ribosomal S6 protein (Engelman et al., 2006).

The major negative regulator of the pathway is the tumor suppressor phosphatase and tensin homolog (PTEN), which dephosphorylates PIP3 to PIP2, thereby terminating PI3K-dependent

signaling (Liu et al., 2009). In addition, inositol polyphosphate-4-phosphatase type II (INPP4B) also negatively regulates the pathway by converting PIP2 to phosphatidylinositol 3-bisphosphate (Gewinner et al., 2009). Another level of negative feedback is mediated through the activation of the S6 kinase (S6K) by mTORC1. The S6-kinase inhibits mTORC2, which negatively feeds back to diminish PI3K activation (Dibble & Manning, 2009). In addition, S6K negatively regulates the PI3K/AKT/mTOR pathway through inhibition of the insulin receptor substrate-1 (Carracedo & Pandolfi, 2008). The PI3K signaling pathway is summarized in Figure 9.
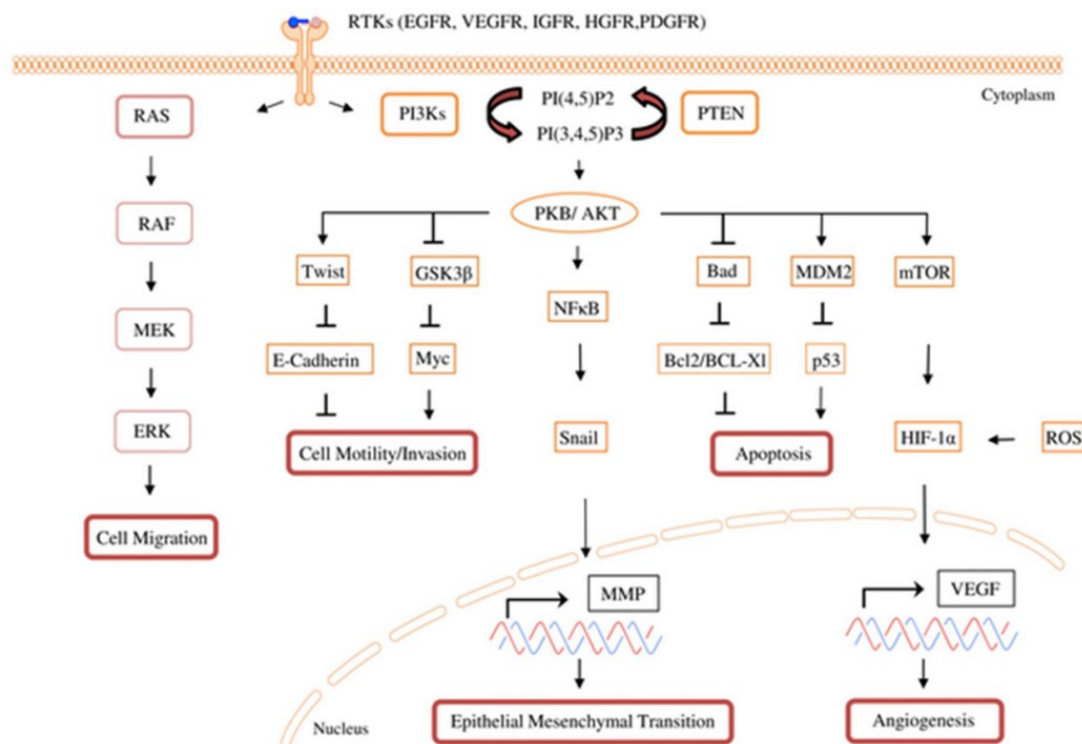
Figure 9: The phosphatidylinositol 3-kinase (PI3K) signaling cascade
The PI3K/AKT signaling pathway internalizes the effects of external growth factors and of membrane tyrosine kinases. Activation of membrane kinases initiates receptor dimerization and subsequent events to activate intracellular pathways that lead to cell growth, survival, metabolism and metastasis. Taken from (Crespo, Kind, & Arcaro, 2016) under a Creative Commons Attribution-NonCommercial-ShareAlike 3.0 License.

The role of the PI3K signaling pathway in tumor progression is well known. In many cancers, this pathway is mutated and overactive, resulting in reduced apoptosis and increased proliferation of tumor cells. The main alterations include mutations and/or amplification of genes encoding receptor tyrosine kinases (e.g., HER2 or EGFR), PIK3CA mutations, PTEN mutation/loss, and KRAS mutations (Dienstmann, Rodon, Serra, & Tabernero, 2014).

Interestingly, this pathway has been shown to play a role not only in primary tumors but also in brain metastases. In this context, Brastianos et al. performed a whole exome sequencing analysis on 86

'trios' of patient-matched brain metastases, primary tumors and normal samples in order to determine whether clinically sampled brain metastases harbor distinct potentially clinically informative mutations not detected in paired primary tumor samples. Remarkably, they detected the activation of the PI3K signaling pathway, and alterations associated with sensitivity to PI3K/AKT/mTOR inhibitors only in the brain metastases counterparts (Brastianos et al., 2015).

The fact that the PI3K signaling pathway is activated in brain metastases, and that it may serve integral functions for stromal cells in the tumor microenvironment, like TAM, points out the PI3K as a feasible therapeutic target for macrophage-associated colonization in the CNS.

1.2.1.1.3 Targeting the PI3K/Akt signaling pathway with the PI3K inhibitor BKM120

The key role of the PI3K/Akt signaling pathway in tumor progression and metastasis has motivated the pharmaceutical industry to develop several PI3K inhibitors with different profiles, such as dual mTOR/PI3K, pan-PI3K, and isoform-specific PI3K inhibitors for clinical application. One of these inhibitors is BKM120, also known as buparlisib. BKM120 is an oral pan-PI3K inhibitor developed by Novartis Oncology. This inhibitor is a pyrimidine-derived compound that blocks all four isoforms of the PI3K class I by competitive binding of the lipid kinase domain on its ATP-binding site (Clarke & Workman, 2012; Maira et al., 2012) (see Figure 10).
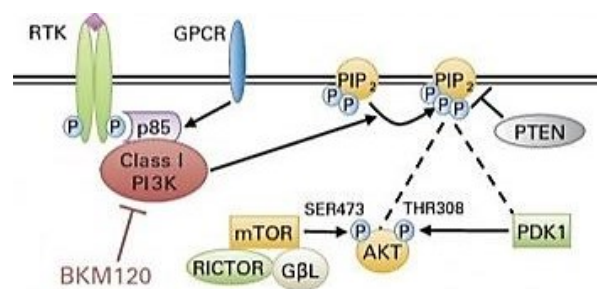
Figure 10: BKM120 blocks the class I PI3-kinase

BKM120 specifically inhibits class I PIK3 in the PI3K/AKT signaling pathway in an ATP-competitive manner, thereby inhibiting the production of the secondary messenger phosphatidylinositol-3,4,5-trisphosphate and the activation of the PI3K signaling pathway. Modified from (Clarke & Workman, 2012) with permission from the American Society of Clinical Oncology (ASCO).

BKM120 has shown preliminary activity in preclinical models of solid tumors as well as favorable tolerability profiles, with the most common adverse events having to deal with "on-target" effects (Maira et al., 2012). Buparlisib is currently in Phase III of clinical trials and is especially indicated in the case of breast cancer patients.

Of note, it has been shown that BKM120 can cross the blood brain barrier (Nanni et al., 2012), a fact that makes this compound especially interesting for the treatment of brain metastasis. However, despite the studies of Brastianos et al., in which they indicated a high sensitivity of brain metastases to PI3K/AKT/mTOR inhibitors, there are only few studies regarding the role of BKM120 in brain metastasis. One of these studies aimed to treat multi-organ metastatic spread with BKM120. However, this study made use of human metastatic HER2+ breast cancer cells and was thus performed in a highly immuno-deficient double knockout mouse model, which lacks T, B and NK cell activity (Nanni et al., 2012). Another study performed by Niessner et al. could prove the anti-tumor effects of BKM120 in metastatic melanoma. However, this study made use of melanoma cell lines, thus missing the influence of the microenvironment in a living animal (Niessner et al., 2016).

That means that, to date, there are no studies that specifically target the PI3-kinase in the tumor microenvironment in the context of brain colonization.

1.3   Aims of the study

My thesis project is included in the so-called "MetastaSys e:Bio" consortium, which aims to analyze molecular markers and pathways in cancer cells and their microenvironment, that govern the fate and localization of tumor metastases. The project is funded by the Federal Ministry of Education and Research (BMBF) within the framework "Systems Biology e:Bio".

MetastaSys makes use of the data generated from in vitro cell line experiments, which are screened in vivo and finally verified in patient samples to generate bioinformatic models and try to identify clinically relevant activation patterns. Eleven sub-projects (work packages - WP) are involved in this consortium (see Figure 11). My contribution to the MetastaSys e:Bio project consists of: i) providing the ex vivo and in vivo platforms to screen the metastatic potential of breast and colon cancer cell lines in the mouse brain, and ii) identifying the influence of the microenvironment on metastasis formation.
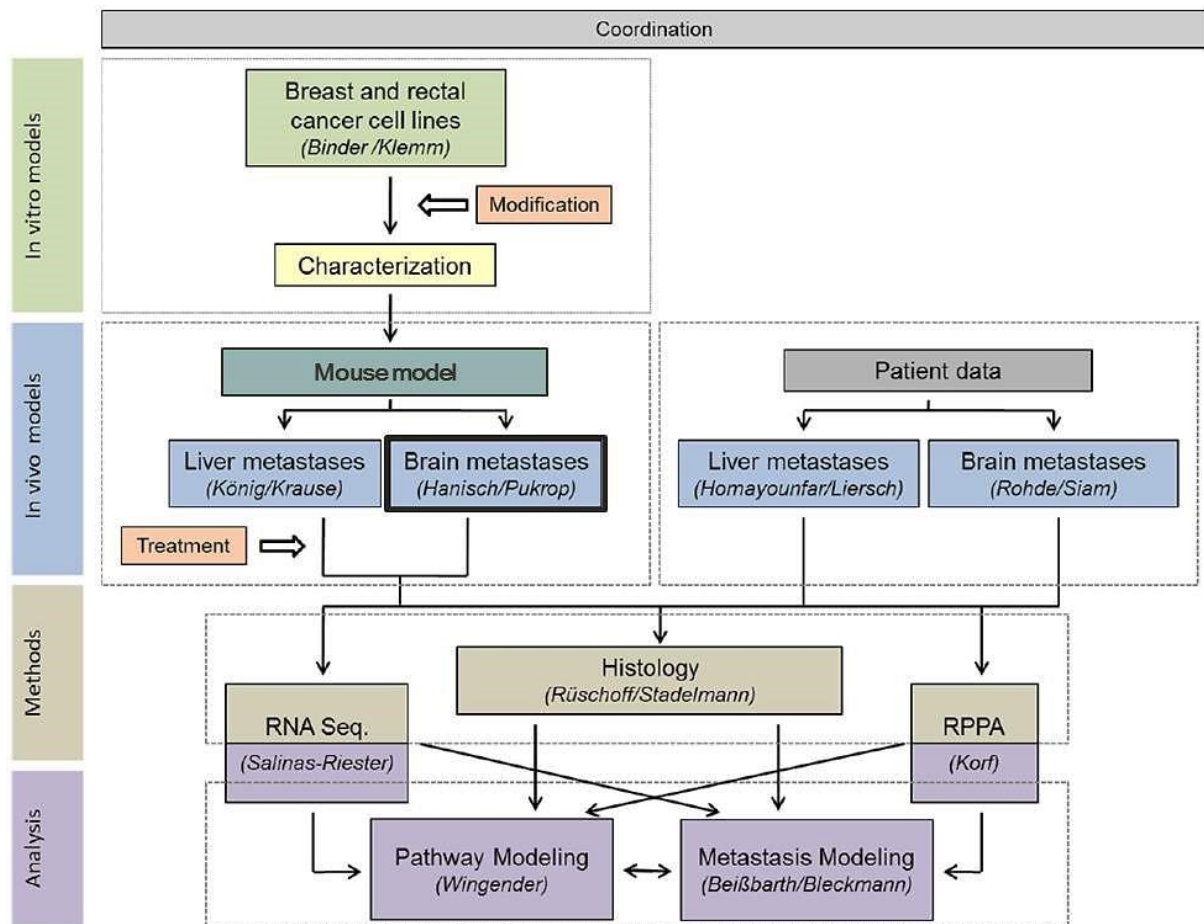
Figure 11: Distribution of the different projects (work packages) involved in MetastaSys e:Bio
The MetastaSys e:Bio consortium consists of eleven work-packages which collaborate to generate bioinformatic models and try to identify clinically relevant activation patterns.

As explained previously, metastasis formation is a complex, branched evolutionary and very inefficient process, especially during the colonization step. However, despite the clinical relevance of this process, the colonization of the brain during metastasis remains ununderstood. Moreover, the role of the tumor-associated microenvironment during colonization also needs to be further investigated. For these reasons, in this study I develop colonization models to look for triggers of metastasis, and investigate the specific role of the microenvironment (especially tumor-associated macrophages) during the colonization of the brain.

Specifically, following aims are pursued in this study:

1) Establishment and characterization of suitable brain colonization in vivo models.

2) Comparison of the colonization models to search for triggers of metastasis.

3) Study of the role of the tumor-associated macrophages (TAM) in the colonization of the brain.

4) Therapeutical inhibition of PI3K to block the tumor-promoting function of macrophages and stop brain colonization.

2   Materials and Methods

2.1   Materials

2.1.1 Biological material

2.1.1.1   Cell lines

The cell lines used in this study are listed in Table 1.

Table 1: Cell lines

Name	Cell type / species	Background	Origin / obtained from	Reference
4T1	mouse breast cancer	BALB/c	Prof. F. Balkwill (London)	(Aslakson & Miller, 1992)
410.4	mouse breast cancer	BALB/c	Prof. F. Balkwill (London)	(Miller, Miller, & Heppner, 1983)
L929	mouse fibroblasts	C3H/An	Prof. U.K. Hanisch (Göttingen)	(Sanford, Hobbs, & Earle, 1956)
MCF-7	human breast cancer	-	DSMZ (Braunschweig)	(Soule et al., 1973)
MDA-MB-231	human breast cancer	-	ATCC (Wesel)	(Cailleau, Young, Olive, & Reeves, 1974)
SK-BR-3	human breast cancer	-	ATCC (Wesel)	(Trempe, 1976)

2.1.1.2   Primary cells

Monocyte-derived macrophages (MDM) were isolated from the bone marrow of adult mice (10-12 week-old). Microglia and astrocytes were isolated from primary glial cell cultures of newborn mice (0-1 day-old).

2.1.1.3   Mouse strains

Adult mice (BALB/c) were obtained from Charles River (Hannover, Germany) and kept in the animal facility for about 15 weeks under standard conditions. All animals became a soy-free diet.

Newborn mice were bred and obtained from the animal facility of the University Medicine Göttingen and the University Hospital Regensburg (Germany).

2.1.2 Cell culture media and additives

All media and additives used for the culture of cell lines and primary cells are listed in Table 2.

Table 2: Cell culture media and additives

Product	Company
Accutase solution	Sigma-Aldrich (Steinheim)
DMEM medium (1 g/l glucose)	Merck Millipore (Berlin)
Dulbecco's Phosphate Buffered Saline (PBS) without Ca^{2+}, Mg^{2+}	Sigma-Aldrich (Steinheim)
Fetal calf serum (FCS)	PAN Biotech (Aidenbach)
Geneticin (G418 Solution)	Roche (Mannheim)
Glucose 40%	B. Braun (Melsungen)
Hank's balanced salt solution (HBSS)	Gibco / ThermoFisher (Darmstadt)
L-Glutamine-Penicillin-Streptomycin Solution	Sigma-Aldrich (Steinheim)
Minimum essential medium (MEM)	Gibco / ThermoFisher (Darmstadt)
Normal goat serum (NGS)	Sigma-Aldrich (Steinheim)
Normal horse serum (NHS)	Gibco / ThermoFisher (Darmstadt)
Penicillin/Streptomycin (P/S)	Merck Millipore (Berlin)
RPMI-1640 medium	Gibco / ThermoFisher (Darmstadt)
Sodium Pyruvate	Sigma-Aldrich (Steinheim)
Trypsin (1:250), 2.5 % in PBS, without Ca^{2+}, Mg^{2+}	Merck Millipore (Berlin)
Trypsin-EDTA (10X)	Sigma-Aldrich (Steinheim)

2.1.3 Chemicals, enzymes and other reagents

All used chemicals, enzymes as well as other reagents are listed in Table 3.

Table 3: Chemicals, enzymes and other reagents

Product	Company
2-Mercaptoethanol	Sigma-Aldrich (Steinheim)
Acetic Acid	Merck Millipore (Berlin)
Agarose HEEO Ultra	Carl Roth (Karlsruhe)
Albumin Fraction V (BSA)	Carl Roth (Karlsruhe)
Ammonium Persulfate (APS)	VWR (Ismaning)
Antibody Diluent	Dako (Jena)
BKM120 (buparlisib, PI3K inhibitor)	Novartis Pharma (Nürnberg)
Blotting-Grade Blocker (nonfat dry milk)	Bio-Rad (Munich)
Bovine Serum Albumin (BSA) Standard Ampules	Gibco / ThermoFisher (Darmstadt)
Clodronate, Disodium Salt	Merck Millipore / Calbiochem (Darmstadt)
Deoxycholic acid sodium salt	Carl Roth (Karlsruhe)
Deoxyribonuclease I (DNAse I)	Worthington / CellSystems (Troisdorf)
Diethil Ether	Merck Millipore (Berlin)
Dimethiyl Sulfoxide (DMSO)	Sigma-Aldrich (Steinheim)
DNase I (10 U/µl)	Roche (Mannheim)
DNase I Incubation Buffer (10x)	Roche (Mannheim)
Eosin Y solution	Carl Roth (Karlsruhe)
Ethanol	Merck Millipore (Berlin)
Ethylenediaminetetraacetic acid (EDTA)	Merck Millipore (Berlin)
Extracellular Matrix (ECM)	R&D Systems (Wiesbaden)
ExtrAvidin-Peroxidase	Sigma-Aldrich (Steinheim)
Fluorescent mounting medium	Dako (Jena)
Formic acid	Carl Roth (Karlsruhe)
Glycine	Carl Roth (Karlsruhe)
Hematoxylin solution	Carl Roth (Karlsruhe)

Isopropanol	Merck Millipore (Berlin)
iTaq Universal SYBR Green Supermix	Bio-Rad (Munich)
Laemmli loading buffer Roti-Load 1 (reducing, 4x)	Carl Roth (Karlsruhe)
Methanol	Merck Millipore (Berlin)
NaCl 0.9%	B. Braun (Melsungen)
Paraformaldehyde (PFA)	Merck Millipore (Berlin)
Paraplast Plus	Sigma-Aldrich (Steinheim)
Perhydrol Hydrogen peroxide 30%	Merck Millipore (Berlin)
Phosphatase inhibitor PhosSTOP (10x)	Roche (Mannheim)
Poly-L-lysine	Sigma-Aldrich (Steinheim)
Ponceau S Solution (0.1 % (w/v) in 5% acetic acid)	Sigma-Aldrich (Steinheim)
Precision Plus Protein Dual Xtra	Bio-Rad (Munich)
Protease Inhibitor cocktail tablets, EDTA free	Roche (Mannheim)
RNase OUT (40 U/µl)	Invitrogen / ThermoFisher (Karlsruhe)
Roti Phenol/Chloroform/Isoamyl alcohol	Carl Roth (Karlsruhe)
Roti-Histokitt II	Carl Roth (Karlsruhe)
Rotiphorese Gel 30 (30% acrylamide/bisacrylamide solution)	Carl Roth (Karlsruhe)
Rotipuran Trichloromethane/Chloroform	Carl Roth (Karlsruhe)
Sodium Acetat Water-free	Carl Roth (Karlsruhe)
Sodium Dodecyl Sulphate (SDS)	Carl Roth (Karlsruhe)
Target Retrieval Solution (Citrate buffer, pH 6)	Dako (Jena)
Tetramethylethylendiamin (TEMED)	Sigma-Aldrich (Steinheim)
Thiazolyl Blue Tetrazolium Bromide (MTT)	Sigma-Aldrich (Steinheim)
Tris-Wash Buffer (pH 6)	Merck Millipore (Berlin)
Triton X-100	Sigma-Aldrich (Steinheim)
Trizma (Tris-Base)	Sigma-Aldrich (Steinheim)
TRIzol Reagent	Invitrogen / ThermoFisher (Karlsruhe)
Tween 20	Sigma-Aldrich (Steinheim)
UltraPure DNase/RNase-Free Distilled Water	Invitrogen / ThermoFisher (Karlsruhe)
Xylol	Carl Roth (Karlsruhe)

2.1.4 Antibodies and fluorescence dyes

The antibodies and fluorescence dyes used in this study are listed in Table 4.

Table 4: Antibodies and fluorescence dyes

Name	Source	Label	Application / Dilution	Company / Cat. Nr.
Akt	Rabbit	-	WB (1:1000)	Cell Signaling (#9272)
Alexa Fluor 568 isolectin GS-IB4 conjugate	Griffonia simplicifolia	Alexa Fluor 568	IF (1:500)	ThermoFisher (#I21412)
Alexa Fluor 647 isolectin GS-IB4 conjugate	Griffonia simplicifolia	Alexa Fluor 647	IF (1:500)	ThermoFisher (#I32450)
CD3	Rabbit	-	IHC (1:150)	DCS Innovative (#CI597R01)
Cytokeratin 8 (phospho-Ser431)	Rabbit	-	WB (1:1000) IHC (1:100)	Abcam (#ab59434)
DAPI	-	-	IF (1:1000)	Sigma-Aldrich (#D9542)
E-Cadherin (24E10)	Rabbit	-	WB (1:1000), IHC (1:200)	Cell Signaling (#3795)
E-Cadherin (Clone 36)	Mouse	-	WB (1:5000)	BD Biosciences (#610181)
Glial Fibrillary Acidic Protein (GFAP)	Rabbit	-	IHC (1:200)	Dako (#Z0334)
Glial Fibrillary Acidic Protein (GFAP) (G-A-5)	Mouse	-	IF (1:100)	Sigma-Aldrich (#G3893)
GSK-3β (27C10)	Rabbit	-	WB (1:2000)	Cell Signaling (#9315)
HSP 90α/β (F-8)	Mouse	-	WB (1:10000)	Santa Cruz (#sc-13119)
Iba1	Rabbit	-	IHC (1:1000)	Wako (#019-19741)
Mouse IgG, F(ab')$_2$-FITC	Goat	FITC	IF (1:200)	Santa Cruz (#sc-3699)
Mouse IgG, F(ab')$_2$-TRITC	Goat	TRITC	IF (1:200)	Santa Cruz (#sc-3796)
Mouse IgG-HRP	Goat	HRP	WB (1:2000)	Santa Cruz (#sc-2005)

Phospho-Akt (Ser473) (D9E)	Rabbit	-	WB (1:1000)	Cell Signaling (#4060)
Phospho-GSK-3α/β (Ser21/9)	Rabbit	-	WB (1:2000)	Cell Signaling (#9331)
Rabbit IgG (H+L)-Biotin	Goat	Biotin	IHC (1:250)	Dianova (#111-065-144)
Rabbit IgG-HRP	Goat	HRP	WB (1:2000)	Santa Cruz (#sc-2004)
Vimentin (D21H3)	Rabbit	-	WB (1:1000)	Cell Signaling (#5741)
β-Actin (AC-15)	Mouse	-	WB (1:10000)	Sigma-Aldrich (#A5441)

2.1.5 Oligonucleotides and plasmid constructs

Table 5 depicts all oligonucleotides, Table 6 all plasmids used for this study.

Table 5: Oligonucleotides

Name	Description	Direction	Sequence (5´ - 3´)
mmCCL8	Chemokine (C-C motif) ligand 8	Forward	ATGTACTAAAGCTGAAGATCCC
		Reverse	GCACTGGATATTGTTGATTCTC
mmCD3E	CD3e Molecule, Epsilon (CD3-TCR Complex)	Forward	TACTTGTACCTGAAAGCTCG
		Reverse	CTTGCTCCAGTAATAAATGACC
mmCDH1	Cadherin 1 (E-Cadherin)	Forward	GAAATCACATCTTATACCGCTC
		Reverse	CGTCTTCTCTGTCCATCTC
mmCSF1	Colony Stimulating Factor 1	Forward	GCGCTTTAAAGACAACACCC
		Reverse	ATGGAAAGTTCGGACACAGG
mmCSF1R	Colony Stimulating Factor 1 Receptor	Forward	CACCATCCACTTGTATGTC
		Reverse	CTCAACCACTGTCACCTC
mmGAPDH	Glyceraldehyde-3-Phosphate Dehydrogenase	Forward	CATCTTGGGCTACACTGAG
		Reverse	CTGTAGCCGTATTCATTGTC

mmGFAP	Glial Fibrillary Acidic Protein	Forward	AACCTGGCTGCGTATAGAC
		Reverse	CCAGCGATTCAACCTTTCTC
mmIBA1	Ionized calcium binding adaptor molecule 1	Forward	TTCAGCTACTCTGACTTTCTC
		Reverse	GAATCATTCTCAAGATGGCAG
mmIL34	Interleukin 34	Forward	TGGCTTTGGGAAACGAGAAT
		Reverse	CCCTCATAAGGCACAGCAAT
mmKRT8	Keratin 8	Forward	ATGAACAAGGTGGAACTAGAG
		Reverse	ATCTCCTCTTCATGGATCTG
mmPD-L1	Programmed Cell Death 1 Ligand 1	Forward	CGTTTACTGCTGCATAATCAG
		Reverse	TAGTTCATGCTCAGAAGTGG
mmPGK1	Phosphoglycerate Kinase 1	Forward	TGTCCAAACTAGGAGATGTC
		Reverse	CCTTGGCAAAGTAGTTCAG
mmPU1	Hematopoietic Transcription Factor PU.1 Proviral Integration Oncogene (Spi1)	Forward	CTTACGATTCAGAGCTATACCA
		Reverse	TCAGGGAAGTTCTCAAACTC
mmTYROBP	TYRO Protein Tyrosine Kinase Binding Protein	Forward	AAACAACACATTGCTGAGAC
		Reverse	CATCTGTAATATTGCCTCTGTG
mmVIM	Vimentin	Forward	CGGCTGCGAGAGAAATTGC
		Reverse	CCACTTTCCGTTCAAGGTCAAG

Table 6: Plasmids

Plasmid	Characteristics / Genotype	Reference
pTurboGFP-N (FP512)	Mammalian GFP Expression Vector	Evrogen Inc. (Heidelberg)

2.1.6 Commercial kits

All commercial kits are listed in Table 7.

Table 7: Commercial kits

Product	Company
Amersham ECL Prime Western Blotting Detection Reagent	GE Healthcare (Freiburg)
DC (detergent compatible) protein assay	Bio-Rad (Munich)
Detection System Alkaline Phosphatase/RED Kit	Dako (Jena)
EndoFree Plasmid Maxi Kit	Qiagen (Hilden)
High Pure RNA Isolation Kit	Roche (Mannheim)
iScript cDNA synthesis Kit	Bio-Rad (Munich)
Liquid DAB+ Substrate-Chromogen System	Dako (Jena)
Nanofectin Transfection Kit	PAA (Cölbe)
ZytoChem-Plus HRP Kit	Zytomed Systems GmbH (Berlin)

2.1.7 Consumables

All consumables used in this study are listed in Table 8.

Table 8: Consumables

Product	Company
10 cm Petri dish (coated)	Nunc (Langenselbold)
10 cm Petri dish (un-coated)	Sarstedt (Nümbrecht)
12-well plates	Sarstedt (Nümbrecht)
24-well plates	Sarstedt (Nümbrecht)
384-well plates	Greiner Bio-one (Frickenhausen)
6-well plates	Nunc (Langenselbold)
96-well plates	Nunc (Langenselbold)
Amersham Protran Membrane (0.45 µm, nitrocellulose)	Sigma-Aldrich (Steinheim)
Blades Wilkinson Sword Classic	Wilkinson (Solingen)
Cell culture flasks (25, 75, 175 cm^2)	Sarstedt (Nümbrecht)

Cell scrapper 25 cm	Sarstedt (Nümbrecht)
Centrifuge tubes (15, 50 ml)	Sarstedt (Nümbrecht)
Combitips advanced (0.1 ml)	Eppendorf (Hamburg)
Cover glasses (18 x 18 mm)	Carl Roth (Karlsruhe)
Cyanoacrylate glue	Renfert (Hilzingen)
Disposable Pestle Tissue Homogenizer (1.5 ml)	VWR (Ismaning)
Dubois decapitation scissors	Hermle (Tuttlingen)
Embedding cassettes	NeoLab (Heidelberg)
E-Plate 16	Roche (Mannheim)
ES-Compresses	Hartmann (Heidenheim)
Glass Pasteur Pipettes (150, 230 mm)	Brand (Wertheim)
Hamilton microliter syringe (10 µl)	Sigma-Aldrich (Steinheim)
Metallic spacer (3.8 mm diameter)	Kig GmbG (Kirkel)
Microscope slides (25 x 75 x 1 mm)	Carl Roth (Karlsruhe)
Millicell cell culture inserts (12 mm, 0.45 µm pore size)	Merck Millipore (Berlin)
Noyes eye scissors	Hermle (Tuttlingen)
Pipette tips (10 / 100 / 1000 µl)	Sarstedt (Nümbrecht)
Polycarbonate membrane (10 µm pore size)	Pieper Filter (Bad Zwischenahn)
Polycarbonate membrane insert (6-Well, 0.4 µm pore size)	BD Falcon (Heidelberg)
Polystrene round-bottom FACS tubes (5 ml)	Falcon (Amsterdam)
Reaction tubes (0.2, 0.5, 1.5, 2 ml)	Sarstedt (Nümbrecht)
Rotilabo Blotting papers (1.5 mm)	Carl Roth (Karlsruhe)
Sealing-Folie (AMPLIseal, transparent)	Greiner Bio-one (Frickenhausen)
Semkin standard forceps	Hermle (Tuttlingen)
Seralon polyamide suture (DR-009, USP 7/0, EP 0.5)	Serag-Wiessner GmbH (Naila)
Serological pipettes (5, 10, 25 ml)	Sarstedt (Nümbrecht)
Sterican needle Gr. 17, 18, 20	B. Braun (Melsungen)
Sterile scalpel	Hermle (Tuttlingen)
Steritop-Filter (0.22 µm pore size)	Merck Millipore (Darmstadt)
Syringe with Luer-Lok connection fitting (1, 5, 10 ml)	B. Braun (Melsungen)
Tissue forceps	Hermle (Tuttlingen)

| Wecker spatula | Hermle (Tuttlingen) |
| Whatman qualitative round filter paper (90 mm diameter) | Sigma-Aldrich (Steinheim) |

2.1.8 Equipment and software

All lab equipment and software used for the experiments is listed in Table 9.

Table 9: Equipment and software

Product	Company
ABI 7900HT Fast Real-Time PCR System	Applied Biosystems (Weiterstadt)
Accu-jet pro pipette controller	Brand (Wertheim)
Autoclave Varioklav	Thermo Scientific (Bonn)
Cell sorter BD FACSAria II	BD Biosciences (Heidelberg)
Centrifuge 1-15K	Sigma-Aldrich (Steinheim)
Centrifuge 5415 C	Eppendorf (Hamburg)
Centrifuge Universal 30RF	Hettich (Tuttlingen)
CO_2 incubator CB150	Binder (Tuttlingen)
Confocal laser scanning microscope LSM 510	Carl Zeiss (Göttingen)
GraphPad Prism Software (version 6 for Windows)	GraphPad Software (La Jolla, CA)
Heated operating table	Medax (Neumünster)
ImageQuant LAS-4000	Fujifilm (Freiburg)
Microliter pipettes (10, 100, 1000 µl)	Eppendorf (Hamburg)
MilliQ water purification system	Millipore (Schwalbach)
Mirax Desk Slides Scanner System	Carl Zeiss (Göttingen)
Mirax Viewer Software (version 1.12 for Windows)	Carl Zeiss (Göttingen)
NanoDrop ND-1000 spectrophotometer	Peqlab (Erlangen)
Neubauer Improved cell counting chamber	Blaubrand (Wertheim)
Olympus CX40 microscope	Olympus (Hamburg)
Orbital shaker incubator ES-20	Grant Bio / Omnilab (Munich)
Oven Heraeus UT6200	Thermo Fisher Scientific (Dreieich)
PerlPrimer Software (version 1.1.21 for Windows)	SourceForge.net

pH meter 761 Calimatic	Knick Elektronische Messgeräte (Berlin)
Photometer Infinite F50	Tecan (Crailsheim)
Roller Shaker RS-TR05	Phoenix Intrument (Garbsen)
Safety microbiological workbench (UVF 6.12S)	BDK (Sonnenbühl-Genkingen)
SDS Software (version 2.4 for Windows)	Applied Biosystems (Weiterstadt)
Sliding microtome HM 400 R	Microm (Walldorf)
Stereotaxic Drill-Jacobs Chuck (18000 rpm)	Kopf Instruments (Düsseldorf)
Thermal cycler DNA Engine	Bio-Rad (Munich)
Thermomixer 5436	Eppendorf (Hamburg)
Ultra-Precise Small Animal Stereotaxic Instrument (Model 963)	Kopf Instruments (Düsseldorf)
Vibratome Leica VT1000S	Leica (Wetzlar)
Vortex shaker Genius 3	IKA Lab equipment (Staufen)
Water bath	Köttermann (Hänigsen)
xCELLigence RTCA DP Analyzer	OMNI Life Science (Bremen)
Zeiss Axio Observer Z1 Inverted Fluorescence Microscope	Carl Zeiss (Jena)

2.2   Methods

2.2.1 Cell culture methods

2.2.1.1   Maintenance of tumor cell lines

Tumor cells were grown at 37°C and 5% CO_2 in a humidified incubator. To passage the cells, they were washed once with PBS (Sigma-Aldrich), detached by incubation with 1 ml Trypsin-EDTA (1X) (Sigma-Aldrich) for up to 10 min and split in a ratio of 1:5-1:10. All cell lines were routinely tested for contamination with mycoplasma. To maintain cells over a longer period of time, they were frozen in DMSO (Sigma-Aldrich) with 90% FCS (PAN Biotech) and stored in liquid nitrogen.

2.2.1.2   Stable transfection with a GFP Vector

In order to evaluate the invasiveness of tumor cells in our organotypic brain slice cocultures, tumor cells were stably transfected with a GFP vector (see Figure 12). Briefly, $2x10^6$ cells were seeded in T75 cell culture flasks and allowed to adhere overnight. Stable transfection with the mammalian expression vector encoding green fluorescence protein (pTurboGFP-N, FP512, Evrogen) was performed with the Nanofectin Kit (PAA) according to the manufacturer's instructions. This method is based on nanoparticles which contain DNA-binding positively charged polymers and mediate transfer of the DNA into the target cells. Each cell line was transfected with 16 μg plasmid in a DNA/Nanofectin ratio of 3. Cells were maintained in cell culture medium supplemented with G418 (Roche) to assure selection of stable transformants for at least three weeks. To obtain a homogenous cell population, GFP positive cells were sorted using a cell sorter (BD FACSAria II, BD Biosciences).
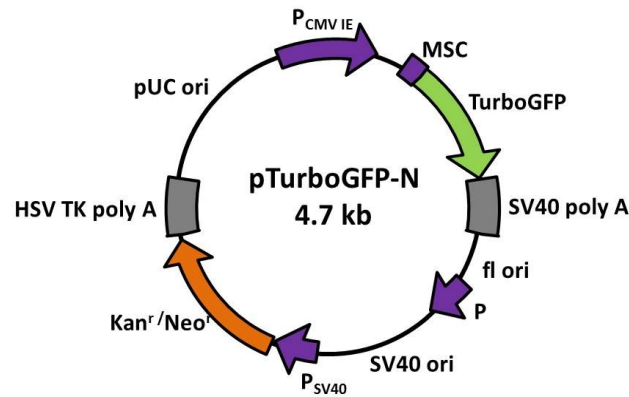
Figure 12: Structure of the pTurboGFP-N vector

pTurboGFP-N is a mammalian expression vector encoding the green fluorescent protein TurboGFP. The CMV promoter provides strong, constitutive expression of TurboGFP in eukaryotic cells. SV40 early promoter (P$_{SV40}$) provides neomycin resistance gene (Neo^r) expression to select stably transfected eukaryotic cells using G418.

2.2.1.3   Primary cell isolation and culture

2.2.1.3.1 Primary cultures of microglia and astrocytes

This method was performed as describe previously (Hanisch et al., 2004). Briefly, after dissection and careful removal of the meninges and blood vessels from whole brains of newborn mice (postnatal day 0, P0), both hemispheres were dissociated mechanically in 2.5% trypsin (Merck Millipore) at 37°C for 10 min. DNAse I (0.4 mg/ml, CellSystems) was added to stop the enzymatic reaction for a further 5 min, followed by centrifugation at 4°C for 10 min. Cells were resuspended and further cultivated in DMEM medium supplemented with 10% FCS, 100 U/ml penicillin and 100 µg/ml streptomycin (Merck Millipore) in T75 flasks coated with poly-L-lysine (200 µg/ml, Sigma-Aldrich) at 37°C and 5% CO_2 in a humidified atmosphere. The culture medium was changed every 48 h. After 10 to 14 days, microglia were harvested by shaking them off the astrocytic monolayer with an orbital shaker incubator (Grant Bio). The purity of microglia was assessed by using immunohistochemistry staining for the ionized calcium binding adaptor molecule 1 (IBA1) and Griffonia simplicifolia isolectin B4 (ILB4) as described before (Hassan, Rifat, Campbell, McCawley, & Douglas, 1991).

To obtain pure primary cultures of astrocytes, glial cells were treated with clodronate (200 µg/ml, Calbiochem) for 48 h to deplete microglial cells. Astrocytic cells were cultivated in DMEM medium supplemented with 10% FCS, 100 U/ml penicillin and 100 µg/ml streptomycin at 37°C and 5% CO2. The purity of astrocytes was assessed by using immunohistochemistry staining for the Glial Fibrillary Acidic Protein (GFAP).

2.2.1.3.2 Primary cultures of monocyte-derived macrophages (MDM)

This method was performed as described before (Reiling et al., 2001) with slight modifications. Briefly, after sacrificing 10 to 12 week-old BALB/c mice by CO_2 asphyxiation, the skin was disinfected with 70% ethanol, and an incision at the top of each hind leg was performed. The skin was peeled off down over the foot and the exposed muscles were removed with sterile scissors and forceps (Hermle). In order to take out the intact femur, I cut distally from the knee joint and carefully pulled the femoral head out of the hip joint. Femurs were placed in a petri dish, sprayed with 70% ethanol and gently cleaned with compresses (Hartmann) to remove remaining tissue. After cutting the femur near each joint under sterile conditions, the bone marrow was flushed with Pluznik Medium into a coated petri dish (Nunc) by inserting a fine needle (Gr. 17, B. Braun) into the femoral bone cavity. Fibroblasts, osteoclasts, and other cells present in the bone marrow adhere to the bottom of coated petri dishes, whereas macrophage progenitors stay as suspension cells. Therefore, after 24 h incubation at 37°C and 5% CO_2, the supernatant was collected and centrifuged 10 min at 1200 rpm and room temperature. The cell pellet containing MDM was resuspended in 40 ml Pluznik medium and seeded in four un-coated petri dishes (Sarstedt). Cells were allowed to adhere and differentiate to mature monocyte-derived macrophages during the following six days at 37°C and 5% CO_2. Medium change was performed after 72 h. For further experiments, MDM were harvested on day seven by the addition of 1 ml Accutase (Sigma-Aldrich) and seeded in MDM-culture medium.

Pluznik Medium:
- DMEM
- 10% FCS
- 5% NHS
- 30% L929 conditioned medium
- 0.01 mM Na-pyruvat
- 0.05 mM β-Mercaptoethanol
- 100 U/ml penicillin
- 100 mg/ml streptomycin

MDM-culture medium:
- DMEM
- 10% FCS
- 15% L929 conditioned medium

The culture medium was supplemented with L929 conditioned medium, which contains macrophage colony-stimulating factor (M-CSF), a growth factor required for the differentiation of monocytes into macrophages (Stanley, 1985). The CSF1 containing conditioned medium was obtained from the L929 murine fibroblast cell line as described before (Pfannes, Muller, Korner, Bessler, & Hoffmann, 2001). Briefly, 10×10^6 L929 cells were seeded in a T175 with 100 ml DMEM and incubated for seven days at 37°C and 5% CO_2. The conditioned medium was then collected, centrifuged at 2000 g, filtered with a Steritop-Filter (0.22 µm pore size, Merck Millipore) and kept at -20°C.

2.2.1.4   Assessment of cell vitality and proliferation

2.2.1.4.1 MTT assay

The MTT assay (Mosmann, 1983) is a colorimetric assay that measures the number of viable cells by assessing their metabolic activity. NAD(P)H-dependent cellular oxidoreductase enzymes in the endoplasmic reticulum reduce the tetrazolium dye MTT 3-(4,5-dimethylthiazol-2-yl)-2,5-diphenyltetrazolium bromide (MTT, Sigma-Aldrich) to its insoluble formazan, which has a purple color. This process can only be carried out by living cells and is therefore impaired in apoptotic or necrotic cells with an altered cell metabolism. For the MTT assay, $5x10^4$ microglia, MDM, astrocytes, $4x10^4$ MCF-7, SK-BR-3, 410.4, $2x10^4$ 4T1, or $1x10^4$ MDA-MB-231 per well were seeded in a 24-well-plate and incubated with the BKM120 inhibitor at the indicated concentrations for 72 h. Subsequently, the cells were incubated with 500 µl culture medium + 10% MTT (stock solution 5 mg/ml) for 4 h at 37°C and 5% CO_2. The medium was aspired and cells lysed in 500 µl lysis buffer for 10 min at room temperature. The extinction at 540 nm was measured in triplicate in a photometer (Infinite F50, Tecan) and related to the extinction values of the untreated control.

Lysis Buffer:
- 95% isopropanol
- 5% formic acid

2.2.1.4.2 xCELLigence

The xCELLigence RTCA DP Analyzer (OMNI Life Science) is a non-invasive electrical impedance monitoring method that quantifies cell proliferation in a label-free, real-time manner. In this assay, the cells are seeded in a special multi-well plate (E-Plate 16, Roche) with gold microelectrodes on the

bottom surface. When submersed in an electrically conductive solution (such as standard culture medium), the presence of adherent cells at the electrode-solution interface impedes the electron flow (see Figure 13). The impedance of electron flow caused by adherent cells can be measured with the Cell Index (CI), where CI = (impedance at time point n – impedance in the absence of cells) / nominal impedance value. For my experiments I seeded $2.5x10^3$ 4T1, $5x10^3$ 410.4 and MDM and $2.5x10^4$ microglia and astrocytes per well and stimulated them with the indicated concentrations of BKM120 for 48 h at 37°C.
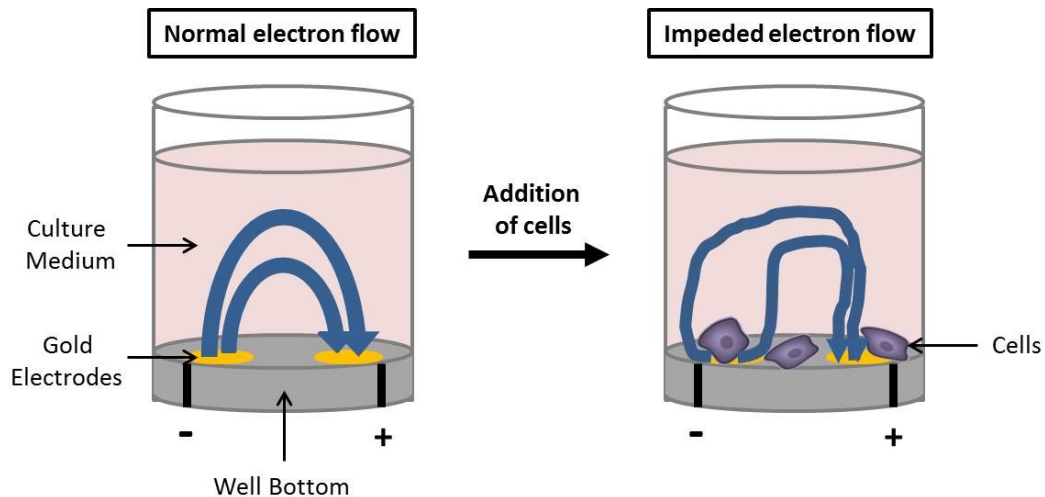
Figure 13: Overview of the xCELLigence RTCA DP Analyzer
A side view of a single well is shown, before and after cells have been added. In the absence of cells electric current flows freely through culture medium, completing the circuit between the electrodes. As cells adhere to and proliferate on the electrodes current flow is impeded, providing an extremely sensitive readout of cell number, cell size/morphology, and cell-substrate attachment quality.

2.2.1.5   Cell invasion assay in a modified Boyden chamber

The Boyden chamber is a useful tool to study cell invasion. In my experiments I used a modified Boyden chamber assay (Hagemann et al., 2004) in which $1x10^5$ tumor cells (4T1 or 410.4) were seeded in the upper wells of the chamber. The lower wells were filled with culture medium and the chamber was then sealed with a polycarbonate membrane (10 µm pore diameter, Pieper Filter) which was coated with ECM (R&D Systems) diluted 1:4 in cell culture medium without FCS. To investigate whether immune cells would affect the invasion capacity of tumor cells, $1.5x10^5$ immune cells (microglia, MDM or astrocytes) were added in a cell culture insert (Merck Millipore) in the upper chamber and treated with or without the BKM120 inhibitor (see Figure 14). After incubating the chamber for 96 h at 37°C and 5% CO_2, the content of the lower chamber with floating as well as adherent cells was collected and pelleted by centrifugation. The cell pellet was resuspended in 200 µl

of PBS and the number of invasive tumor cells which had successfully degraded the ECM gel and invaded through the membrane into the lower wells was determined with a Neubauer Counting Chamber (Blaubrand) and related to the control.
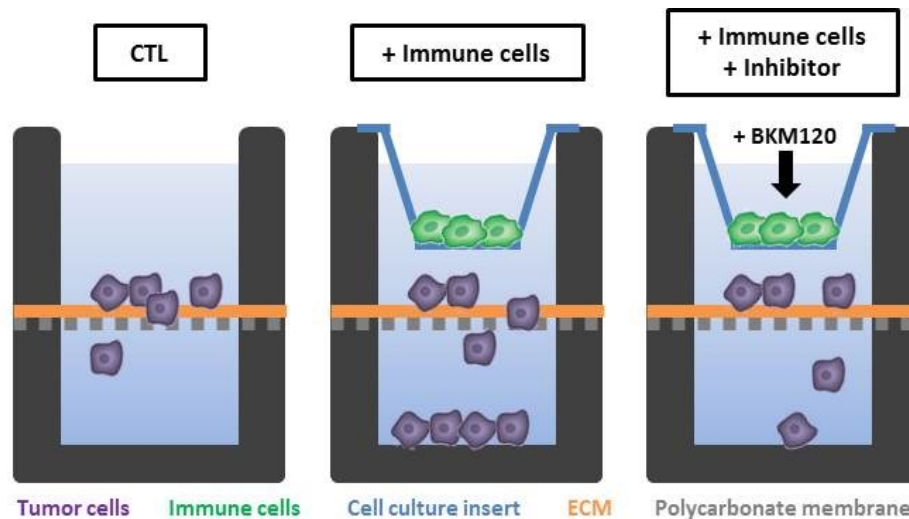
Figure 14: Schematic representation of the modified Boyden chamber assay
The tumor cells are seeded in the upper wells of the chamber and cocultured with immune cells in transwell inserts. Immune cells are treated with or without BKM120. The invasion of the tumor cells alone or in coculture with the immune cells can be assessed after 96 h and related to the unstimulated control (CTL).

2.2.1.6   Organotypic brain slice coculture system

This method (Pukrop et al., 2010) is an adaptation of a previously published organotypic hippocampal brain slice approach (De Simoni & Yu, 2006; Fuller & Dailey, 2007; Kreutz, Koch, Ghadban, Korf, & Dehghani, 2007; Stoppini, Buchs, & Muller, 1991) which was modified to our own needs. Briefly, a matrigel plug containing the tumor cells is cocultured with a living mouse brain slice for 96 h. This method allows us to investigate the invasion of the tumor cells and their interactions with the immune cells present in the brain slice. This technique is illustrated in Figure 15.

Young mice (postnatal day 6-8, P6-P8) were decapitated and the brain was rapidly removed from the skull under sterile conditions and transferred to ice-cold dissection medium (B). After removal of the frontal pole and the cerebellum (C), the brain was fixed in a platform using agarose blocks (D) and horizontal brain sections of 350 μm thickness were prepared using a vibratome (VT1200S, Leica) (A, E-F). Four to five whole brain slices can be collected from a single mouse brain, depending on the age of the mouse (G). Brain slices were placed on a 0.4 μm polycarbonate membrane of a transwell membrane insert (BD Falcon) in 6-well plates with incubation medium and cultured overnight at 37°C and 5% CO_2 in a humidified atmosphere.

On the next day, 1×10^5 tumor cells were embedded in 20 µl gel matrix, consisting of 30% cell culture medium and 70% ECM (R&D Systems). Each cell plug was then placed into a sterile metallic spacer (Kig GmbG) directly adjacent to the cortical region of the organotypic brain slice (H). After 1.5 h, the spacer was removed and the tumor cell plug was placed just adjacent to the organotypic brain slice. The brain slice coculture was cultivated for 72 to 96 h at 37°C and 5% CO_2 in a humidified atmosphere (I). Medium change was performed after 48 h. Cocultures were then analyzed by immunoflourescence staining and confocal microscopy (J).

Dissection medium:

- MEM
- 0.2 mM glutamine
- 100 U/ml penicillin
- 100 mg/ml streptomycin
- 4.5 mg/ml glucose

Incubation medium:

- 50% MEM
- 25% HBSS
- 25% NHS
- 0.2 mM glutamine
- 100 U/ml penicillin
- 100 mg/ml streptomycin
- 4.5 mg/ml glucose

Figure 15: Overview of the organotypic brain slice coculture system

Brain slices were obtained from P6-8 mice using a vibratome VT1200S (Leica) **(A)**. The brain was isolated from the skull **(B)** and the frontal pole and the cerebellum were removed **(C)**. The brain was fixed in a platform using agarose blocks **(D)** and sliced using a vibratome **(E-F)**. Approximately 4 to 5 horizontal brain sections of 350 μm thickness were obtained from each mouse **(G)**. Brain slices were placed on a cell culture insert for 16 h, followed by a cell plug setting into a 3.8 mm diameter spacer adjacent to the cortical region of the brain slice **(H)**. The brain slice coculture was cultivated for 72 to 96 h **(I)** and analyzed by immunoflourescence staining and confocal microscopy **(J)**.

2.2.2 Stereotactical intracortical injection

For the establishment of our brain colonization in vivo models, tumor cells were stereotactically injected in the cortical region of syngeneic mice. This process is described in Figure 16. Briefly, 10 to 12-week-old BALB/c mice were put under anesthetic by intraperitoneal injection of the anesthetic solution (10 μl/g KW) (A-B). After making a small incision in the middle of the head, the periosteum

of the right skull cup was carefully removed with the help of a sterile scalpel (C). The mouse was then placed into a stereotaxic frame (David Kopf Instruments) and fixed with ear bars so that the skull remained horizontal to the surface (D). Using a tooth-technical drill (David Kopf Instruments) a drill hole of approx. 1 mm of diameter was stereotactically bored 1 mm right rostral and 2 mm lateral of the bregma (E). During this process, the dura mater is neither opened nor damaged.

Next, the cells were trypsinized and counted in a Neubauer Chamber. The desired number of cells were centrifuged and resuspended in 3 µl gel matrix, consisting of 1 µl cell culture medium and 2 µl ECM gel (Sigma). This cell suspension was mixed and drawn up in a 10 µl Hamilton syringe (Sigma-Aldrich) with beveled cannula. The syringe was placed in the holder of the frame vertically to the skull hole and with the open end of the cannula to the left. The cannula was introduced 3.5 mm deep in the brain through the skull hole and pulled back 0.5 mm in order to form a small cavity for the cell content. In this position, the cells are injected directly into the cortical region of the brain. The injection takes place during the first minute, and the needle remains in the same position two minutes more to assure the establishment of the cells in the brain parenchyma (F). Afterwards the needle was removed and the lesion was simultaneously washed with NaCl.

Finally, the skin was stitched up with a polyamide suture (Seralon, Serag-Wiessner GmbH) (G). Painkillers were injected subcutaneously (5 µg/g KW) (H) and the mouse was laid down on a thermal plate (Medax) until it came out of the anesthetic (I).

Anesthetic solution:

- Ketamin   100 mg/kg
- Domitor   0.25 mg/kg
- NaCl   ad 10ml

Painkillers:

- Rimadyl   5 mg/kg
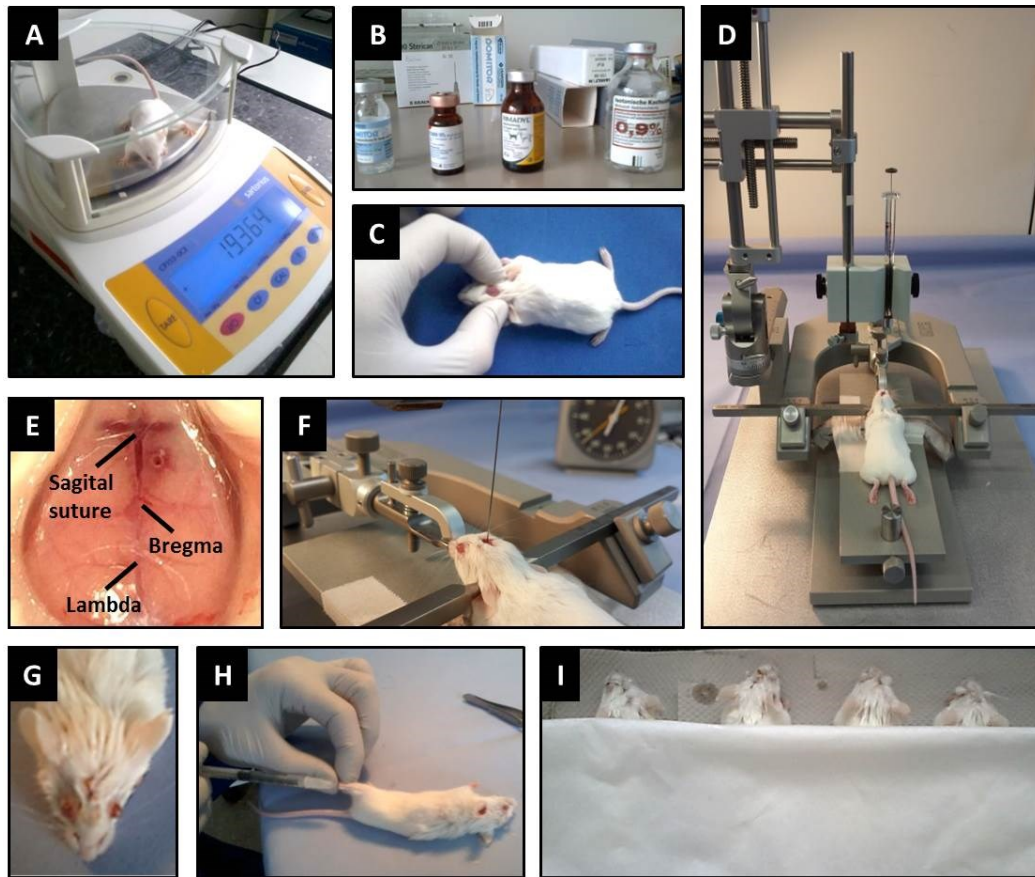
Figure 16: Stereotactical intracortical injection of tumor cells

10 to 12-week-old BALB/c mice are weighted **(A)** and put under anesthetic by intraperitoneal injection **(B)**. After making a small incision in the middle of the head, the periosteum of the right skull cup is removed carefully with the help of a sterile scalpel **(C)**. The mouse is then placed into a stereotaxic frame **(D)** and a drill hole of approx. 1 mm of diameter is stereotactically bored 1 mm right rostral and 2 mm lateral of the bregma **(E)**. The cell suspension (3 µl) is stereotactically injected into the cortex using a 10 µl Hamilton syringe **(F)**. Afterwards the skin is stitched up **(G)** and painkillers are administered subcutaneously **(H)**. The mice are allowed to recover on a thermal plate **(I)**.

2.2.3 Protein biochemistry

2.2.3.1   Protein isolation

To generate lysates from whole cells, 1×10^6 cells per well were seeded in 6-well plates and allowed to adhere overnight at 37°C and 5% CO_2. After that, cells were washed once with PBS and then detached from the well with a cell scraper on ice in 50-100 µl RIPA lysis buffer. Protease inhibitors as well as phosphatase inhibitors (Roche) were added fresh to the lysis buffer. Samples used in the second part of this thesis were incubated with the indicated concentrations of the BKM120 inhibitor for 2 h and then harvested. Lysates were then centrifuged for 10 min at 20000 g and 4°C to pellet cell debris and DNA. Supernatants were collected and stored at -20°C.

RIPA lysis buffer:

- 50 mM Tris (pH 7.2)
- 150 mM NaCl
- 0.1% SDS
- 0.5% Na-deoxycholate
- 1% Triton X-100

2.2.3.2   Protein quantification by Lowry assay

The DC (detergent compatible) protein assay (Bio-Rad) is a colorimetric method for determining the total level of protein in a solution. It is similar to the well-documented Lowry assay (Lowry, Rosebrough, Farr, & Randall, 1951), but modified to save time. The Lowry assay is based on the formation of complexes between copper (II) ions and peptide bonds of the test sample in alkaline medium. They are subsequently reduced to monovalent cations and can react with the Folin-Ciocalteu reagent which results in a blue color (Peterson, 1979). The total protein concentration is exhibited by a color change of the sample solution in proportion to the protein concentration, which can then be measured in a photometer (Tecan) at 750 nm in relation to a BSA standard curve (Gibco). For my purposes, samples were diluted in 10 µl ddH$_2$O (1:5 for immune cells and 1:10 for tumor cells) and the assay was carried out according to the manufacturer's instructions.

2.2.3.3   SDS-PAGE

In order to analyze the protein expression in whole cell lysates by Western Blotting (see 2.2.3.4), proteins were first separated according to their molecular weight by discontinuous SDS polyacrylamide gel electrophoresis (SDS-PAGE) (Laemmli, 1970) consisting of two separate gels cast at different pH values. The resolving gel (10%) was prepared and after its polymerization the stacking gel (5%) was layered on top. Protein samples (10-20 µg) were mixed with 4x Laemmli loading buffer (Carl Roth) and heated for 5 min at 95°C. The loading buffer contains 2-mercaptoethanol which reduces the protein disulfide bonds. Additionally, this buffer also comprises SDS that quantitatively binds to proteins, thereby applying a negative charge in proportion to their mass; thus, the mobility of the proteins inside the resolving gel during the electrophoresis is solely influenced by their molecular weight. The samples were loaded onto the gel and focused in the stacking gel for 30 min at 90 V. Subsequently, proteins were resolved for around 90 min at 130 V. For determination of the protein size, a protein standard (Bio-Rad) was applied.

Stacking gel (5%):

- 1.5 M Tris + 2% SDS (pH 6.8)   630 µl
- Acrylamide/Bisacrylamide (30%)   830 µl
- APS (10% w/v)   50 µl
- TEMED   5 µl
- H$_2$O bidest.   3.45 ml

Resolving gel (10%):

- 1.5 M Tris + 2% SDS (pH 8.8)   5 ml
- Acrylamide/Bisacrylamide (30%)   6.7 ml
- APS 10% (w/v)   200 µl
- TEMED   20 µl
- H$_2$O bidest.   7.9 ml

Electrophoresis buffer (1x):

- 25 mM Tris   3 g
- 192 mM Glycine   14.4 g
- SDS 0.1% (w/v)   1 g
- H$_2$O bidest.   ad 1 l

2.2.3.4   Western Blot

After electrophoresis, proteins were blotted onto a nitrocellulose membrane (Sigma-Aldrich) where they can then be detected by specific antibodies. The resolving gel was put on top of the nitrocellulose membrane which had been equilibrated in transfer buffer. The blot sandwich was covered by three sheets of Whatman blotting paper (Carl Roth) on each side. Blotting was performed using a semi-dry transfer system at 15 V for 90 min at room temperature. Afterwards the membrane was routinely stained with 0.5% Ponceau S (Sigma-Aldrich) as loading control and to confirm transfer efficiency. For protein detection, the membrane was blocked for 1 h in 5% MMP (Bio-Rad) or 5% BSA (Carl Roth) in TBST at room temperature to saturate unspecific binding sites and subsequently incubated with the specific primary antibodies (see 2.1.4) in the corresponding blocking solution (MMP or BSA) overnight at 4°C. After three wash steps with TBST for 5 min each, the membrane was incubated with secondary antibodies conjugated to horseradish peroxidase (HRP) (see 2.1.4) in the corresponding blocking solution for 1 h at room temperature and rinsed again three times in TBST for 5 min each.

TBST (1x):

- 20 mM Tris   2.4 g
- 137 mM NaCl   8 g
- H$_2$O bidest.   ad 1 l (adjust to pH 7.6)
- 0.1% (v/v) Tween-20   1 ml

Transfer buffer (1x):

- 25 mM Tris   3 g
- 192 mM glycine   14.4 g
- 20% (v/v) methanol   200 ml
- H$_2$O bidest.   ad 1 l (adjust to pH 8.3)

HRP is an enzyme that catalyzes the oxidation of luminol, thereby producing a chemoluminescence signal which can be detected in a biomolecular imager. Therefore, signals were detected using the ECLPrime detection reagent (GE Healthcare) in the LAS-4000 Imager (Fujifilm).

2.2.4 Gene expression analysis

2.2.4.1   Isolation of total RNA from murine tissue samples

The isolation of total RNA from murine brain metastases samples was carried out with the TRIzol (Invitrogen) reagent. First, small tissue samples were homogenized in 1 ml TRIzol, before 200 µl chloroform (Carl Roth) were added, mixed and incubated for 5 min at room temperature. Centrifugation at 20000 g for 15 min at 4°C yields three phases with the RNA being present in the colorless upper aqueous phase. The upper phase was transferred to a new tube and 500 µl isopropanol were added. For the precipitation of the RNA, the sample was incubated for 10 min at room temperature followed by centrifugation at 13000 g and 4°C for 30 min. The pellet was washed in 1 ml 70% ethanol at 20000 g and 4°C for 5 min and afterwards air dried for 5-10 min. To remove contaminating DNA, the pellet was resuspended in 50 µl DNA digestion mix and incubated for 20 min at 37°C. To purify the remaining RNA, 150 µl nuclease-free water (Invitrogen) and 200 µl phenol/chloroform/isoamyl alcohol (Carl Roth) were added. The sample was vortexed for 30 sec and subsequently centrifuged for 2 min at 20000 g and 4°C. The upper aqueous phase which contains the RNA was transferred to a new tube. 20 µl sodium acetate (3 M, pH 4.8) (Carl Roth) and 200 µl isopropanol were added and the sample was incubated for 30 min at 4°C. Afterwards, samples were centrifuged for 30 min at 20000 g and 4°C to precipitate the RNA. The pellet was washed twice in 1

ml 70% ethanol for 5 min each at 20000 g and 4°C and was air dried afterwards. The RNA was resuspended in 20 µl nuclease-free water and the concentration and purity determined at the NanoDrop ND-1000 spectrophotometer (Peqlab).

DNA digestion mix:

- DNase I (10 U/µl, Roche)   1 µl
- RNase OUT (40 U/µl, Invitrogen)   0.5 µl
- DNase I incubation buffer (10x, Roche)   5 µl
- Nuclease-free water   ad 50 µl

2.2.4.2   Isolation of mRNA from eukaryotic cells

The isolation of mRNA from cultured cells was carried out with the spin column-based High Pure RNA isolation kit (Roche) according to the manufacturer's instructions. Briefly, $1x10^6$ cells were seeded in 6-well plates and allowed to adhere overnight at 37°C and 5% CO_2. Subsequently, cells were washed once with PBS and lysed in 400 µl of the lysis/binding buffer supplemented with 200 µl PBS. While RNases are inactivated, the buffer further contains Triton X-100 which mediates permeabilization of the cell membrane and guanidine hydrochloride which induces protein denaturation. The samples were vortexed for 15 sec to help cell lysis and subsequently applied onto a spin column consisting of glass fiber fleece. Columns were centrifuged at 8000 g for 15 sec which leads to the binding of the nucleic acids to the column, while proteins, salts and cellular debris are eluted. Contaminating DNA was digested directly on the column by incubation with DNase I for 15 min at room temperature. The remaining RNA was washed three times, before 50 µl nuclease-free water were added to the column for elution of the isolated RNA. Concentration and purity were measured with the NanoDrop ND-1000 spectrophotometer (Peqlab).

2.2.4.3   Reverse transcription

For the analysis of gene expression changes by qRT-PCR, the isolated RNA was transcribed into complementary DNA (cDNA) using the iScript cDNA synthesis kit (Bio-Rad). The reaction is carried out by the reverse transcriptase, an RNA-dependent DNA polymerase. The enzyme binds to the random hexamer oligonucleotides and oligo (dT) primers which are contained in the kit. The latter are complementary to the poly-A tail of eukaryotic mRNA allowing reverse transcription of all mRNA in the sample. The reaction setup was prepared as follows:

5x iScript reaction mix	4 µl
iScript reverse transcriptase	1 µl
RNA template (1 µg)	x µl
Nuclease-free water	y µl
Total volume	20 µl

The prepared reaction mix was incubated in a thermal cycler (DNA Engine, Bio-Rad) for 5 min at 25°C, followed by 30 min at 42°C, and 5 min at 85°C. Each sample was diluted in a ratio of 1:5 with nuclease-free water and kept at -20°C.

2.2.4.4   Quantitative real-time PCR (qRT-PCR)

Changes in gene expression were analyzed by quantitative real-time PCR (qRT-PCR) using SYBR green detection. The basic principle of this method is a conventional PCR reaction. After activation of the hot-start polymerase, the gene of interest is amplified during 40 cycles of DNA denaturation, followed by annealing of gene-specific primers and extension of the product. Every cycle is completed by measurement of the fluorescence of SYBR green (Bio-Rad) which is an intercalating dye that emits a fluorescent signal when bound to double-stranded DNA. Since the copy number of the gene of interest is amplified with every cycle, the fluorescence increases proportionally and can be plotted versus the cycle number. The number of the cycle in which the fluorescence reaches the threshold level is called Ct value and was normalized on the expression of two house-keeping genes (=ΔCt value).

The primers used in this study were designed as described in 2.2.4.4.1 and are listed in Table 5. Murine samples were normalized on *Gapdh* and *Pgk1* expression. For each gene 8 µl from the prepared PCR reaction mix were pipetted into a 384-well plate (Greiner Bio-One) in triplicates. To each well 2 µl cDNA (10ng) diluted in nuclease-free water were added. The plate was sealed, spun down (5 min, 750 g) and RT-PCR was carried out according to the following protocol in the Taqman ABI PRISM 7900 HT detection system (Applied Biosystems).

Standard qRT-PCR program:

- Activation of taq-polymerase:	95°C	12 min	
- Denaturation:	95°C	15 sec	40 cycles
- Annealing and elongation:	60°C	1 min	
- Melting curve analysis:	95°C	15 sec	
	60-95°C	2°C/min	

PCR reaction mix:

- SYBR green master mix   5.6 µl
- fw-primer (10 µM)   0.3 µl
- rv-primer (10 µM)   0.3 µl
- Nuclease-free water   1.8 µl

The qRT-PCR was analyzed with the SDS software (version 2.4, Applied Biosystems) and ΔCt values were plotted with the GraphPad Prism software (version 6, GraphPad Software).

2.2.4.4.1 Establishment of primers for qRT-PCR reactions

Primer pairs for qRT-PCR analyses were designed with the PerlPrimer software (version 1.1.21, SourgeGorge.net) (Marshall, 2004) and then tested for their efficiency. Since analysis of relative gene expression by the ΔΔCt-method assumes an amplification efficiency of 100%, comparable primer efficiencies are important. A primer efficiency of 100% means that during each PCR cycle the PCR product is exactly doubled. To test primer efficiency, a cell line or tissue with high expression of the gene of interest was chosen from the BioGPS database (Wu et al., 2009) and a serial dilution series of the cDNA with known concentrations was prepared. The measured Ct values were plotted versus the amount of input cDNA and the slope of the resulting graph calculated with the SDS software. A slope of -3.33 equals a primer efficiency of 100%. Primers with an efficiency of 90-110% were chosen for further analysis.

2.2.5 Staining

2.2.5.1   Immunofluorescence (IF) staining

Organotypic brain slice cocultures (described in 2.2.1.6) were fixed with 4% PFA (Merck Millipore) overnight at 4°C. The organotypic whole brain slices and adjacent cell plugs were removed together from the cell culture inserts by cutting out the underlying membrane, followed by placing them into a 12-well plate and rinsing with PBST (0.2% Triton X-100 in PBS). Non-specific binding was blocked by adding normal goat serum (NGS, Sigma-Aldrich) (1:20 in PBST) at room temperature for 1 h. Astrocytes were stained with anti-GFAP (1:100 in PBST and 0.5% BSA) for 36 h in the dark at 4°C followed by incubation with anti-mouse-IgG-TRITC (1:200 in PBST and 0.5% BSA) for 2h in the dark at room temperature. Microglia were then stained with ILB4-Alexa Fluor 647 (1:500 in PBST and 0.5%

BSA) at room temperature in the dark for 1 h. After washing with PBST, nuclei were counterstained with DAPI (Sigma-Aldrich) (1:1000 in PBST and 0.5% BSA) for 5 min at room temperature in the dark. After washing, samples were mounted on a slide with fluorescent mounting medium (Dako), coverslipped and analyzed with a confocal laser scanning microscope (LSM 510, Zeiss).

2.2.5.2   Hematoxylin & Eosin (H&E) staining

Hematoxylin and eosin (H&E) stains have been used for at least a century and are still essential for recognizing various tissue types and the morphologic changes that form the basis of contemporary cancer diagnosis. Hematoxylin has a deep blue-purple color and stains nucleic acids. Eosin is pink and stains proteins nonspecifically. In a typical tissue, nuclei are stained blue, whereas the cytoplasm and extracellular matrix have varying degrees of pink staining (Cardiff, Miller, & Munn, 2014).

First, tissue samples were fixed with 4% PFA for 48 h at room temperature. Next, they were embedded in paraffin (Sigma-Aldrich), sectioned into 3 µm-slices with a sliding microtome (HM 400 R, Microm) and placed on a slide by a technical assistant. After that, they were dried in an oven (Heraeus, Thermo Fisher Scientific) for 30 min at 60°C. For the staining, slides were taken through short changes of xylol (Carl Roth), alcohol and water to 'hydrate' the tissue. Slides were then stained with the nuclear dye hematoxylin (Carl Roth), rinsed, and counterstained with eosin (Carl Roth). After staining, samples were rinsed again, taken back through water, alcohol, and xylene, and finally coverslipped using Dako Mounting Media. Finally, samples were examined under a bright field microscope (Olympus) and scanned with the Mirax Desk Scanner (Zeiss). For further analysis, the Mirax Viewer Software (version 1.12, Zeiss) was used.

2.2.5.3   Immunohistochemistry (IHC) staining

For the immunohistochemistry staining protocols, tissue samples were first fixed and sectioned as already described in 2.2.5.2. Next, they were taken through short changes of xylol (Carl Roth), alcohol and water to 'hydrate' the tissue. After staining, samples were rinsed, taken back through water, alcohol, and xylene, and coverslipped using Roti-Histokitt II (Carl Roth). Finally, samples were scanned using the Mirax Desk Scanner, and analyzed with the Mirax Viewer Software.

2.2.5.3.1 CK8, IBA1, CD3

After hydrating the tissue, slides were immersed in citrate buffer (pH 6) (Dako) and placed in a microwave for 32 min and 300 W. After cooling down the samples, they were washed with ddH$_2$O and subsequently with Tris buffer (pH 6) (Merck Millipore) for 10 min at room temperature. Next, the samples were incubated in a peroxidase solution (3%) (Merck Millipore) for a further 10 min at room temperature. The samples were washed again with Tris buffer and blocked for 20 min with antibody diluent (Dako). Next the slides were stained with the corresponding first antibodies (see 2.1.4) overnight at room temperature. On the next day, the samples were washed with Tris buffer and incubated with the secondary antibody (anti-rabbit-biotinylated, 1:250) 1 h at room temperature. After washing again, the slides were incubated with ExtrAvidin-Peroxidase (1:1000) (Sigma-Aldrich) for 1 h at room temperature and washed again. Next, samples were incubated in DAB-Solution (1:50) (Dako) for 10 min at room temperature in the dark. After washing again, the slides were stained with hematoxylin for 20 sec and washed briefly with warm water.

2.2.5.3.2 ECAD

After hydrating the tissue, slides were then immersed in citrate buffer (pH 6) and placed in the microwave for 32 min and 300 W. After cooling down the samples, they were washed with ddH$_2$O and stored overnight at 4°C. On the next day, samples were washed with Tris buffer (pH 6) for 10 min at room temperature and then incubated in a peroxidase solution (3%) for a further 10 min. The samples were washed again with Tris buffer and blocked for 8 min with antibody diluent. Next the slides were stained with the first antibody (see 2.1.4) 3 h at room temperature, washed with Tris buffer and incubated with the secondary antibody (anti-rabbit IgG (H+L)-Biotin, 1:250) 30 min at room temperature and subsequently with Streptavidin HRP-Conjugate (ZytoCham-Plus, Zytomed Systems) for 15 min at room temperature. After washing again, the slides were incubated with DAB-Solution (1:50) for 10 min at room temperature in the dark. The slides were then stained with hematoxylin for 2 min and washed briefly with warm water.

2.2.5.3.3 GFAP

After hydrating the tissue, slides were then immersed in citrate buffer (pH 6) and placed in the microwave for 32 min and 300 W. After cooling down the samples, they were washed with ddH$_2$O and stored overnight at 4°C. On the next day, samples were washed with Tris buffer (pH 6) for 10 min at room temperature and then incubated in a peroxidase solution (3%) for a further 10 min. The

samples were washed again with Tris buffer and blocked for 20 min with antibody diluent. Next the slides were stained with the first antibody (see 2.1.4) 1 h at room temperature, washed with Tris buffer and incubated with Alkaline Phosphatase/RED Streptavidin (Dako) for 15 min at room temperature and subsequently with chromogen for 1.5 min at room temperature. After washing again, the slides were stained with hematoxylin for 20 sec and washed briefly with warm water.

2.2.6 Microscopy

2.2.6.1   Bright field microscopy

Cell morphology of 4T1 and 410.4 cells was evaluated by bright field microscopy. For this, 7.5×10^5 cells were seeded in 6-well plates and allowed to adhere for 24 h at 37°C and 5% CO_2. After washing the cells with PBS, cell morphology was visualized using the Axio Observer Z1 Inverted Fluorescence Microscope (Zeiss).

2.2.6.2   Confocal microscopy

The grade of invasion of the tumor cells in the organotypic brain slice cocultures was evaluated with a Zeiss confocal laser scanning microscope (LSM 510, Zeiss) using the following scoring system: "+++" ≥ 2/3, "++" > 2/3 and "+" ≤ 1/3, relating to the fraction of contact section being invaded by tumor cells. A rank of "0" was given when no or only single invasive cells were detectable. Furthermore, the area of the tumor plug occupied by microglial cells, as well as the length of the astrocytes inside the tumor plug was also evaluated.

2.2.7 Statistical analysis

All experiments were performed at least in biological triplicates. Data are displayed as means ± SD of the mean (SEM) and statistical significance was calculated with a two-sided student's t-test, unless indicated otherwise. P-values under 0.05 were considered statistically significant (*$p < 0.05$; **$p < 0.01$; ***$p < 0.001$). Data were plotted with GraphPad Prism software (version 6, GraphPad Software).

3   Results

As already explained in the Introduction (see 1.3), this thesis project is included in a consortium (MetastaSys e:Bio), whose main aim is to analyze and to model molecular pathways in cancer cells and their microenvironment that govern the colonization of carcinoma cells in the liver and brain. My contribution to the consortium consisted in the generation of reliable brain metastasis colonization mouse models for the investigation of two key signaling pathways in colon (β-catenin) and breast cancer (EGFR). These pathways had to be validated in a liver colonization model, where the incidence of metastases of colon cancer is about 25% (Damiens et al., 2012); and in a brain colonization model, where the incidence of metastases of breast cancer reaches 30% (E. I. Chen et al., 2007).

A new syngeneic breast cancer colonization mouse model (410.4) had already been established in our group (in the framework of Britta Wenske's PhD thesis project). The 410.4 is the parental cell line of the 4T1. The 410.4 cell line has been poorly described in the literature. Miller et al. demonstrated a moderate metastatic potential of 410.4 (Miller et al., 1983). On the other hand, the 4T1 model is a well-established model to study spontaneous metastasis of breast cancer. The 4T1 has the features to metastasize at multiple distant sites including lymph nodes, lung, brain, and bone when tumor cells are orthotopically transplanted into the mammary fat pad (Pulaski & Ostrand-Rosenberg, 2001). Due to this metastatic potential, the 4T1 is widely used as a spontaneous model for breast cancer brain metastasis. However, to date, there are no publications comparing the colonization potential of the parental 410.4 with their derivate 4T1. They seem different in their metastatic potency regarding the first steps of metastasis, but whether they show a significant difference in their colonization capacity, is unknown. If that was the case, this pair would be an ideal model system to define new molecular targets and mechanisms during colonization. However, to our knowledge, there are no studies comparing the parental 410.4 and the 4T1, in particular no systematic comparison of their capacity to colonize distant organs. Therefore, the aim of the first part of my thesis was the establishment of the 4T1 in a brain colonization model, and the direct comparison between the parental cell line 410.4 and the potentially better colonizing derivate 4T1.

Additionally, we compare in the framework of the e:Bio consortium the colonization capacity of the 410.4 breast cancer cell line in the liver and the brain and seek candidates that trigger metastasis in both organs combining bioinformatic tools and biological validation. The results in the second part of my thesis underline the importance of the microenvironment in the formation of metastasis. In this context, I further study the interaction of the tumor cells and the surrounding stromal cells, especially monocyte-derive macrophages, during the colonization of the brain. I also show how

tumor-associated macrophages can be pharmacologically re-educated with a PI3-kinase inhibitor and switched into a tumor-suppressing phenotype in order to stop the formation of brain metastases.

3.1 Comparison of the colonization potential of the parental 410.4 with the 4T1 in syngeneic mouse models of breast cancer brain metastases

To carry out the following parts of this study I first developed a colonization model for the study of brain metastases. The importance of this very inefficient but key step in the metastatic cascade has already been explained in the Introduction (see 1.1.2.1). Despite the huge relevance of the colonization in the formation of metastases, very few have focused their attention on it. There are many in vivo systems that try to model one or more steps of the metastatic cascade. A huge effort was indeed made in the last decades in understanding how tumor cells leave the original lesion and invade the adjacent tissue before they get into the circulation and disseminate to distant organs. However, the way the tumor cells arrive at the target organ and colonize the secondary tissue remains almost unexplored.

Since the colonization of the brain represents the bottleneck of the metastatic cascade (Vanharanta & Massague, 2013), I believe that understanding the mechanisms underlying this decisive process may provide new therapeutic tools to combat brain metastases. To this end, I chose a specific colonization model consisting of the stereotactic implantation of tumor cells into the brain cortex of 10-12 week-old syngeneic mice (see 2.2.2). Our group has been using this system for many years, since it models the colonization of the brain, and moreover, the metastases reliably reflect those lesions seen in patients.

3.1.1 Characterization and comparison of murine breast cancer cell lines

As already mentioned, the experiments included in this work are conducted in syngeneic mice. For this reason I use murine cell lines that are stereotactically injected in 10-12 week-old mice with the same genetic background. A very important advantage of syngeneic mouse models is that they allow the investigation of the interaction of tumor cells with an intact immune system (see 1.1.3.2.1).

For the breast cancer brain metastasis mouse models two related cell lines were used. On the one hand, I chose the 4T1, a highly tumorigenic cell line which simulates the stage IV of human triple negative breast cancer. This cell line is commercially available and has been shown to spontaneously metastasize to distant organs, including the brain. The 4T1 cell line is a thioguanine-resistant variant

that was selected from another murine breast cancer cell line, the 410.4, without mutagen treatment (Aslakson & Miller, 1992). The 410.4, on the other hand, were isolated from a single spontaneously arising mammary tumor from a BALB/cfC3H mouse. This cell line has a moderate metastatic potential when injected intravenously, into mammary fat pads or subcutaneously (Miller et al., 1983).

Both cell lines are adherent and display an epithelial phenotype (see Figure 17 A). This characteristic makes them especially adequate for my purposes, as they mimic the human disease. The 410.4 exhibit a more marked epithelial phenotype in vitro in comparison to the 4T1, as they tend to grow in compact islets forming a thicket structure. Furthermore, the 410.4 express higher protein and RNA levels of E-cadherin and lower levels of vimentin compared to the 4T1 (see Figure 17 B-C). As will be discuss further in this work, the lower expression of E-cadherin in the 4T1 cells could be associated with their more aggressive behavior, as this marker is known as an important gatekeeper in breast cancer tumorigenesis and malignant progression (Berx & Van Roy, 2001; Kowalski, Rubin, & Kleer, 2003).
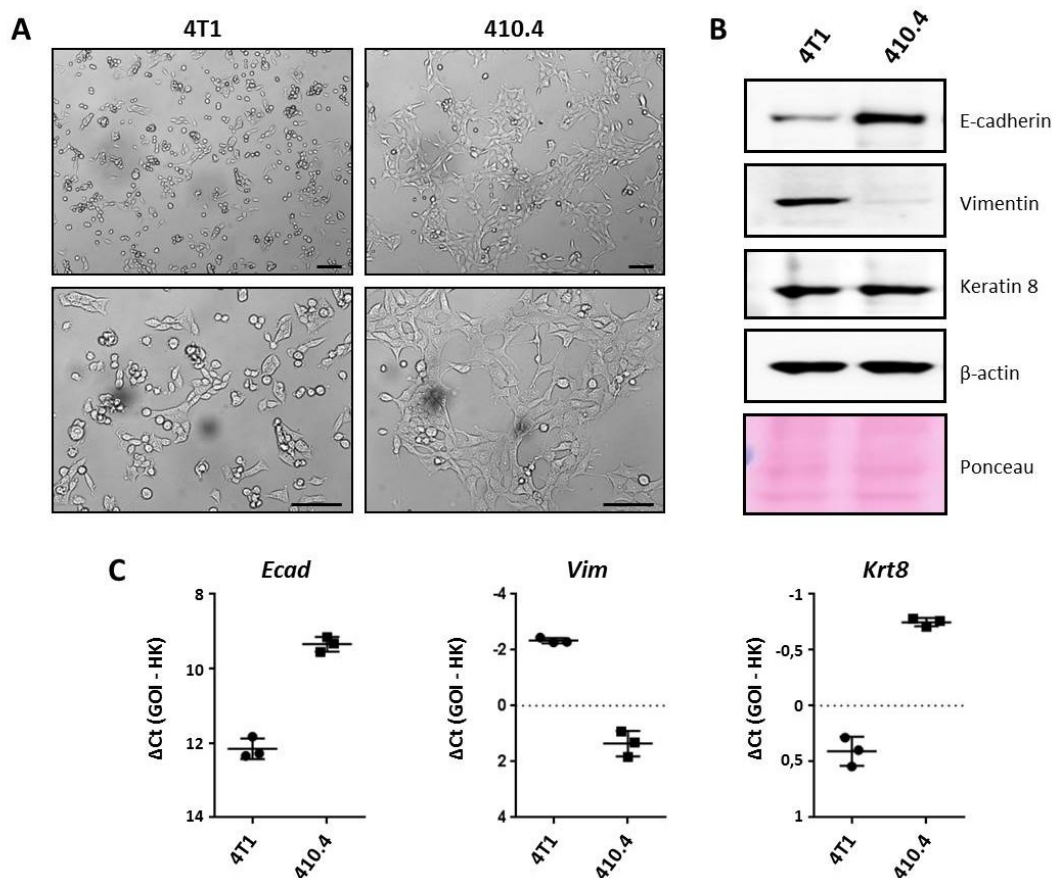
Figure 17: Characterization of murine breast cancer cell lines
A) Representative pictures of murine breast cancer cell lines (4T1, 410.4) were taken with a bright field microscope. Scale bars represent 100 µm. **B)** Western Blot analysis of epithelial (E-cadherin and keratin 8) and mesenchymal markers (vimentin) in murine breast cancer cell lines (4T1, 410.4). β-actin and Ponceau were used as loading controls. **C)** Real time PCR analysis of E-cadherin (*Ecad*), vimentin (*Vim*) and keratin 8 (*Krt8*) in murine breast cancer cell lines (4T1, 410.4). *Gapdh* and *Pgk1* were used as house-keeping (HK) genes.

3.1.2 Establishment, characterization and comparison of mouse models for brain colonization

As already indicated, the first aim of my thesis was to compare the colonization potential of the parental 410.4 and the 4T1 in vivo. To this end, I stereotactically injected the selected cell lines into the right hemisphere of syngeneic mice. In all models the number of injected cells was previously titrated and optimized in order to obtain reliable brain metastases at a high frequency (>80%) in an acceptable period of time (within 100 days). When the first neurological symptoms appeared, mice were submitted to the Hanging Wire test. This test assesses muscle strength, coordination and orientation of the mice, and is useful to identify neurological symptoms caused by brain metastases. Mice were sacrificed in case of failing the test. The resulting brain metastases were further examined by immunohistochemistry (IHC) and quantitative real time PCR (qRT-PCR) analysis.

The 410.4 mouse model has not yet been fully described in the literature. Miller et al. showed that this cell line has a moderate metastatic potential when injected intravenously, into mammary fat pads or subcutaneously (Miller et al., 1983). However, it is not a popular model for the study of brain colonization due to its low metastatic rate. On the other hand, the 4T1 cells, selected from the parental 410.4, have demonstrated a high metastatic potential in vivo. For this reason, this model is one of the preferred syngeneic systems for the study of metastatic breast cancer (Tao, Fang, Alroy, & Sahagian, 2008). However, the behavior of these breast cancer cell lines hasn't been studied in a colonization model until now. For this reason, the aim of the first part of my thesis was the establishment and characterization of the colonization models and the direct comparison of the parental cell line 410.4 and the potentially better colonizing derivate 4T1.

3.1.2.1   410.4 breast cancer brain colonization mouse model

The first model to be described is the 410.4. This model had already been established in our group. In this case, I stereotactically injected 100000 cells in the right hemisphere of 10 to 12 week-old syngeneic mice and the metastases appeared after approximately 7-8 weeks (median OS = 50 days) in 10 out of 11 mice (see Figure 18 A).

For the detection of metastatic foci in the brain parenchyma I made use of two epithelial markers: keratin 8 and E-cadherin. Keratin 8 (KRT8) is a luminal epithelial cell marker which is widely used for the pathological diagnosis of adenocarcinoma. E-cadherin (ECAD), also known as Cadherin 1 (CDH1), is a cell-cell adhesion receptor, which has been largely described as playing an important role in tumor progression, serving as a suppressor of invasion and metastasis in many contexts (Berx & Van

Roy, 2001; Jeanes, Gottardi, & Yap, 2008). These two markers were assessed in the brain tissue samples both by real time PCR and immunohistochemistry analyses.

The analysis of the metastatic tissue by real time PCR revealed a significant higher expression of the tumor markers *Krt8* and *Ecad* in the mice injected with 410.4 compared to the control mice (see Figure 18 B). Remarkably, one of the injected mice didn't develop any metastases. Interestingly, this mouse expresses levels of keratin 8 and E-cadherin which are comparable to those of the controls. These data were confirmed by negative IHC staining (data not shown). This observation reinforces the robustness of the choice markers for the detection and confirmation of brain metastases.

The immunohistochemistry analysis confirmed the presence of metastases in the brain tissue (see Figure 18 C). Furthermore, the hematoxylin/eosin (H&E) and keratin 8 (KRT8) staining revealed a cohort infiltration pattern of the 410.4 tumor cells into the adjacent brain parenchyma (see Figure 17 C, left and middle panel). As already described by our group, this is a typical infiltration pattern of breast cancer cells, in which strands and detached infiltrating cohorts and clusters of cells invade the brain tissue (Siam et al., 2015). Furthermore, E-cadherin positive cells could be observed at the invasion front of the 410.4 metastasis (see Figure 18 C, right panel).

Figure 18: Characterization of the 410.4 breast cancer brain colonization mouse model
A) Overall survival of mice injected with the breast cancer cell line 410.4 (Met-410.4). BALB/c mice solely injected with ECM were used as control (CTL). P-value was calculated with the Log-rank (Mantel-Cox) test (***p<0.001). **B)** Real time PCR analysis of keratin 8 (*Krt8*) and E-cadherin (*Ecad*) in 410.4 metastasis (410.4 Met), 410.4 cell line (410.4 cells) and ECM injected controls (CTL). The orange square indicates the mouse without the event of metastases. *Gapdh* and *Pgk1* were used as house-keeping (HK) genes. P-value was calculated with the unpaired t-test (***p<0.001). **C)** Immunohistochemistry (IHC) staining of Hematoxylin & Eosin (H&E), keratin 8 (KRT8) and E-cadherin (ECAD) in brain metastases of 410.4. Representative microphotographs of sagittal brain sections at the level of the anterior striatum are shown.

3.1.2.2   4T1 breast cancer brain colonization mouse model

Next, I characterized the well-known 4T1 breast cancer model, but in our colonization in vivo system. Previous works where these cells are injected orthotopically in the mammary fat pad or ectopically in the left ventricle of the heart have described the 4T1 as highly tumorigenic (Pulaski & Ostrand-

Rosenberg, 2001; Tao et al., 2008). In contrast to these models, I only injected 1000 cells into the mouse cortex. The very low amount of implanted cells is possible due to the local injection technique, in which there is no loss of tumor cells because of dissemination steps and all cells (usually) grow into the target organ when both entities are compatible.

As Figure 19 A shows, the injection of only 1000 cells results in the formation of symptomatic metastases with a very high success rate in a short period of time. In other words, all mice injected with 4T1 develop metastases after approximately 3 weeks (median OS = 20 days). This result confirms the observations made by others regarding the aggressiveness of this cell line in vivo.

As can be observed in Figure 19 B, the real time PCR analysis of the metastatic tissue reveals a high significant increase in the expression of *Krt8* and *Ecad* in mice injected with tumor cells (4T1 Met) in comparison to the control mice injected only with ECM (CTL). The immunohistochemistry examination of the metastatic tissue revealed the presence of metastases in the brain tissue that reliably reflect the human disease. As in the case of the 410.4, the 4T1 also display a cohort infiltration pattern in the brain parenchyma (see Figure 19 C, left and middle panel).

A very interesting finding is the low expression of E-cadherin in the metastatic tissue. As has already been shown in Figure 17, 4T1 cells express low levels of this marker, which may be associated with their higher metastatic potential (Berx & Van Roy, 2001). Moreover, in the metastatic tissue E-cadherin is almost absent (see Figure 19 C, right panel). This observation may indicate that the re-expression of E-cadherin by tumor cells during brain colonization (mesenchymal to epithelial transition) is not mandatory in the establishment of metastasis, and other features may confer tumor cells the ability to infiltrate the brain parenchyma in an effective manner.
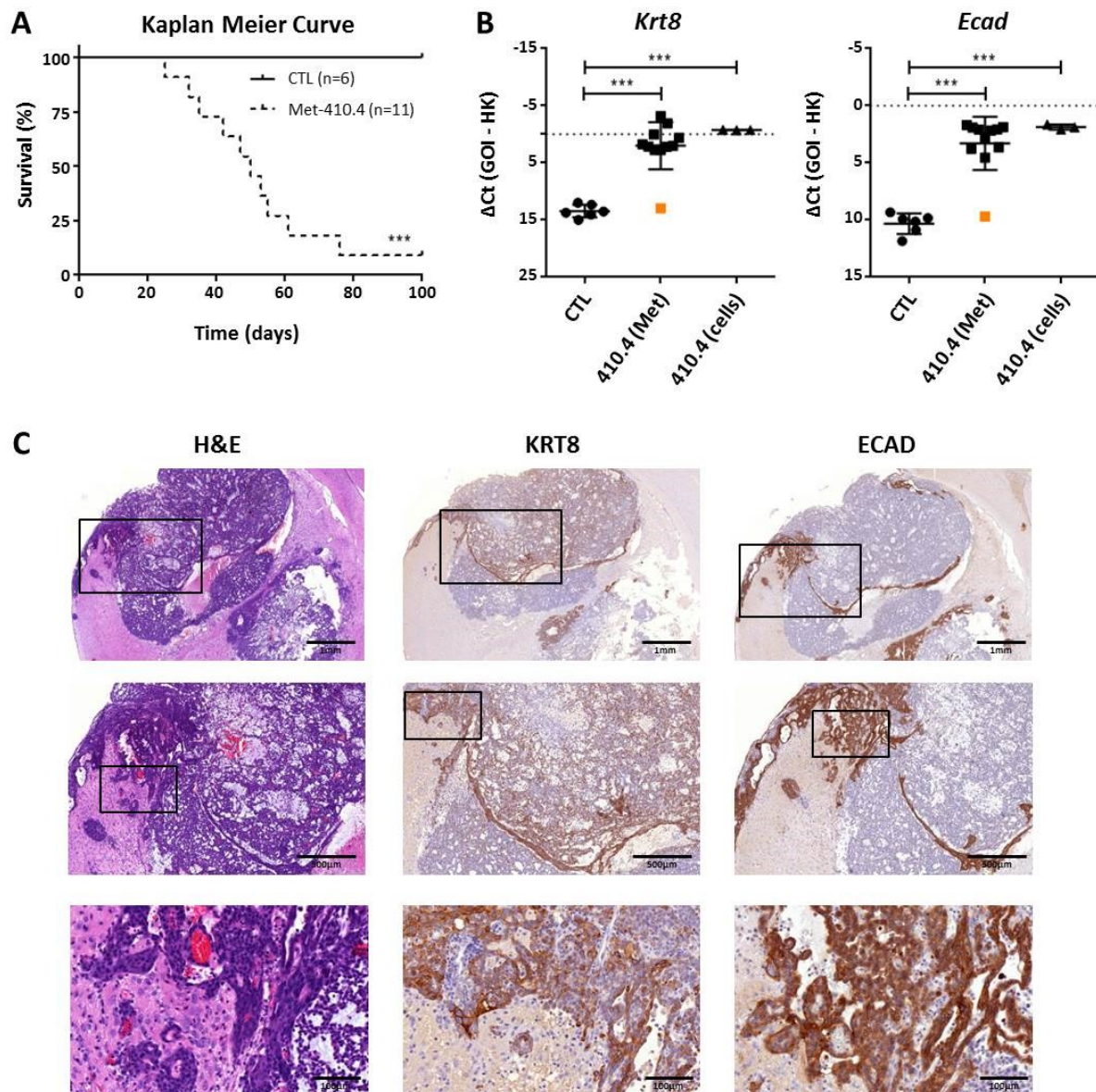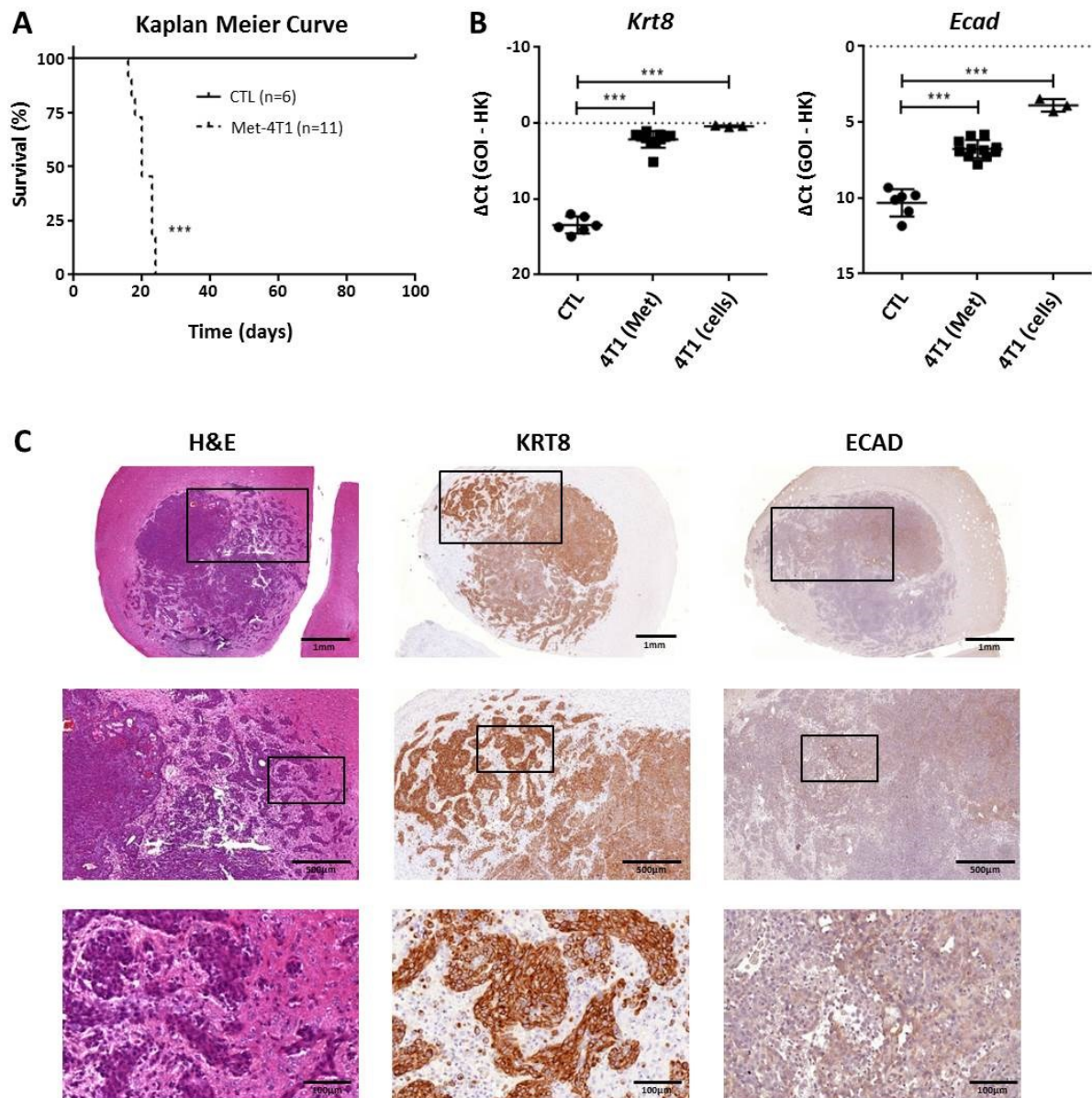
Figure 19: Characterization of the 4T1 breast cancer brain colonization mouse model
A) Overall survival of mice injected with the breast cancer cell line 4T1 (Met-4T1). BALB/c mice injected solely with ECM and without 4T1 cells were used as control (CTL). P-value was calculated with the Log-rank (Mantel-Cox) test (***p<0.001). **B)** Real time PCR analysis of keratin 8 (*Krt8*) and E-cadherin (*Ecad*) in 4T1 metastasis (4T1 Met), 4T1 cell line (4T1 cells) and ECM injected controls (CTL). *Gapdh* and *Pgk1* were used as house-keeping (HK) genes. P-value was calculated with the unpaired t-test (***p<0.001). **C)** Immunohistochemistry (IHC) staining of Hematoxylin & Eosin (H&E), keratin 8 (KRT8) and E-cadherin (ECAD) in brain metastases of 4T1. Representative microphotographs of sagittal brain sections at the level of the anterior striatum are shown.

To sum up, two breast cancer brain colonization mouse models with different colonization skills have been developed. On the one hand, the 410.4 have a slow and/or moderate colonization pattern, since they need almost 8 weeks and 100000 cells to colonize the brain. However, these cells provide reproducible metastases that reflect the human disease. On the other hand, the 4T1, a thioguanine resistant variant of the 410.4, display a much higher metastatic potential in vivo, since they rapidly

colonize the brain parenchyma and cause wide spread metastases by only injecting 1000 cells. Either way, both cell lines show a cohort infiltration pattern, characteristic of breast cancer brain metastasis, and can be detected by means of epithelial markers like keratin 8. Table 10 summarizes all parameters studied and described in both models.

	410.4		4T1	
	Cell line	Metastasis	Cell line	Metastasis
Cytokeratin 8	High	High	High	High
E-cadherin	High	Moderate	Low	Low
Vimentin	Low	-	High	-
Injected cells (n)	-	100000	-	1000
Event of metastasis (N/M)	-	10/11	-	11/11
Median OS (days)	-	50	-	20
Infiltration pattern	-	Cohort	-	Cohort

Table 10: Characteristics of breast cancer brain metastases mouse models

The epithelial markers (cytokeratin 8 and E-cadherin) were evaluated for the cell line and the metastases and the mesenchymal marker (vimentin) for the cell lines. The number of injected cells, the number of mice with symptomatic metastases and the median overall survival of the mice was measured. The infiltration pattern of the cells in the brain parenchyma was also described.

3.1.3 The Colonization Index

The characterization of the breast cancer brain metastases in vivo colonization models revealed that both cell lines display a similar infiltration pattern into the brain parenchyma. Both the 4T1 and 410.4 demonstrate a cohort infiltration pattern, in which strands and detached infiltrating cohorts and clusters of cells invade the brain tissue. Despite this similarity, a significant difference in the colonization capacity of these two related cell lines can be guessed. Several parameters to assess the different colonization potential of the cell lines have been described (see Table 10); but a precise and accurate method, in which the most relevant characteristics of the models are included, was needed.

In the literature, most studies associate the aggressiveness of the cell lines with the number of mice that develop metastases. However, if we reduce the colonization potential only to the percentage of successful colonization [(N/M) = %] important information to demonstrate the real difference in the colonization capacity of the cells would be lost. In our models I could also identify other deciding factors that were different between both models. For example, the 4T1 needs a lower amount of

cells and less time to produce brain metastases. Furthermore, all mice injected with these cells develop symptomatic metastases, while in the case of the 410.4 one mouse survives in spite of the fact that the number of injected cells is 100 times higher.

Thus, these parameters must also be taken into account to demonstrate the real difference in the colonization capacity of the cells. To solve this problem I developed an equation that I called "the Colonization Index" which includes three important parameters for the quantification of the colonization potential: the rate of successful colonization of the brain, the number of injected cells, and the median overall survival of the mice (see Figure 20). Therefore, the Colonization Index (CI) is a new quantification tool which allows a much more accurate and precise comparison of different cell lines in their colonization capacity as the single parameters alone, and demonstrates more potent differences among the models. According to the Colonization Index, the 4T1 is a much more aggressive cell line than the parental cells 410.4, as it causes symptomatic metastases in all mice, in a shorter period of time, and the number of injected cells is much lower. All these parameters are summarized in Figure 20.

$$\text{Colonization Index (CI)} = \frac{\text{Successful Colonization (\%)}}{\text{Injected cells (n) x Median OS (d)}} \times 100$$

Cell line	Injected cells (n)	Successful colonization (%)	Median overall survival (days)	Colonization Index (CI)
4T1	1000	100	20	0.5
410.4	100000	91	50	0.0018
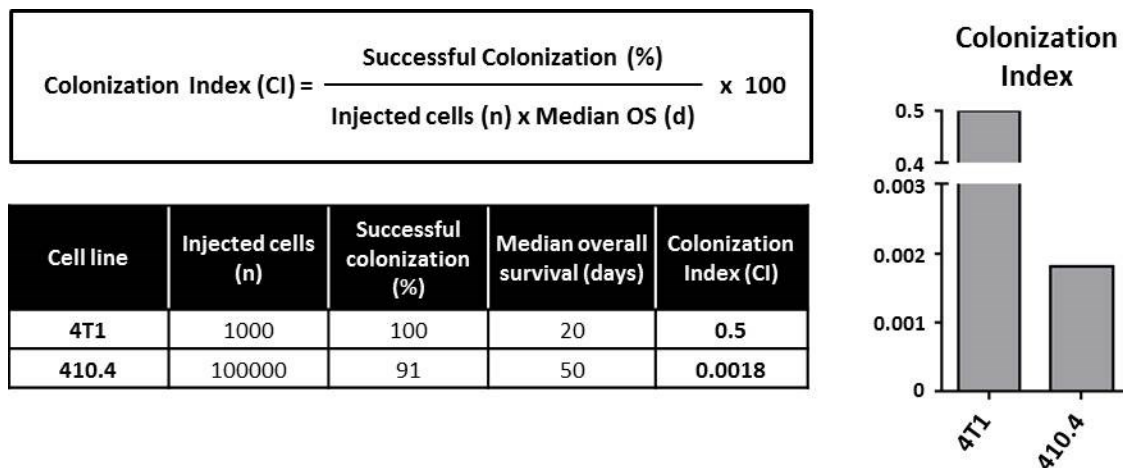
Figure 20: The Colonization Index (CI)
The rate of successful colonization, the number of injected cells, and the median overall survival of the mice are included in this equation to compare the colonization potential of the breast cancer cell lines 4T1 and 410.4 in vivo. The 4T1 have a much higher colonization index and are thus considered more aggressive than the 410.4.

Taken together, I have demonstrated that the 4T1 and the parental 410.4 are suitable models for the study of breast cancer brain colonization. Additionally, I developed a new quantification tool, the Colonization Index, which makes possible the comparison of both models regarding their colonization skills. According to this equation, both breast cancer cell lines display different colonization potentials, from low/moderate (410.4) to highly aggressive (4T1). For this reason, this pair is an ideal model system to define new molecular targets and mechanisms during colonization.

3.1.4 The role of the microenvironment in brain metastasis

As already commented in the introduction (see 1.2.1), the microenvironment plays a very important role in tumor progression and metastasis (Hart & Fidler, 1980a). The microenvironment can exert inhibitory effects on malignant cells. However, during tumor progression, tumor cells usually evade these inhibitory signals and misuse the surrounding stromal cells to promote tumor progression and ultimately metastasis (Chuang, van Rossum, et al., 2013; Pukrop et al., 2010). Thus, immune reactions within the tumor may influence clinical outcome (Galon et al., 2006; Galon, Fridman, & Pages, 2007; Pages et al., 2005).

The central nervous system (CNS) has a markedly different milieu than other organs. We and others have already proven that, in the brain, the tumor-associated parenchymal cells such as vascular cells, peripheral immune cells, microglia, and astrocytes play a key role in controlling the course of disease (Charles, Holland, Gilbertson, Glass, & Kettenmann, 2012; Chuang, van Rossum, et al., 2013; Pukrop et al., 2010). For this reason, I also characterized the presence and role of the microenvironment (especially microglia/macrophages, astrocytes and T cells) in the brain colonization mouse models.

3.1.4.1 Characterization of microglia/macrophages in the metastatic brain tissue

Microglia are the main immune effectors of the CNS. They are usually activated in case of injury and act as antigen-presenting cells for the T cells, together with peripheral macrophages (Berghoff & Preusser, 2015; Winkler, 2015). However, microglia can also suppress the anti-tumor T cell response via activation of CTLA-4 or PD-1, and therefore participate in the generation of an immune suppressive tumor microenvironment (Berghoff & Preusser, 2015). Our group has also demonstrated that microglia enhance the invasion and colonization of the brain tissue by cancer cells by serving both as active transporters and guiding rails (Pukrop et al., 2010).

In the syngeneic breast cancer brain colonization models, I found activated microglia/macrophages in the brain parenchyma. Interestingly, they appeared inside and around the metastatic lesion, but not in the hemisphere that had not been infiltrated by tumor cells or in the mice that had only been injected with ECM and no tumor cells (see Figure 21 A). Furthermore high levels of *Iba1* were detected in the brain tissue from those mice that developed metastasis; however, the expression of this marker in the mouse without metastasis was comparable to that seen in the control mice (see Figure 21 B). This fact discards the possibility that the activation of the microglia was due to an injection-induced damage.
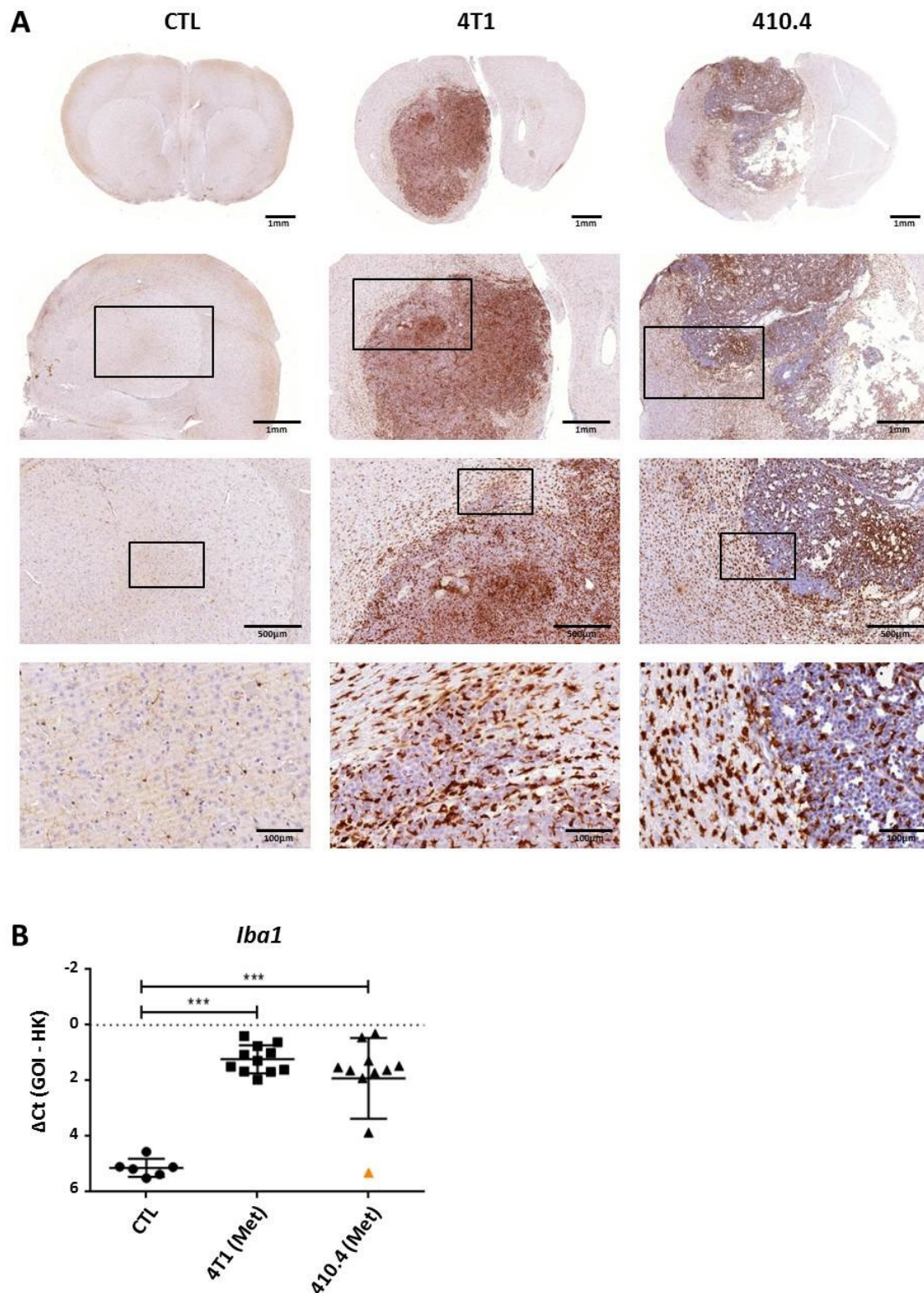
Figure 21: Characterization of microglia in the metastatic brain tissue

A) Immunohistochemistry (IHC) staining of microglia/macrophages (IBA1) in mice injected only with ECM and no tumor cells (CTL) and breast cancer brain metastasis of 4T1 and 410.4. Representative microphotographs of sagittal brain sections at the level of the anterior striatum are shown. **B)** Real time PCR analysis of microglia/macrophages (*Iba1*) in ECM injected controls (CTL) and brain metastasis of 4T1 (4T1-Met) and 410.4 (410.4-Met). The orange arrow indicates a mouse without the event of metastases. *Gapdh* and *Pgk1* were used as house-keeping (HK) genes. P-value was calculated with the unpaired t-test (***p<0.001).

3.1.4.2   Characterization of astrocytes in the metastatic brain tissue

Astrocytes are the characteristic star-shaped and the most abundant glial cells of the CNS (Xing et al., 2013). They form part of the blood brain barrier (BBB) together with endothelial cells, provide nutrients to the nervous tissue, and play an important role in repair processes of the brain after traumatic injuries. However, these cells can also be switched into a reactive phenotype induced by the tumor microenvironment and can then secrete a number of factors that influence tumor progression (Charles et al., 2012).

As can be seen in Figure 22, astrocytes were highly activated in the brain parenchyma from those mice that developed brain metastasis compared to the mice injected only with ECM, as also happens with microglial cells. This could be predominantly observed in the hemisphere where the tumor cells had been injected. Interestingly, astrocytic cells didn't appear inside the metastases (as in the case of microglia) but around them, forming some kind of surrounding layer (see Figure 22 A). These observations could be confirmed and quantified by means of real time PCR (see Figure 22 B). Remarkably, in the case of the mouse that didn't develop symptomatic metastases, this activation didn't take place at all, and the levels of *Gfap* were comparable to those of the control mice.
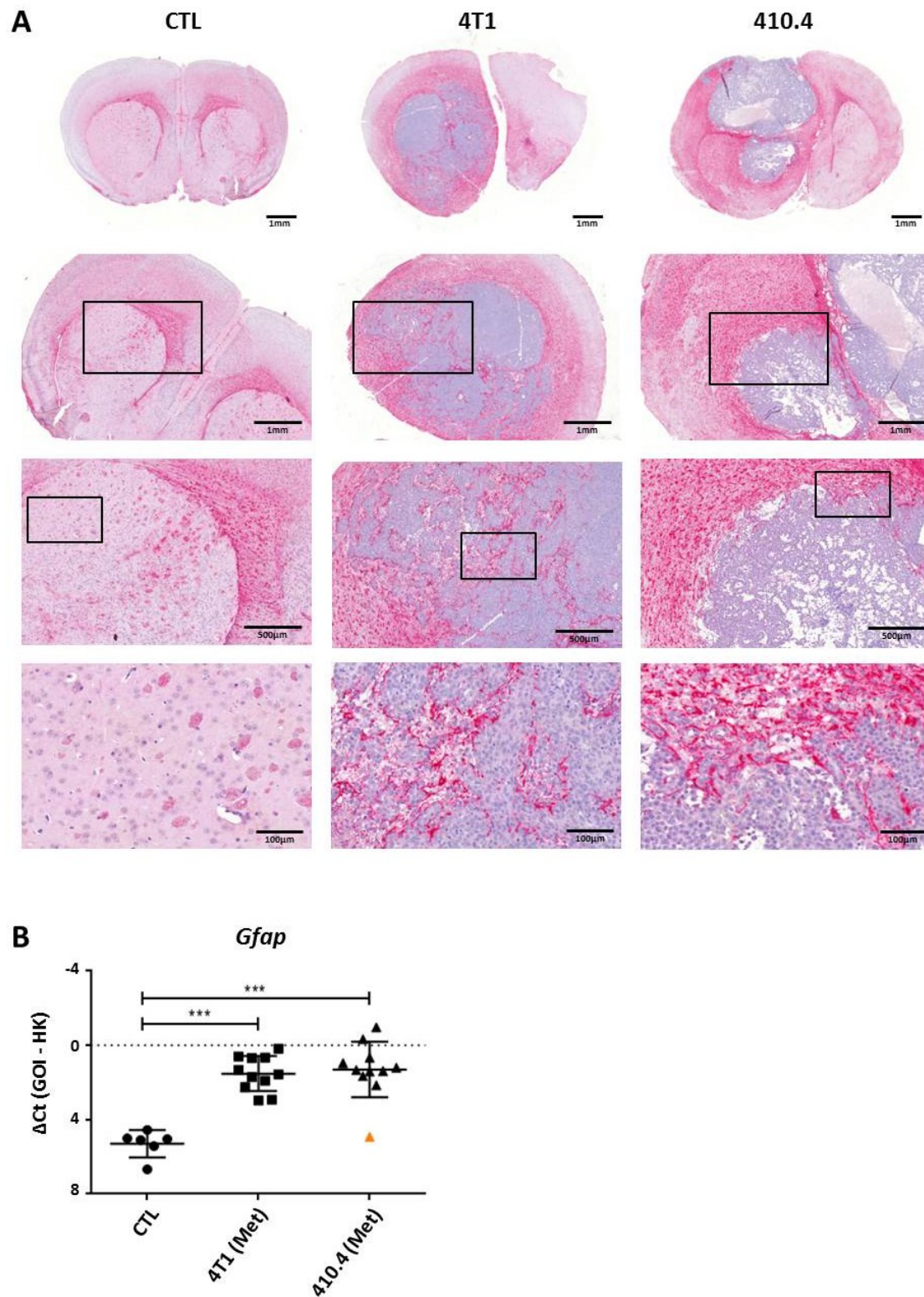
Figure 22: Characterization of astrocytes in the metastatic brain tissue
A) Immunohistochemistry (IHC) staining of astrocytes (GFAP) in mice injected only with ECM and no tumor cells (CTL) and breast cancer brain metastasis of 4T1 and 410.4. Representative microphotographs of sagittal brain sections at the level of the anterior striatum are shown. **B)** Real time PCR analysis of astrocytes (*Gfap*) in ECM injected controls (CTL) and brain metastasis of 4T1 (4T1-Met) and 410.4 (410.4-Met). The orange arrow indicates a mouse without the event of metastases. *Gapdh* and *Pgk1* were used as house-keeping (HK) genes. P-value was calculated with the unpaired t-test (***p<0.001).

3.1.4.3   Characterization of T cells in the metastatic brain tissue

T cells are the main effector cells of the adaptive immune system. Lymphocytes are mostly absent in the healthy brain parenchyma and only migrate into the CNS under pathological conditions (Platten, Ochs, Lemke, Opitz, & Wick, 2014). Cytotoxic T cells (CD8+) display a tumor suppressive function. Regulatory T cells (CD4+), on the contrary, have an immunosuppressive function; they suppress CD8+ cytotoxic T cells and participate in the generation of an immune-suppressive microenvironment (Berghoff & Preusser, 2015).

In the in vivo models, infiltrating T cells (CD3+) could be detected in the tumor mass. This observation is particularly evident in the 410.4 model (see Figure 23 A, right panel). In the 4T1 model I was also able to see some T cells but in a lower amount (middle panel). As also happens with microglial and astrocytic cells, T cells were absent in the brain parenchyma of mice stereotactically injected with ECM or those that didn't develop symptomatic metastases. These observations were also confirmed by means of real time PCR (see Figure 23 B).
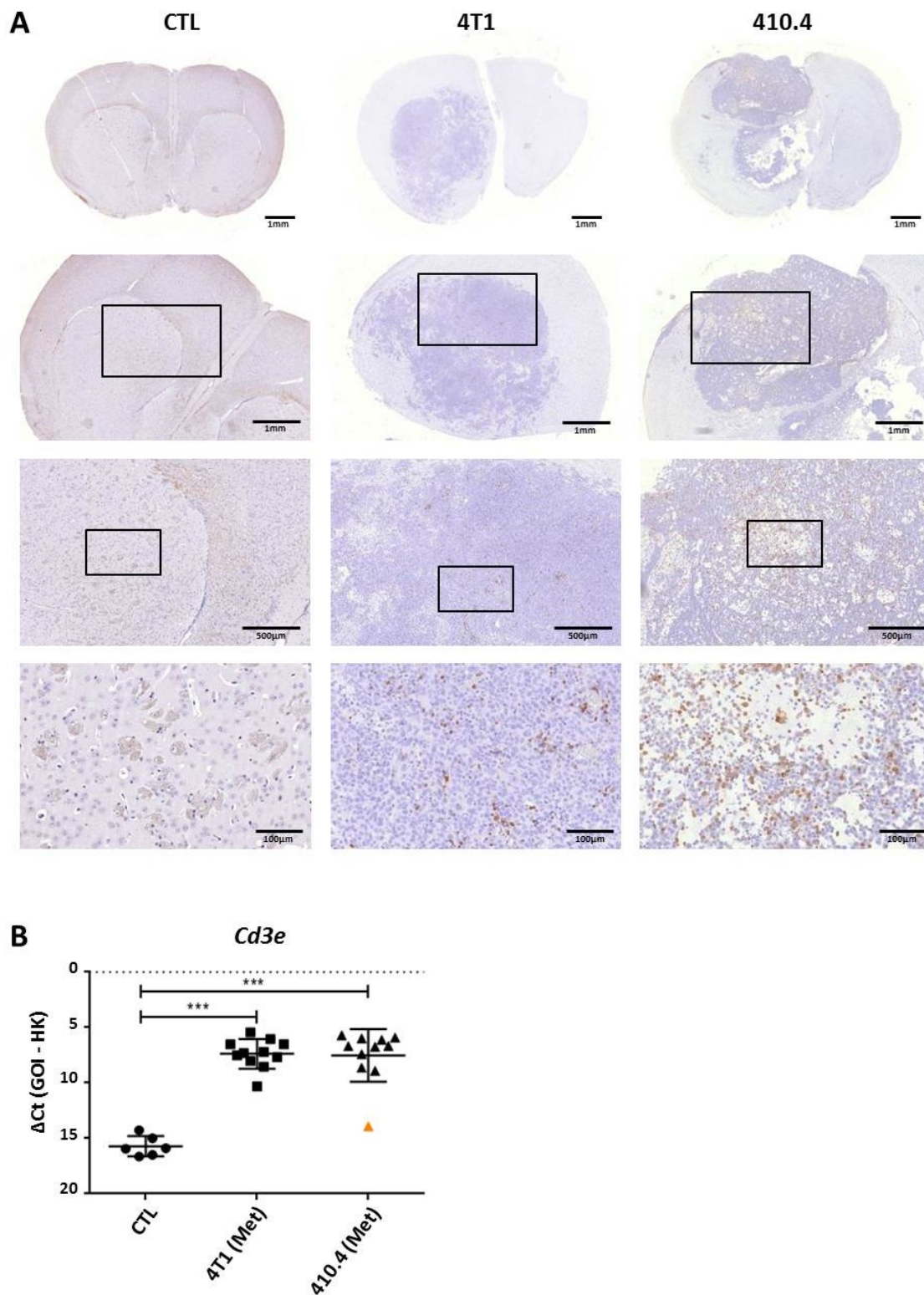
Figure 23: Characterization of T cells in the metastatic brain tissue
A) Immunohistochemistry (IHC) staining of T cells (CD3) in mice injected only with ECM and no tumor cells (CTL) and breast cancer brain metastasis of 4T1 and 410.4. Representative microphotographs of sagittal brain sections at the level of the anterior striatum are shown. **B)** Real time PCR analysis of T cells (*Cd3e*) in ECM injected controls (CTL) and brain metastasis of 4T1 (4T1-Met) and 410.4 (410.4-Met). The orange arrow indicates a mouse without the event of metastases. *Gapdh* and *Pgk1* were used as house-keeping (HK) genes. P-value was calculated with the unpaired t-test (***p<0.001).

3.1.5 Looking for candidate triggers of metastasis

In order to better understand which factors are really implicated in the formation of metastasis, we persuaded a Differentially Expressed Gene (DEG) analysis in the framework of the BMBF e:Bio MetastaSys consortium in collaboration with the department of General and Visceral Surgery, the department of Medical Statistics, and the Transcriptome and Genome Analysis Laboratory (TAL) in Göttingen. This computational approach aims to identify the differentially expressed genes in metastatic samples of the liver and the brain. Therefore the samples were sequenced by means of RNA-seq, and the differentially expressed genes were selected based on a combination of expression change threshold and score cutoff based on P values generated by statistical modeling (Rapaport et al., 2013).

For our purposes, we compared the 410.4 breast cancer cell line with the metastatic tissue either in the liver or in the brain and looked for common differentially expressed genes in order to identify candidate genes that trigger the metastatic process in itself, independently of the target organ (see Figure 24). My task was to stereotactically inject the breast cancer cells 410.4 (n=5) into the right brain hemisphere of syngeneic mice and also provide ECM-control mice (n=5) for the subsequent analysis. To this end, I isolated RNA from the metastatic tissue and provided high qualitative material for further sequencing and bioinformatic analysis. The liver metastasis samples were provided by other partners of the consortium.

* Clean metastatic tissue = metastase − control tissue
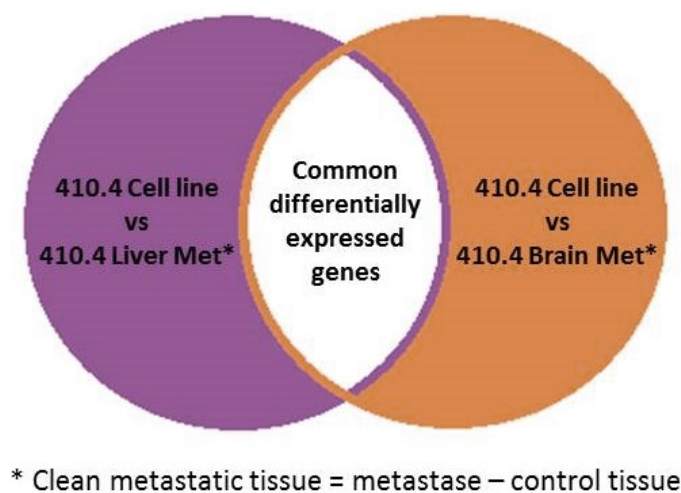
Figure 24: Schematic view of the sample comparison for DEG analysis
After RNA sequencing, the gene expression data of the breast cancer cell line 410.4 (410.4 Cell line) was compared with the murine metastatic tissue after injection of the cell line either in the liver (410.4 Liver Met) or in the brain (410.4 Brain Met), in order to identify common differentially expressed genes that trigger the metastatic process.

In this common approach the consortium identified 27 common differentially expressed genes, most of them associated with chemokine signaling, extracellular matrix proteins, cell death and inflammation, and immune-modulating molecules (see Table 11). For my project we chose 3 of them for further biological validation (*Iba1/Aif1*, *Tyrobp* and *Ccl8*). These genes are related to the activation of the tumor microenvironment/innate immunity during metastasis progression.

Gene Name	Description	Ensembl gene ID
CCL8	chemokine (C-C motif) ligand 8 [Source:MGI Symbol;Acc:MGI:101878]	ENSMUSG00000009185
TYROBP	TYRO protein tyrosine kinase binding protein [Source:MGI Symbol;Acc:MGI:1277211]	ENSMUSG00000030579
AIF1	allograft inflammatory factor 1 [Source:MGI Symbol;Acc:MGI:1343098]	ENSMUSG00000024397
CCL5	chemokine (C-C motif) ligand 5 [Source:MGI Symbol;Acc:MGI:98262]	ENSMUSG00000035042
CASP1	caspase 1 [Source:MGI Symbol;Acc:MGI:96544]	ENSMUSG00000025888
SPI1	spleen focus forming virus (SFFV) proviral integration oncogene [Source:MGI Symbol;Acc:MGI:98282]	ENSMUSG00000002111
VAV1	vav 1 oncogene [Source:MGI Symbol;Acc:MGI:98923]	ENSMUSG00000034116
CD14	CD14 antigen [Source:MGI Symbol;Acc:MGI:88318]	ENSMUSG00000051439
CLEC4A2/DCIR	C-type lectin domain family 4, member a2 [Source:MGI Symbol;Acc:MGI:1349412]	ENSMUSG00000030148
CD37	CD37 antigen [Source:MGI Symbol;Acc:MGI:88330]	ENSMUSG00000030798
CCL4	chemokine (C-C motif) ligand 4 [Source:MGI Symbol;Acc:MGI:98261]	ENSMUSG00000015437
GZMB	granzyme B [Source:MGI Symbol;Acc:MGI:109267]	ENSMUSG00000022126
IRG1	immunoresponsive gene 1 [Source:MGI Symbol;Acc:MGI:103206]	ENSMUSG00000030793
PYCARD	PYD and CARD domain containing [Source:MGI Symbol;Acc:MGI:1931465]	ENSMUSG00000042784
GPX2	glutathione peroxidase 2 [Source:MGI Symbol;Acc:MGI:106609]	ENSMUSG00000042808
IL12RB1	interleukin 12 receptor, beta 1 [Source:MGI Symbol;Acc:MGI:104579]	ENSMUSG00000000791
PTAFR	platelet-activating factor receptor [Source:MGI Symbol;Acc:MGI:106066]	ENSMUSG00000056529
LY9/SLAMF3	lymphocyte antigen 9 [Source:MGI Symbol;Acc:MGI:96885]	ENSMUSG00000004707
MMP12	matrix metallopeptidase 12 [Source:MGI Symbol;Acc:MGI:97005]	protein_coding
MRC2	mannose receptor, C type 2 [Source:MGI Symbol;Acc:MGI:107818]	ENSMUSG00000020695
NAPSA	napsin A aspartic peptidase [Source:MGI Symbol;Acc:MGI:109365]	protein_coding
MUC1	mucin 1, transmembrane [Source:MGI Symbol;Acc:MGI:97231]	ENSMUSG00000028217
CDH17	cadherin 17 [Source:MGI Symbol;Acc:MGI:1095414]	ENSMUSG00000018930
IHH	Indian hedgehog [Source:MGI Symbol;Acc:MGI:96533]	ENSMUSG00000006538
FERMT1	fermitin family homolog 1 (Drosophila) [Source:MGI Symbol;Acc:MGI:2443583]	ENSMUSG00000027356
MMP7	matrix metallopeptidase 7 [Source:MGI Symbol;Acc:MGI:103189]	ENSMUSG00000018623
GATA3	GATA binding protein 3 [Source:MGI Symbol;Acc:MGI:95663]	ENSMUSG00000015619

Table 11: Common differentially expressed genes in brain and liver metastasis of breast cancer
Common differentially expressed genes of brain and liver metastasis of breast cancer primary tumor are listed on this table. Among them, *Ccl8*, *Tyrobp* and *Iba1/Aif1* were chosen for further biological validation. Data provided by Alexander Wolff (Department of Medical Statistics, Göttingen).

3.1.5.1 Validation of differentially expressed genes in brain and liver metastases

As has already been pointed out, immune reactions during the metastatic process may influence clinical outcome (Galon et al., 2007; Pages et al., 2005). Among the common differentially expressed genes in liver and brain metastases of 410.4 we found many of them related to immune activation. The candidate genes chosen for further validation (*Iba1*, *Tyrobp* and *Ccl8*) are indeed directly associated with the innate immunity.

Iba1 (ionized calcium-binding adapter molecule 1) also known as allograft inflammatory factor 1 (*Aif1*) is induced by cytokines and interferon and may promote macrophage activation and proliferation of T lymphocytes. As can be observed in Figure 25 A, *Iba1* is significantly upregulated both in the brain and in the liver metastasis samples compared to the control tissue. This gene had been already used as a marker of activated macrophages/microglia in brain metastasis (see 3.1.4.1). This finding confirms that *Iba1* is not only a marker for activated macrophages in the CNS, but also for activated macrophages in other organs, like the liver.

The TYRO protein tyrosine kinase binding protein (*Tyrobp*), also known as *Dap12*, is abundantly expressed in myeloid and natural killer (NK) cells. It encodes a transmembrane signaling polypeptide which contains a single immune-receptor tyrosine-based activation motif (ITAM). This immune-receptor adaptor protein recruits and activates tyrosine kinases, which are responsible for T and B cell receptor (TCR and BCR) signal transduction (Lanier, 2009). On the other hand, recent studies have also identified *Tyrobp* as one of the ectopic immune antigens expressed on the cell surface of malignant cells. Interestingly, tumor cells may acquire some "macrophage traits" by expressing these antigens in order to resist immune elimination and overcome the rate-limiting steps of metastasis (Parcesepe, Giordano, Laudanna, Febbraro, & Pancione, 2016; Shabo, Olsson, Stal, & Svanvik, 2013). In this study, I could also confirm the upregulation of *Tyrobp* in all metastatic samples compared to the control tissue and the 410.4 cell line (see Figure 25 B). This observation indicates that *Tyrobp* may be an important mediator of innate immune activation during metastasis.

The chemokine (C-C motif) ligand 8 (*Ccl8*), also known as monocyte chemoattractant protein 2 (*Mcp2*) is a small cytokine belonging to the CC chemokine family. *Ccl8* displays chemotactic activity for monocytes, lymphocytes, basophils and eosinophils. By recruiting leukocytes to sites of inflammation this cytokine may contribute to tumor-associated leukocyte infiltration. Furthermore, recent studies have identified *Ccl8* as a possible host-related factor which might be involved in supporting the metastatic phenotype. In line with that, this gene showed a significantly increased expression in the metastases of different primary tumors (Barbai, Fejos, Puskas, Timar, & Raso, 2015). These data also suggest a metastatic promoting role of *Ccl8*, as it is significantly upregulated in all metastatic samples, both in the brain as in the liver compared to the control tissue and the 410.4 cell line itself (see Figure 25 C).
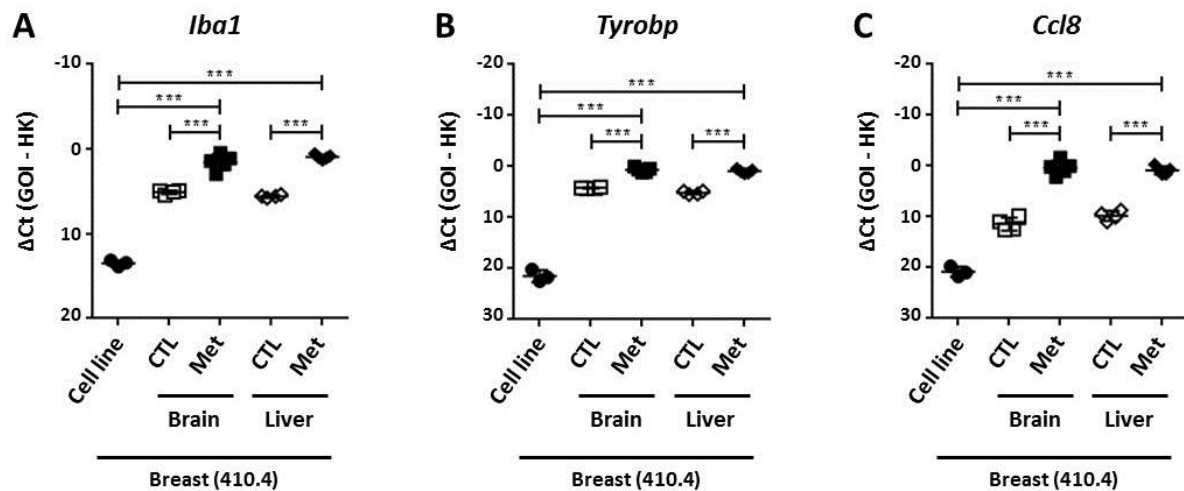
Figure 25: Common genes associated with immune response in brain and liver metastasis
Real time PCR analysis of *Iba1* **(A)**, *Tyrobp* **(B)** and *Ccl8* **(C)** in breast cancer brain and liver metastasis (Met) and in the 410.4 cell line. Liver or brain tissue of BALB/c mice injected with ECM but no cells were used as control (CTL). *Gapdh* and *Pgk1* were used as house-keeping (HK) genes. P-value was calculated with the unpaired t-test (***p<0.001).

3.1.5.2   Validation of DEG in breast cancer brain colonization models

All three genes identified and described above seem to play a role during inflammation and immune response. These candidate genes could also be validated in the brain colonization in vivo models of 4T1 and 410.4, which reinforce their role as triggers of metastasis. As can be seen in Figure 26, these genes are significantly upregulated in the brain metastasis samples of 4T1 and 410.4 compared to the corresponding cell lines and to the control mice only injected with ECM and no tumor cells (see Figure 26).

Figure 26: Genes associated with inflammation in breast cancer brain metastasis
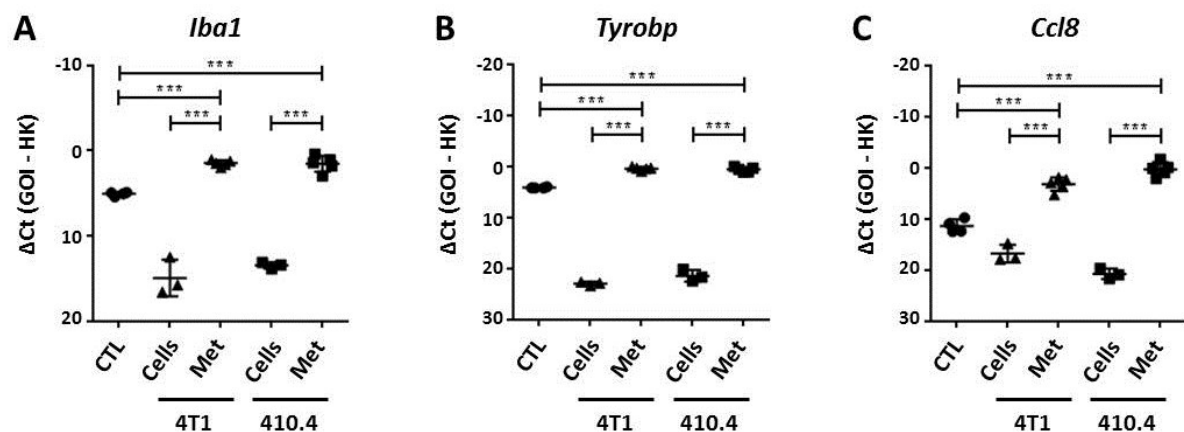Real time PCR analysis of *Iba1* **(A)**, *Tyrobp* **(B)** and *Ccl8* **(C)** in brain metastases (Met) of 4T1 or 410.4, and tumor cells. Brain tissue of BALB/c mice injected with ECM but no cells were used as control (CTL). *Gapdh* and *Pgk1* were used as house-keeping (HK) genes. P-value was calculated with the unpaired t-test (***p<0.001).

Iba1 had been already pointed out by us to be an important marker in metastasis of the CNS. These new data highlight the relevance of activated macrophages/microglia in promoting metastasis. Additionally, two further genes (*Tyrobp* and *Ccl8*) could also be identified as being significantly upregulated in the brain metastasis samples compared to the corresponding cell lines. The identification of these candidate genes as common differentially expressed in brain and liver metastases, and their validation in our two breast cancer brain colonization models, reinforces the theory of a promoting role of stromal cells (especially innate immune cells) in the colonization of the target organ during metastasis.

3.2   Role of tumor-associated macrophages in promoting brain metastasis

In the first part of this work, two breast cancer brain colonization mouse models have been described, and the decisive role of the microenvironment in promoting the colonization of the brain by tumor cells has been highlighted.

In the CNS, metastatic tumors have been shown to be infiltrated by macrophages (Joyce & Pollard, 2009). In spite of this, due to the lack of reliable markers that distinguish microglia and macrophages coming from the bone marrow, it is still unclear whether these macrophage populations consist only of tissue specific macrophages, or whether bone marrow derived macrophages also participate in the colonization of the brain.

For this reason, in this section I focus on the role of monocyte-derived macrophages (coming from the bone marrow) in the colonization of the brain and the formation of metastases. Furthermore, I try to pharmaceutically re-educate those metastasis-promoting macrophages by blocking the PI3K/Akt signaling pathway. As already discussed in the Introduction (see 1.2.1.1.2) the PI3-kinase seems to be a feasible and appealing target for the treatment of the tumor associated microenvironment in brain metastases. In this work, the PI3K is blocked with BKM120 (buparlisib), an oral pan-PI3K inhibitor developed by Novartis Oncology.

3.2.1 BKM120 effectively blocks the PI3K/Akt signaling pathway

In a first approach I tested the effect of BKM120 on a panel of human and murine breast cancer cell lines and primary murine stromal cells. I tried different concentrations ranging from 0.01 nM to 1 µM. As can be seen in Figure 27, BKM120 affects the survival of human breast cancer cell lines (A-C), primary murine stromal cells (D-F) and murine breast cancer cells (G-H) in a dose-dependent manner.

Not surprisingly, the human breast cancer cells MCF-7 showed higher sensitivity to BKM120, probably due to their PIK3CA mutation in the catalytic subunit p110α (Maira et al., 2012). These data confirm the observations made by others regarding the efficiency of BKM120 in vitro.
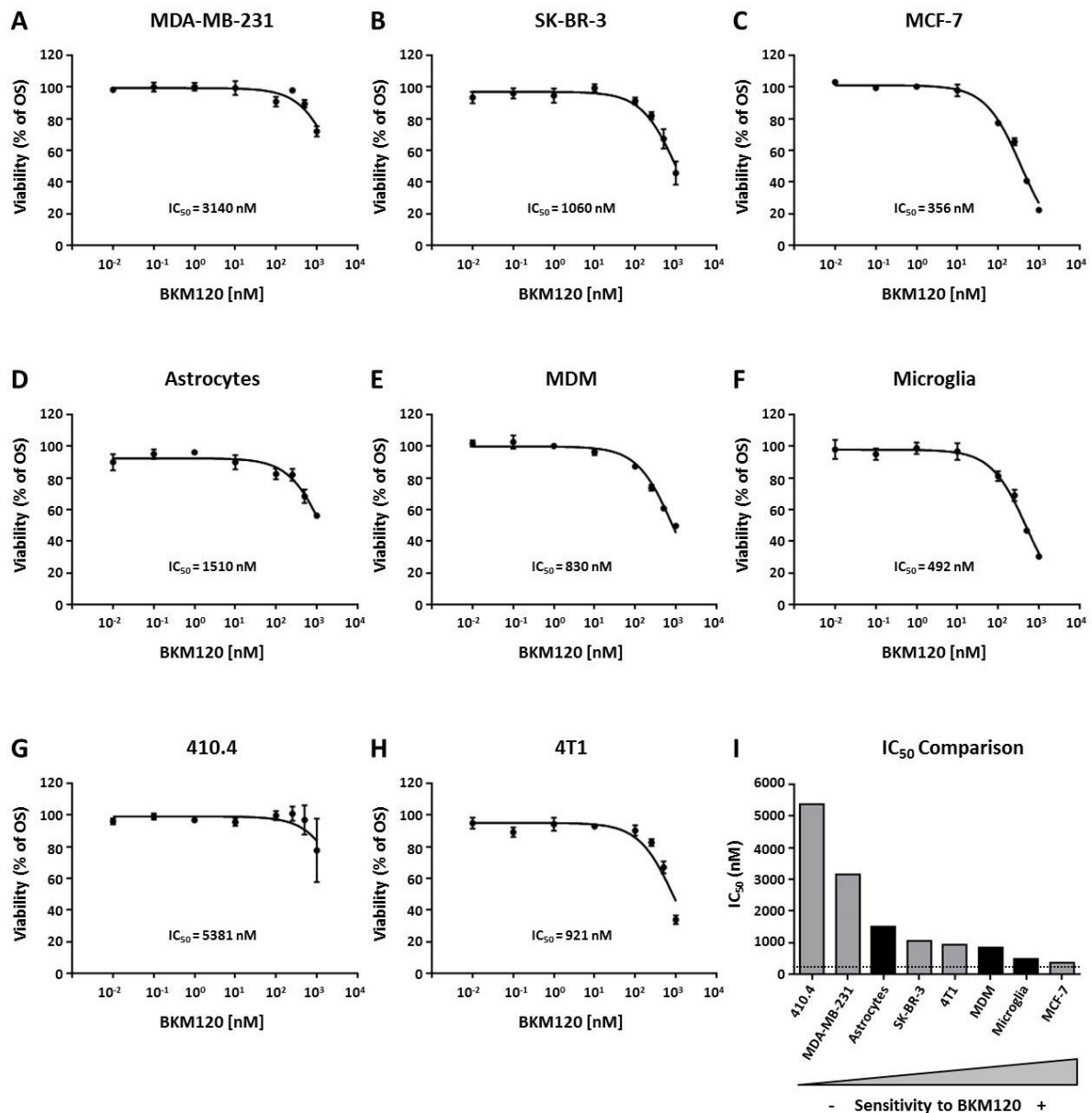
Figure 27: BKM120 has an effect on survival of breast cancer and primary murine stromal cells
MTT assay of human breast cancer cell lines **(A-C)**, primary murine stromal cells **(D-F)** and murine breast cancer cells **(G-H)** incubated for 72 h with increasing concentrations of the BKM120 inhibitor. OS = overall survival; means ± SD, n=3. **(I)** Comparison of the corresponding IC_{50} coefficients.

In the overview (I), it can be clearly seen that not only the breast cancer cell lines but also the primary murine stromal cells (black bars) are sensitive to BKM120. Interestingly, one of the murine breast cancer cell lines, 410.4 is relatively resistant to this compound, while 4T1 show a high

sensitivity. That means that we are provided with two perfect models for the study of the effect of BKM120 on the tumor associated microenvironment during metastasis progression.

According to these data, I decided to work further with a concentration of 250 nM, as this doesn't seem to have toxic effects on any of the breast cancer cell lines tested. At this concentration, BKM120 neither affects the survival nor the proliferation of the primary murine stromal cells (Figure 28 A-C) or murine cell lines (D-E). The cell proliferation was assessed by an xCELLigence assay. Remarkably, microglia show a slight decrease in their cell index when treated with BKM120; however, this reduction is not significant.
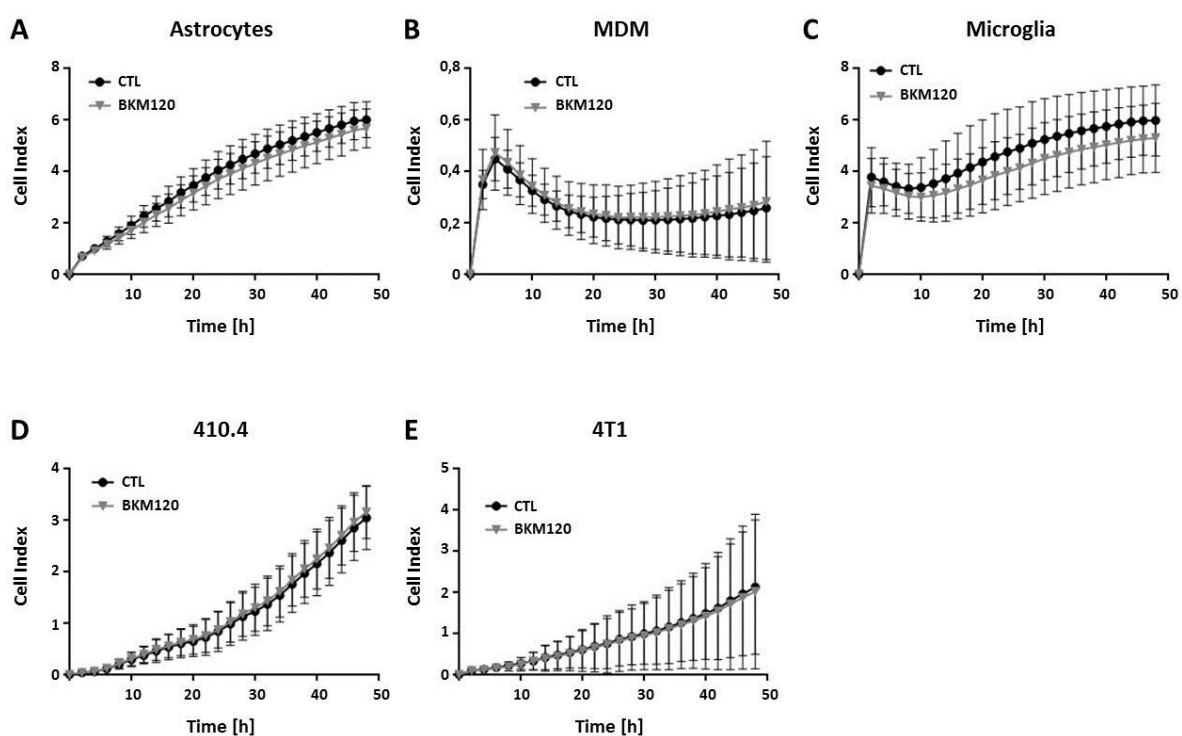
Figure 28: BKM120 does not affect cell proliferation of murine breast cancer or stromal cells
Cell Index (CI) of primary murine stromal cells **(A-C)** and murine breast cancer cells **(D-E)** incubated for 48 h with the BKM120 inhibitor (250 nM). Means ± SD, n=3. P-value was calculated with the unpaired t-test.

In another approach, I also tested whether BKM120 could effectively block the PI3K/Akt signaling pathway. As can be observed in Figure 29, buparlisib inhibited phospho-Akt and phospho-GSK3β (downstream effectors of PI3K), both in the stromal cells (A) and in the breast cancer cells (B), in a dose-dependent manner. In any case, at a concentration of 250 nM all the cells show almost no expression of phospho-Akt, which indicates a successful inhibition of the PI3K pathway. Although the breast cancer cell line 410.4 is rather resistant to BKM120, it also shows a reduced expression in phospho-Akt and phospho-GSK3β protein levels. This could be due to interactions with other signaling pathways.
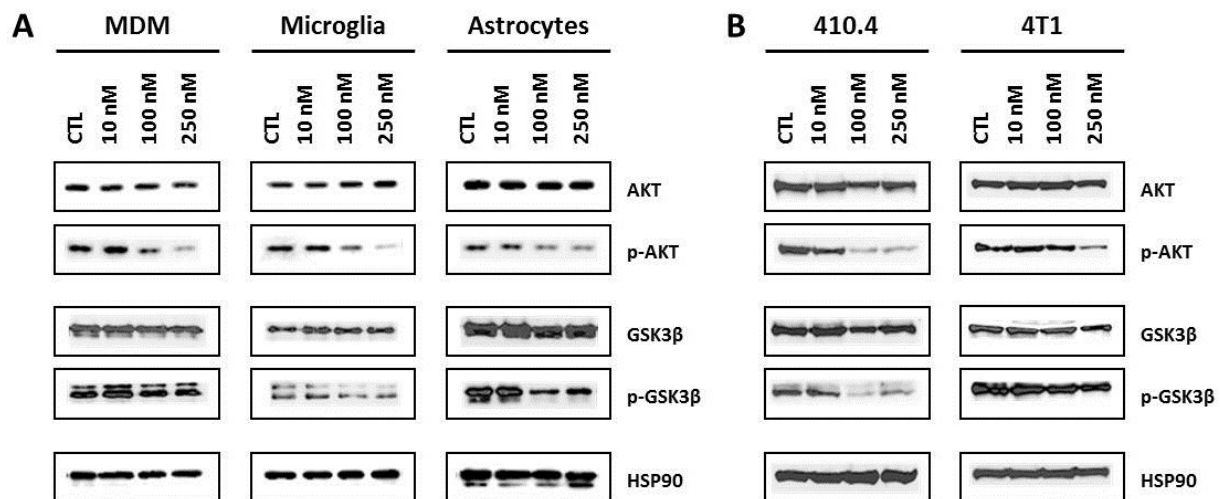
Figure 29: BKM120 effectively blocks the PI3K/Akt signaling pathway
Western Blot analysis of the downstream effectors of the PI3K/Akt signaling pathway, AKT and GSK3β and their phosphorylated forms, in murine primary stromal cells **(A)** and murine breast cancer cells **(B)** treated with the indicated concentrations of BKM120. HSP90 was used as loading control.

3.2.2 BKM120 reduces the stromal cell-induced invasion of tumor cells

In a next step I aimed to investigate the effects of BKM120 on the stromal cell-induced invasion of the breast cancer cell lines. For this purpose, I used a Boyden Chamber assay in which 410.4 are cocultured together with monocyte-derived macrophages (MDM), microglia (MG) or astrocytes (AS).

As can be seen in Figure 30, the addition of the inhibitor alone didn't produce any changes in the tumor cell invasion. However, when stromal cells are present, the invasion of the tumor cells suffers a 2.5-time increase in the case of MDM and microglia and is almost double in the cocultures with astrocytes. Nonetheless, the addition of BKM120 to the cocultures significantly reduced this induced-invasion almost to the control levels (120% in cocultures with MDM and 150% in cocultures with microglia). The invasion of 410.4 cocultured with astrocytes, on the other hand, wasn't affected by the inhibitor, maybe because these glial cells are more resistant to this compound than MDM and MG. Because 410.4 are relatively resistant to BKM120, it can be discarded that the reduction of their invasion is due to effects of BKM120 on the tumor cells, but only on the macrophages. In the case of 4T1 I couldn't detect any changes in their invasion, independently of the addition of stromal cells (data not shown).
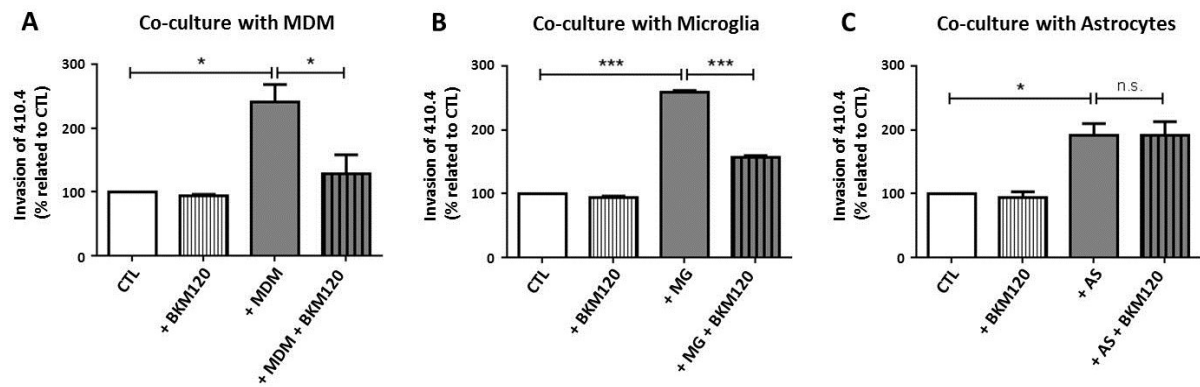
Figure 30: Effect of BKM120 on tumor cell invasion
Boyden chamber assay of the 410.4 breast cancer cell line cocultured with MDM **(A)**, microglia **(B)** or astrocytes **(C)**. The addition of the stromal cells increases the invasion rate of tumor cells. The treatment with BKM120 reduces the stromal cell-induced invasion in cocultures with MDM and microglia. P-values were calculated with the unpaired t-test (means ± SD, n=3; *p<0.05, **p<0.01, ***p<0.001).

In a next approach I also tested the inhibitor in our ex vivo organotypic brain slice model. This model consists of a brain slice cocultured with a matrigel plug, where the tumor cells are embedded (see Figure 31 A). With this method, I studied the invasion of the breast cancer cell line 4T1 into the brain slice. As Figure 31 shows, when BKM120 is not present (CTL), the tumor cells (in green) show high/moderate grades of invasion (+++ and ++). However, the addition of the inhibitor significantly reduces this invasion in a concentration-dependent manner (see Figure 31 B-C).

Furthermore, BKM120 didn't only affect the tumor invasion, but also the activation of microglia/macrophages (in purple) and astrocytes (in red). In the case of microglia/macrophages, I quantified the tumor plug area invaded by them. In this case, I could only observe a tendency to lower amounts of microglial cells present in the tumor plug (see Figure 31 D). However, the length of the astrocytic protrusions into the tumor plug was significantly decreased when BKM120 was added to the cocultures, in a concentration-dependent manner (see Figure 31 E). These data indicate that BKM120 not only affects the behavior of the tumor cells but also the activation of the brain parenchymal cells.
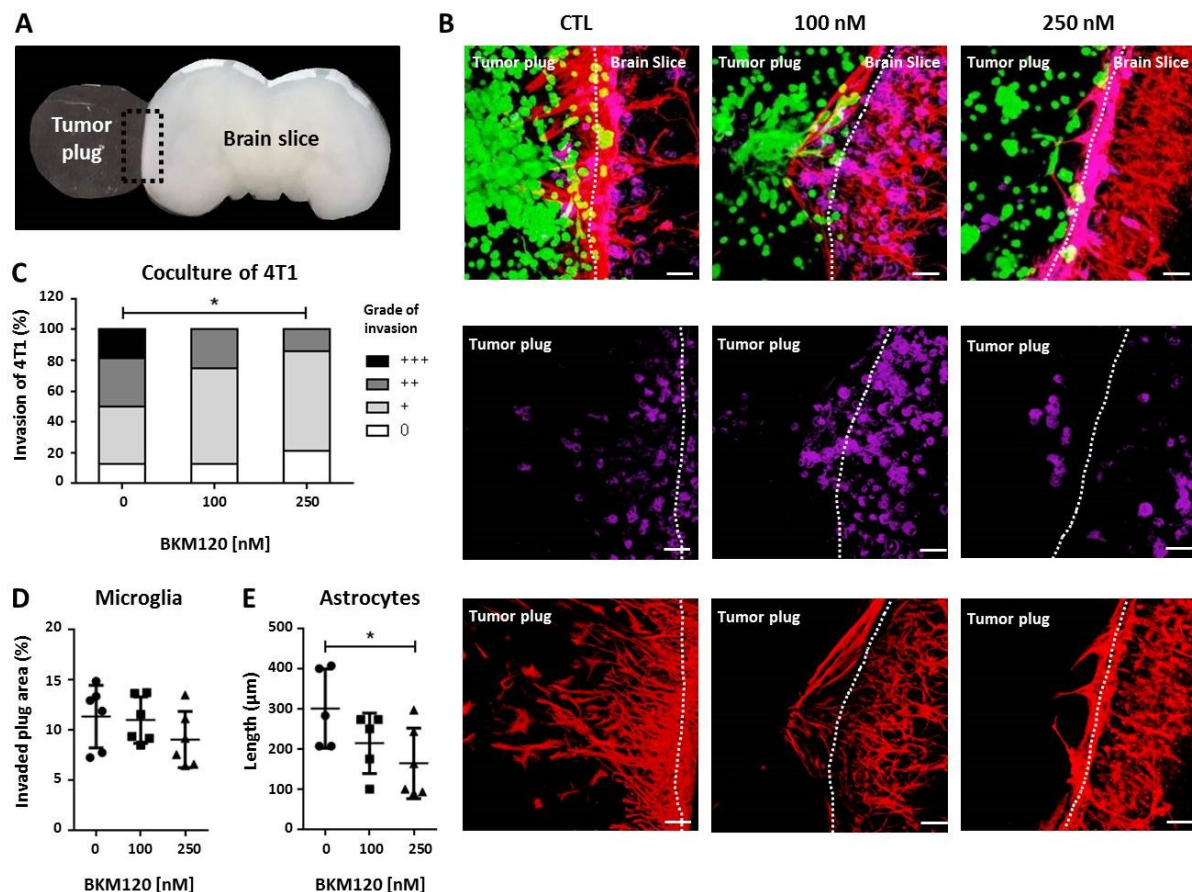
Figure 31: Effect of BKM120 on tumor cell invasion and immune activation

(**A**) Overview of an organotypic brain slice coculture. **(B)** Representative images of the cocultures taken with a confocal microscope (green: GFP-transfected 4T1 cells; violet: microglia/macrophages, stained with ILB4-Alexa Fluor 647; red: astrocytes, stained with GFAP-TRITC). Scale bars represent 50 µm. **(C)** Quantification of invasion of 4T1 cells treated with different concentrations of BKM120 in organotypic brain slice cocultures. Data represent the percentage of the degree of cell invasion into the brain slice. P-values were calculated with the Spearman's test (means ± SD, n≥ 12; *p<0.05, **p<0.01, ***p<0.001). **(D-E)** Quantification of the tumor plug area invaded by microglia/macrophages **(D)** and of the length of astrocytic protrusions **(E)** in organotypic brain slice cocultures treated with the indicated concentrations of BKM120. Data represent the percentage of microglial cell invasion into the brain slice or the length of the astrocytic protrusions. P-values were calculated with the unpaired t-test (means ± SD, n=5; *p<0.05, **p<0.01, ***p<0.001).

3.2.3 Effect of BKM120-treatment of MDM in vivo

Finally, I decided to test BKM120 in the breast cancer colonization mouse models. For this purpose I isolated monocyte-derived macrophages (MDM) from the bone marrow of adult BALB/c mice (10 to 12 week-old) and cultured them for one week. After that, I treated the MDM with BKM120 at a concentration of 250 nM or with PBS (CTL) overnight, and injected them sterotactically together with the breast cancer cells into the right hemisphere of BALB/c mice with the same strain and background. Of note, the tumor cells weren't treated at all with the inhibitor. An overview of the experiment design is illustrated in Figure 32.
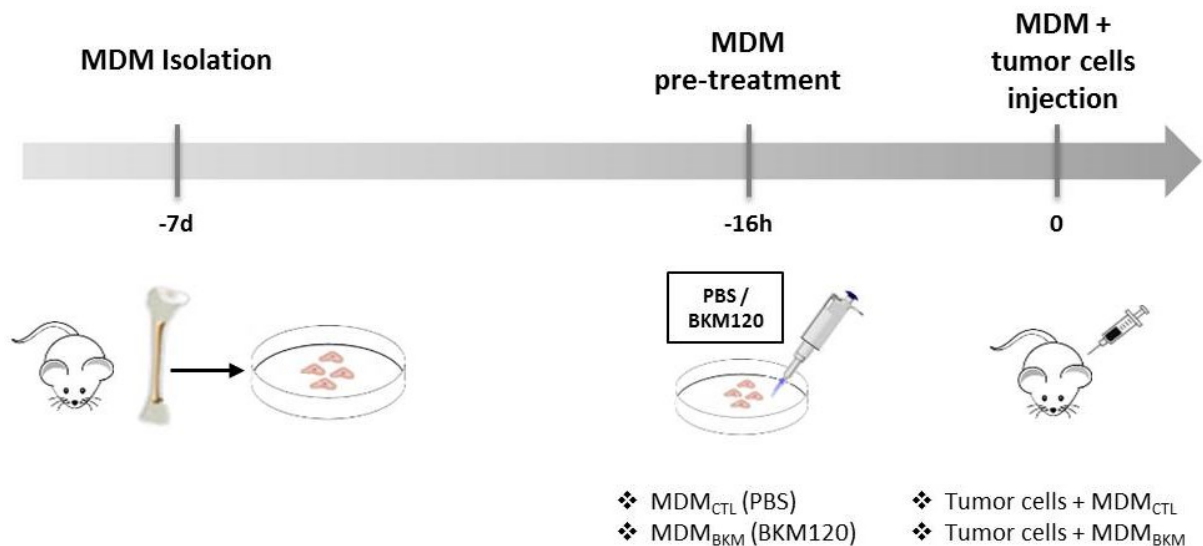
Figure 32: Experiment design

Monocyte-derived macrophages (MDM) were isolated from the bone marrow of adult mice and cultured for one week. The MDM were treated with BKM120 at a concentration of 250 nM or with PBS (CTL) overnight, and sterotactically injected into syngeneic mice together with the breast cancer cells.

3.2.3.1   Effect of BKM120-treatment of MDM in the 410.4 mouse model

In the first approach I stereotactically injected 250000 monocyte-derived macrophages (MDM) into the right hemisphere of 10-12 week-old BALB/c mice together with 100000 410.4 breast cancer cells (ratio 1:2.5) embedded in ECM. In this case, I didn't see any significant difference in the overall survival of the mice injected with the tumor cells and the untreated or pre-treated MDM, but only a cautious tendency (see Figure 33). I suspect that the long duration of the experiment with this cell line (over 12 weeks) could be responsible for these results. In this context, the single treatment of the tumor-associated macrophages with BKM120 may not be enough to get a prolonged protective effect against metastasis formation.

Figure 33: BKM120-treatment of MDM does not prolong survival in the 410.4 model
Overall survival of mice injected with the breast cancer cell line 410.4 and monocyte-derived macrophages treated with PBS (CTL) or BKM120 (BKM). P-value was calculated with the Log-rank (Mantel-Cox) test.

Furthermore, I also analyzed the invasion pattern of the 410.4 in the brain parenchyma of mice stereotactically injected with the breast cancer cells and untreated or BKM120 pre-treated MDM (see Figure 34). Consistently with the survival data, no relevant changes in the brain tissue of the injected mice could be observed; neither in the infiltration pattern of the tumor cells (A-B), nor in the activation status of macrophages/microglia (C) or astrocytes (D).
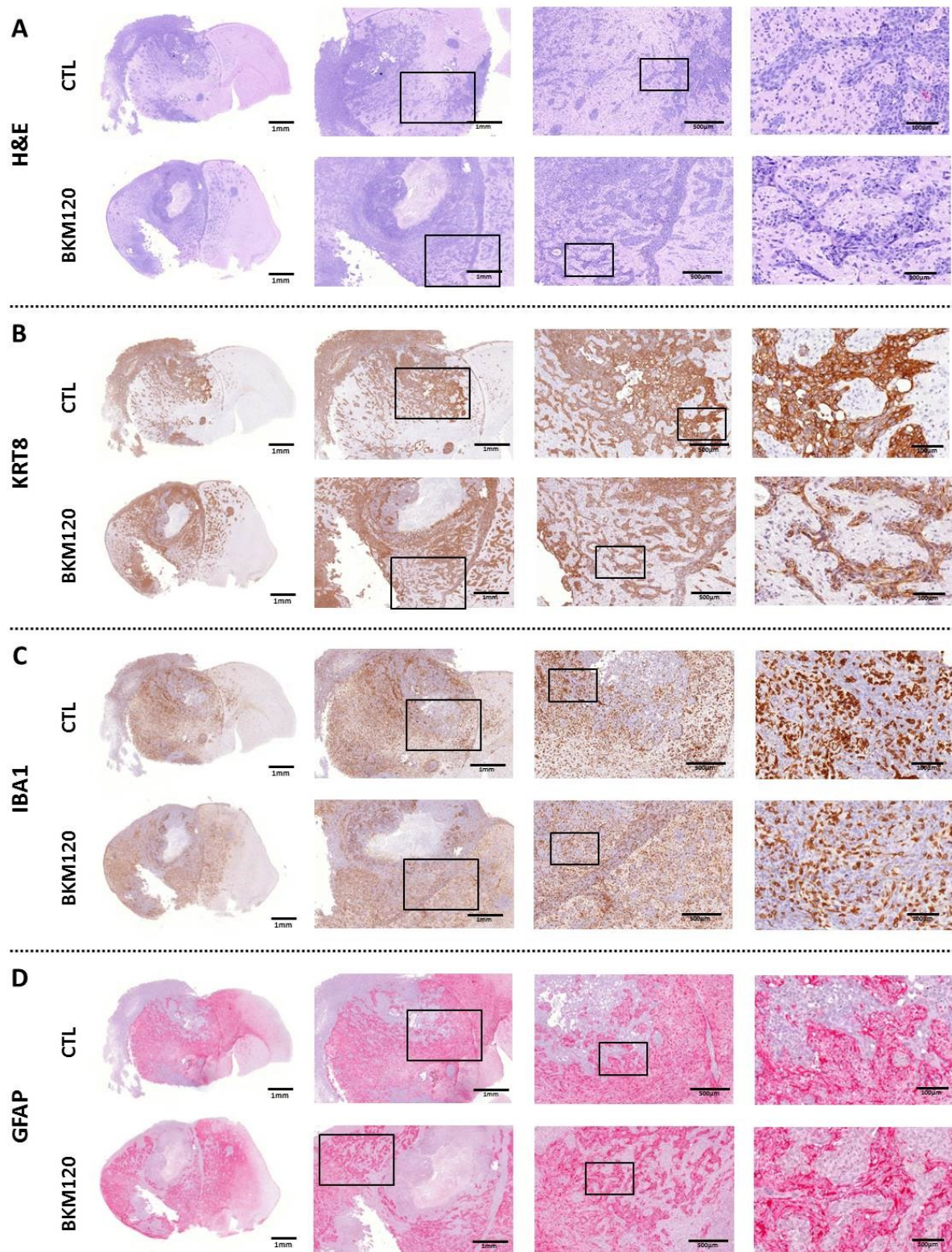
Figure 34: BKM120-treatment of MDM does not change the infiltration pattern of 410.4 cells
Immunohistochemistry (IHC) staining of hematoxylin & eosin **(A)**, keratin 8 **(B)**, microglia/macrophages **(C)** and astrocytes **(D)** in brain metastases of 410.4 injected with untreated (CTL) or BKM120 pre-treated MDM (BKM120). Representative microphotographs of sagittal brain sections at the level of the anterior striatum are shown.

The immunohistochemistry data shown above could be confirmed by means of real time PCR (see Figure 35). In this case, the brain tissue of the mice stereotactically injected with 410.4 and untreated or pre-treated macrophages didn't show any significant differences neither in the tumor load (A), nor in the activation status of microglia/macrophages (B) or astrocytes (C).

Furthermore, I also analyzed markers related to the CSF1 signaling loop. As already explained in the Introduction (see 1.2.1.1.1) this loop may be involved in macrophage-associated tumor promotion. In this context, cancer cells express the colony-stimulating factor 1 (CSF1), which acts as a potent chemoattractant and activator for CSF1R-expressing macrophages. As can be seen in Figure 35, the real time PCR analysis of the metastases from mice stereotactically injected with the breast cancer cell line 410.4 and monocyte-derived macrophages untreated (CTL) or pre-treated with BKM120 (BKM120) didn't reveal any significant differences in the expression levels of the *Csf1r* (D) or its ligands in the CNS, *Csf1* (E) and *Il34* (F).
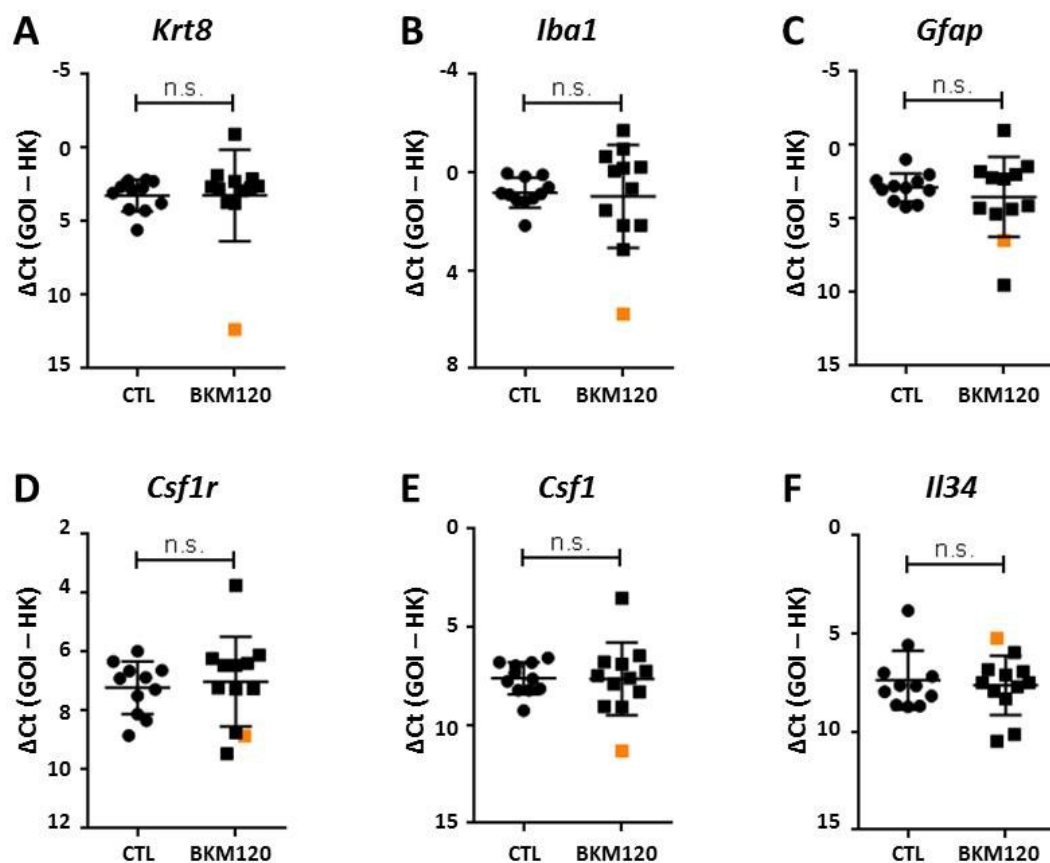
Figure 35: BKM120-treatment of MDM neither reduces the tumor load nor influences the stromal cell activation or the CSF1 signaling

Real time PCR analysis of *Krt8* **(A)**, *Iba1* **(B)**, *Gfap* **(C)**, *Csf1r* **(D)**, *Csf1* **(E)** and *Il34* **(F)** in metastatic tissue of mice stereotactically injected with the breast cancer cell line 410.4 and monocyte-derived macrophages treated with PBS (CTL) or BKM120 (BKM). The orange square indicates the mouse without the event of metastases. *Gapdh* and *Pgk1* were used as house-keeping (HK) genes. P-value was calculated with the unpaired t-test.

3.2.3.2   Effect of BKM120-treatment of MDM in the 4T1 mouse model

In the case of the experiment with 410.4, I could observe a cautious tendency in the overall survival of the mice stereotactically injected with macrophages pre-treated with BKM120. However, the analysis of the brain tissue didn't reveal any differences, neither in the tumor cell infiltration nor in the CSF1R signaling. As already mentioned, the long duration of the experiment could be responsible for these results. Because of that, I repeated the experiment in the 4T1 colonization model. These cells have a much higher Colonization Index and metastases arise approximately 3 weeks after the stereotactical injection of the tumor cells, which could be beneficial to my purposes.

In a first approach with a small number of animals, I stereotactically injected 10000 4T1 tumor cells together with 25000 monocyte-derived macrophages (MDM) (ratio 1:2.5) embedded in ECM into the right hemisphere of 10-12 week-old BALB/c mice. Here, I could already see a tendency in the overall survival of the mice (see Figure 36 A). However, I suspected that the number of injected cells was probably too high, which resulted in shortened disease-free survival for the mice (less than 3 weeks) and could mask the effect of BKM120.

Thus I repeated the experiment but injected a lower amount of 4T1 (1000 cells), maintaining the ratio (1:2.5) with the MDM, in the right hemisphere of syngeneic mice. This time I could see very clearly that the ex vivo pre-treatment of the monocyte-derived macrophages with BKM120 at a concentration of 250 nM had a positive effect on the overall survival in vivo (see Figure 36 B). Interestingly, one of the mice that was stereotactically injected with pre-treated macrophages had indeed a 50% longer OS than the mice injected with the tumor cells and the untreated macrophages. These data indicate that the in vitro effects of BKM120 were mirrored in this murine breast cancer brain colonization model.

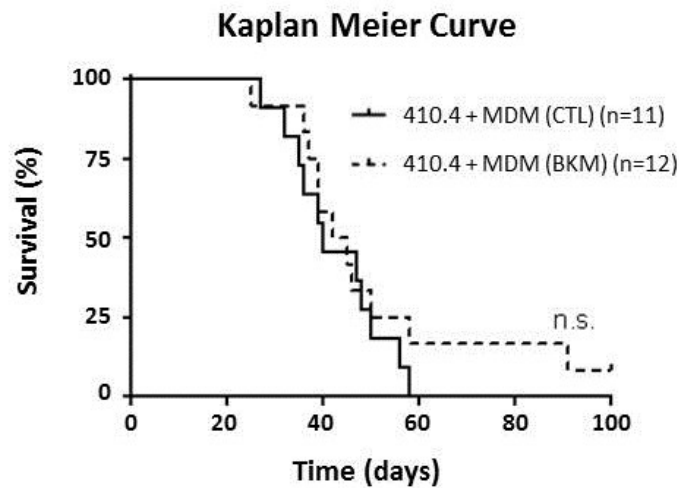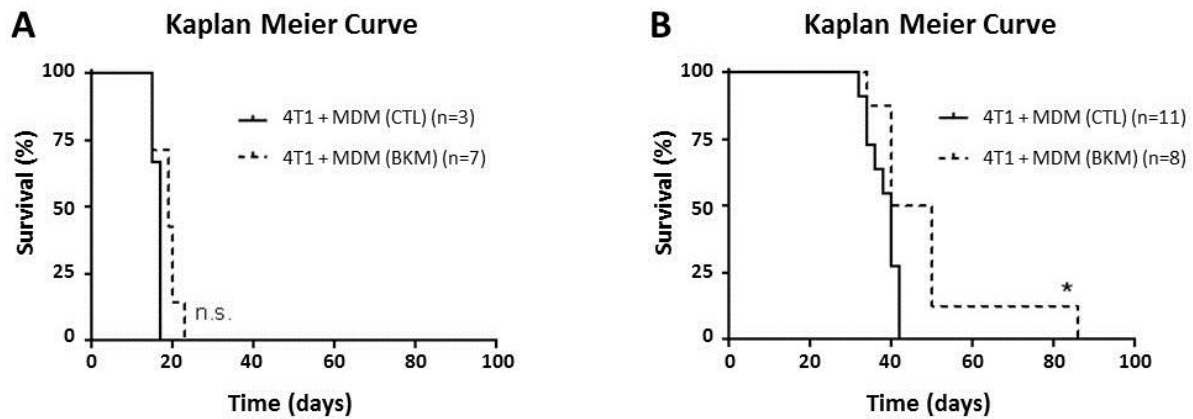**Figure 36: BKM120-treatment of MDM prolongs survival in the 4T1 model**

Overall survival of mice injected with the breast cancer cell line 4T1 and monocyte-derived macrophages treated with PBS (CTL) or BKM120 (BKM). Mice were stereotactically injected with 10000 cells **(A)** or 1000 cells **(B)**. P-value was calculated with the Log-rank (Mantel-Cox) test (*p<0.05).

Of note, I observed a different pattern of infiltration between the mice stereotactically injected with 4T1 and the control MDM, and those injected with BKM120 pre-treated MDM (see Figure 37, A-B). In the case of the control mice, the metastases demonstrated cohorts of infiltrating cells in the brain parenchyma, that were detected in areas far away from the tumor core. On the other hand, the metastases of mice stereotactically injected with 4T1 and the pre-treated macrophages showed a round well-defined pattern, with no infiltration zones. This observation may imply that the activated macrophages that haven't been treated with BKM120 promote the infiltration and colonization of the brain parenchyma, whereas the BKM120-treated macrophages may control tumor infiltration. Interestingly, the activation status of the microglia/macrophages (C) or the astrocytes (D) didn't seem to suffer any changes, as could also be confirmed by real time PCR (see Figure 38).
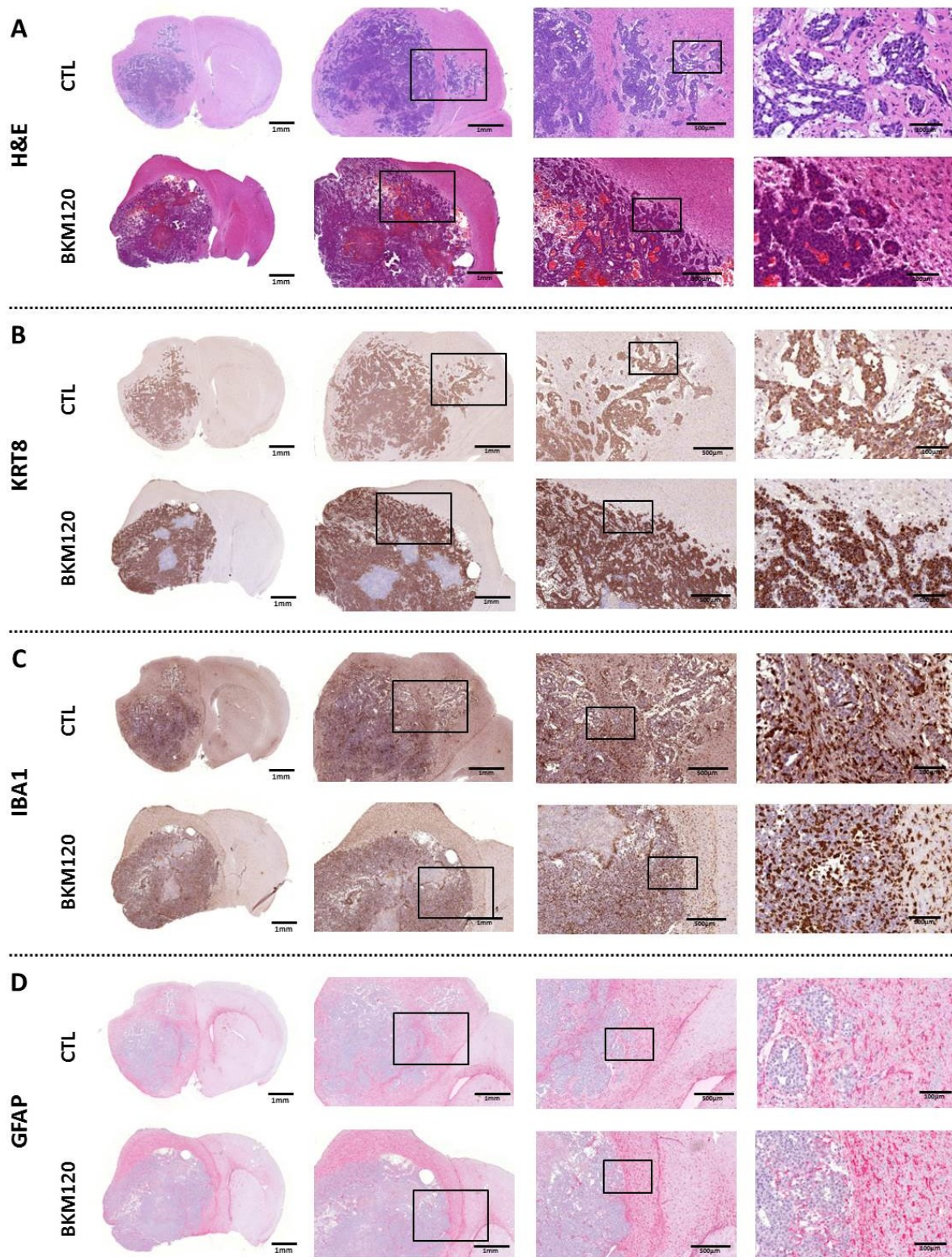
Figure 37: Mice injected with 4T1 and pre-treated MDM show a well-defined infiltration pattern
Immunohistochemistry (IHC) staining of hematoxylin & eosin **(A)**, keratin 8 **(B)**, microglia/macrophages **(C)** and astrocytes **(D)** in brain metastases of 4T1 injected with untreated (CTL) or BKM120 pre-treated macrophages (BKM120). Representative microphotographs of sagittal brain sections at the level of the anterior striatum are shown.

In order to uncover the mechanisms responsible for the positive effects of BKM120 in vivo, I analyzed the brain metastatic tissue by real time PCR and looked for candidate genes at a molecular level (see Figure 38). Interestingly, the tumor load in mice injected with BKM120 pre-treated macrophages was significantly reduced (A), which speaks to the anti-colonizing effects of BKM120. As was already commented, I didn't observe any significant changes in the expression levels of macrophages/microglia (B) or astrocytes (C). However, the treatment of BKM120 resulted in decreased levels of *Csf1r* (D) and *Csf1* (E), as expected. I also checked *Il34* (F), the alternative ligand for *Csf1r* in the CNS, which remained unchanged. These data indicate that the CSF1 signaling loop could be effectively blocked on the macrophages by targeting the PI3-kinase with BKM120.
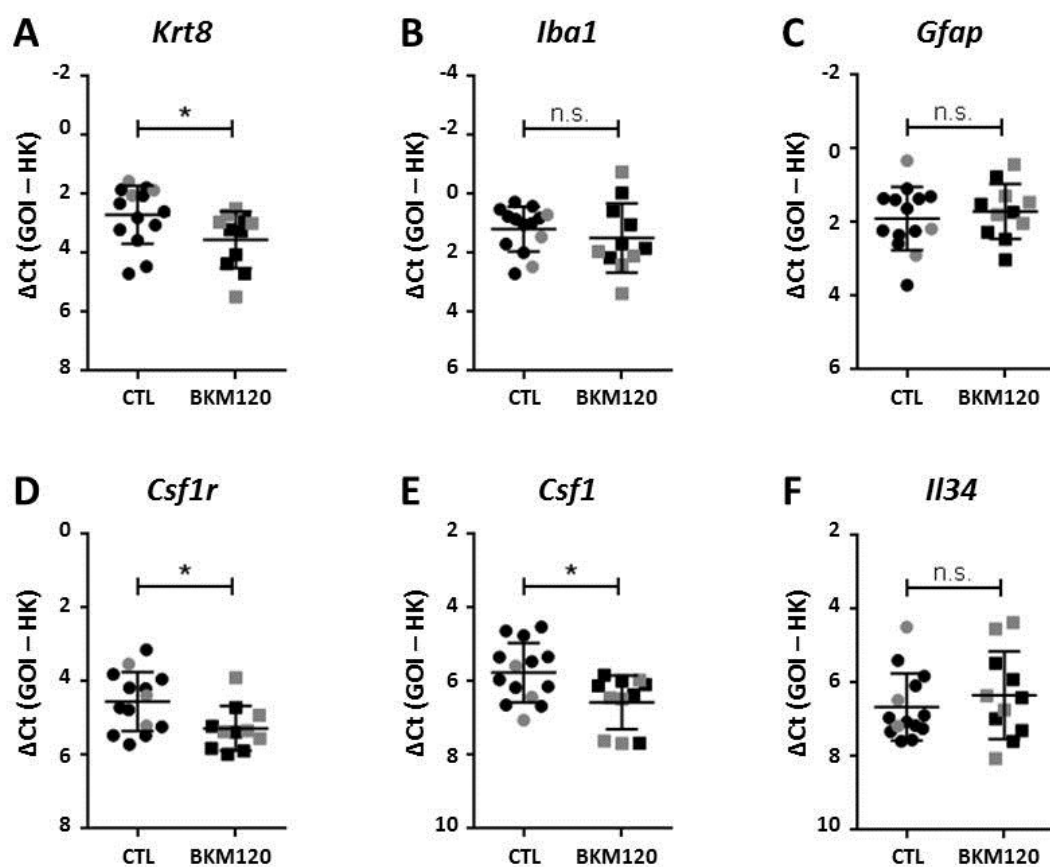
Figure 38: BKM120-treatment of MDM blocks the CSF1 signaling
Real time PCR analysis of *Krt8* **(A)**, *Iba1* **(B)**, *Gfap* **(C)**, *Csf1r* **(D)**, *Csf1* **(E)** and *Il34* **(F)** of mice stereotactically injected with the breast cancer cell line 4T1 and monocyte-derived macrophages treated with PBS (CTL) or BKM120 (BKM). The grey symbols represent the mice injected with 10000 cells. *Gapdh* and *Pgk1* were used as house-keeping (HK) genes. P-value was calculated with the unpaired t-test (*p<0.05).

To sum up, the blockade of PI3K with BKM120 leads to a significant reduction of the CSF1 macrophage activation loop (lower levels of *Csf1* and *Csf1r*, though remaining *Il34*); while the number of macrophages/microglia (*Iba1*), as well as other stromal cells also present in the brain parenchyma like astrocytes (*Gfap*), remain unchanged. All this, results in a reduced tumor load (*Krt8*),

which is reflected by less tumor cell infiltration, and an increased overall survival of the mice injected with tumor cells and pre-treated macrophages.

3.2.4 BKM120 treatment leads to a macrophage-switch

Lastly, I wanted to investigate whether the blockade of the CSF1R by inhibition of the PI3-kinase with BKM120 could provoke a macrophage-switch from a tumor-supporting into a tumor-suppressing phenotype. A bioinformatic analysis revealed the "regulation of transcription" as one of the differential processes between untreated and BKM120 pre-treated monocyte-derived macrophages (data not shown). As has already been explained, tumor-associated macrophages (TAM) are myeloid-derived inflammatory cells. I found in the literature that the most important transcriptional activator involved in the development of myeloid cells is the transcription factor PU.1 (also known as *Spi1*). This hematopoietic transcription factor plays a key role in the differentiation or activation of macrophages (Celada et al., 1996). For this reason, I decided to study the expression of *Spi1* in the metastatic tissue of mice stereotactically injected with untreated or BKM120-treated macrophages by real time PCR. Interestingly, *Spi1* also suffered a significant reduction in the treated mice (see Figure 39 A). Due to its key role in macrophage differentiation, the downregulation of *Spi1* may speak to a change in the activation status of tumor-associated macrophages, which reinforces the theory of a phenotypic switch.

Furthermore, I could also detect the downregulation of the Programmed cell death 1 ligand 1 (*Pdl1)* in treated mice (see Figure 39 B). This factor is notably expressed on tumor-associated macrophages (Loke & Allison, 2003), and cancer cells may misuse the upregulation of Pdl1 to evade the host immune system through cytotoxic T-cell inactivation. Moreover, high tumor expression of Pdl1 has been shown to be associated with higher tumor aggressiveness and an increased risk of death (Thompson et al., 2004). In this context, the downregulation of *Pdl1* in the metastatic tissue may also indicate a positive switch of the macrophages into a tumor-suppressing phenotype.
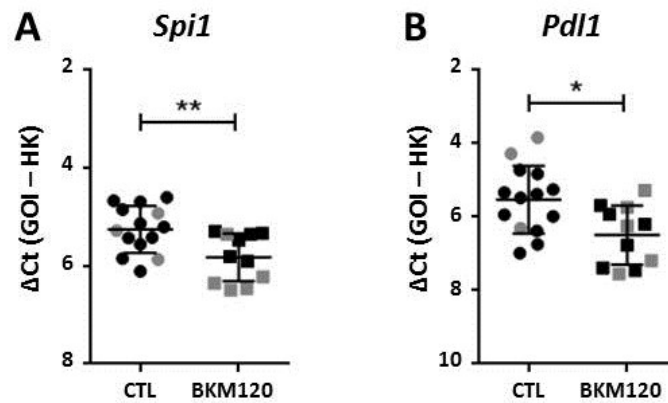
Figure 39: BKM120-treatment provokes a phenotypic switch in MDM

Real time PCR analysis of *Spi1* **(A)** and *Pdl1* **(B)** in metastatic tissue of mice stereotactically injected with the breast cancer cell line 4T1 and monocyte-derived macrophages treated with PBS (CTL) or BKM120 (BKM). The grey symbols represent the mice injected with 10000 cells. *Gapdh* and *Pgk1* were used as house-keeping (HK) genes. P-value was calculated with the unpaired t-test (*$p < 0.05$; **$p < 0.01$).

Taken together, these data indicate that the treatment of the PI3-kinase by BKM120 in monocyte-derived macrophages leads to the blockade of the CSF1R signaling pathway, which in turn provokes a phenotypic switch of the tumor-associated macrophages into a tumor-suppressing phenotype. This change is represented by the downregulation of important tumor-associated macrophage-related factors like *Spi1* and *Pdl1*. All this results in a reduction of the tumor load and prolonged overall survival of the mice injected with the breast cancer cell line 4T1 and the BKM120 pre-treated macrophages.

4   Discussion

4.1   Colonization models: a gap in the metastatic cascade

In the past decades, several experimental systems have been developed to model one or more steps of the metastatic cascade. The first steps of the metastatic cascade are indeed pretty well understood (Kessenbrock et al., 2010; Roussos et al., 2011). However, to date, there are not sufficient adequate models with which to study the most rate limiting and decisive step, namely the colonization of the target organ. Taking into account the key role of the colonization, especially from a clinical point of view (Fidler, 1970; Vanharanta & Massague, 2013), I focused my work on the study of the factors that could influence the colonization of the brain.

4.1.1 Comparison of the 4T1 and 410.4 colonization models

In order to study the colonization of the brain I established a colonization mouse model by means of stereotactically injecting the 4T1 and 410.4 breast cancer cell lines in syngeneic mice. These cell lines had already been described in the literature as high and low/moderate metastatic respectively. Experiments in spontaneous models have indicated that both cell lines seem to differ in their metastatic potency regarding the first steps of metastasis (Aslakson & Miller, 1992; Miller et al., 1983). However, until now, there were no publications comparing the colonization potential of the parental 410.4 with their derivate 4T1. In this study I could confirm that both cell lines show a significant difference in their colonization capacity in the CNS, which makes this pair an ideal model system to study the colonization step in more detail.

My results indicate that the 4T1 is a much more aggressive cell line than the parental cells 410.4, which confirm the observations made by others regarding the metastatic potential of these cell lines. To assess the difference in the colonization potential of both cell lines, several parameters were regarded.

From a clinical point of view, a very important factor that describes how aggressive tumors are, is the overall survival of patients. In fact, this parameter is also used in clinical trials to determine the effectivity of new therapeutic agents. In the colonization models, the median overall survival of the mice stereotactically injected with 4T1 was remarkably shorter than in the case of the 410.4 model. The 4T1 produced clinically symptomatic metastases in approximately 3 weeks; while the 410.4

needed almost 8 weeks. These data indicate that the 4T1 are more aggressive than the parental 410.4.

From the cancer stem cell biology we know that the amount of tumor cells which are needed for tumor formation is a very important factor. According to the hierarchical model, also known as cancer stem cell (CSC) model, only a small subset of tumor cells within the tumor bulk exhibit the capacity to initiate and sustain tumor growth and are responsible for tumor relapse and metastasis (Gupta, Chaffer, & Weinberg, 2009). Thus, the fewer cells needed to initiate metastatic outgrowth, the more tumorigenic the cells are. In this context, the 410.4 colonization model required 100 times more cells than the 4T1 for the development of macro-metastases, which indicate a lower tumorigenicity of the 410.4 compared to 4T1.

Finally, the percentage of successful colonization or uptake has also been used for the description of the aggressiveness of mouse systems (Pulaski & Ostrand-Rosenberg, 2001; Tao et al., 2008). This parameter may therefore provide an idea of the grade of tumorigenicity of the cell lines. In line with that, from 11 mice injected with 410.4, 10 developed metastases, while in the case of 4T1 all mice did. This fact points out again the higher aggressiveness of the 4T1.

4.1.1.1   The Colonization Index as quantification tool of the colonization potential of the 4T1 and 410.4 colonization models

All these parameters described above suggest that both cell lines differ in their colonization potential. However, the analysis of the individual parameters may only partially describe the differences between the models. In order to obtain a detailed and accurate comparison of the real colonization potential of the models, I developed "the Colonization Index". This equation includes the most relevant parameters for the quantification of the colonization potential of the cell lines, namely: the rate of successful colonization of the brain, the number of injected cells, and the median overall survival of the mice.

The Colonization Index is thus a more accurate calculation to compare the colonization potential of different cell lines. This equation not only describes how aggressive a cell line is, but quantifies it. According to my results, it can be concluded that the 4T1 are much more aggressive than the parental 410.4, since their colonization index is 250 times higher (0.5 vs 0.0018). Using the Colonization Index, I could not only confirm the observations made by others regarding the metastatic potential of the cells, but I also added valuable information, namely the quantification.

With this tool, the description of the metastatic potential of the cells is no longer gradual (low/moderate/high), but becomes a number that allows a much more accurate comparison between different models. Therefore, this novel method could be helpful in future to compare the colonization potential between different cell lines in in vivo models.

4.1.2 Investigating the factors responsible for the different colonization potentials

Once I had developed colonization models with the 4T1 and 410.4 and confirmed their different colonization potential by means of the Colonization Index, I wanted to investigate which factors may be responsible for these different colonization skills between the cells. The fact that two related cell lines (on the one hand, the parental cells 410.4; and on the other hand, the much more aggressive derivate 4T1) show very different colonization potentials makes them a very interesting model to investigate which factors are really implicated in the colonization of the CNS.

4.1.2.1   Both models display an epithelial phenotype

In the brain colonization models of 4T1 and 410.4 I was able to demonstrate the formation of brain macro-metastases that closely reflect the human disease. The IHC study of the macro-metastases revealed that both cell lines display the same growth pattern in the brain parenchyma. The 410.4 and 4T1 share the typical epithelial phenotype of carcinomas, characterized by a stratified pattern and the uniform expression of cytokeratin 8 (Painter, Clayton, & Herbert, 2010).

Additionally, in both models the tumor cells infiltrate the adjacent brain parenchyma. However, they don't invade as single cells, as would be the case of mesenchymal cells, like lymphoma. On the contrary, infiltrating cohorts and clusters of cells can be detected in the brain parenchyma. This cohort infiltration pattern observed in the 410.4 and 4T1 colonization models has already been described by our group to be typical for human breast cancer brain metastases (Siam et al., 2015).

The fact that the tumor cells invade the adjacent tissue as groups or cohorts of cells, and that they express high and uniform levels of the epithelial marker KRT8, indicate that both cell lines display an epithelial phenotype. In view of that, the infiltration pattern of the tumor cells can be discarded as a responsible factor for the different colonization potentials between the 4T1 and 410.4 colonization models.

4.1.2.2 EMT as responsible mechanism for the different colonization potentials?

One hallmark of a malignant primary tumor is its tendency to invade and infiltrate local and adjacent structures. Carcinomas develop from epithelial cells. However, cells must lose their epithelial character and acquire mesenchymal features in order to get into the surrounding tissues. This process is called epithelial to mesenchymal transition (EMT) and is associated with high tumorigenicity and poor prognosis. The acquisition of a mesenchymal phenotype requires the downregulation of the epithelial markers E-cadherin and cytokeratin and the upregulation of vimentin. Additionally, disseminated cancer cells must undergo a reverse process, called mesenchymal to epithelial transition (MET), to form epithelial metastases upon arriving at distant sites (Tsai & Yang, 2013). According to the EMT theory, the epithelial tumor cells that infiltrate the brain parenchyma at the metastasis/brain parenchyma interface should, for a second time during the metastatic process, acquire mesenchymal features.

In the case of the carcinoma cells, the 410.4 and the 4T1 fit perfectly into the criteria underlying the EMT theory in primary tumors. The low colonizing parental 410.4 express relative high levels of the epithelial marker E-cadherin and low levels of vimentin. On the contrary, the high aggressive 4T1 cells express low levels of E-cadherin and high vimentin levels, which may be associated with their higher metastatic potential (Berx & Van Roy, 2001; Kowalski et al., 2003).

However, in the metastases, not all criteria of the EMT are matched. In the case of the 410.4, I even detected focal upregulation of E-cadherin at the infiltration front of the metastases. These data indicate that the loss of E-cadherin is not a mandatory event for the invasion of tumor cells, at least in the metastases. On the other hand, the 4T1 could match this theory, since E-cadherin was almost absent in the metastatic tissue. However, the carcinoma cells were not micro-dissected from the metastatic tissue so I cannot rule out the possibility that E-cadherin is locally upregulated in the metastasis. In the metastatic tissue the assessment of vimentin was not performed, since this marker is known to have a very low specificity. In fact, it can be found in some carcinomas and may be co-expressed with CK in a wide range of tumors (Bahrami, Truong, & Ro, 2008).

Nonetheless, these results could indicate that the higher colonization potential of the 4T1 is associated with the loss of E-cadherin and the acquisition of mesenchymal features. However, despite the low or absent expression of E-cadherin in the metastatic tissue, brain metastases of 4T1 still express high and uniform levels of the epithelial marker CK8 and show an epithelial phenotype.

Thus, despite the loss of E-cadherin and expression of vimentin by 4T1 in the metastases, it doesn't necessarily mean that EMT is taking place during the process of colonization.

I suggest that the epithelial 4T1 may acquire some mesenchymal features that allow a higher Colonization Index, but retain their epithelial nature at the same time. In this context, vimentin may induce changes in the cytoskeleton and subsequent mechanical composition of the cells that support the first growth phase after stereotactical injection of the cells, as well as the invasion of the surrounding tissue. In this context, it is well known that vimentin confers elasticity to the tissues. The higher the concentration of vimentin, the more malleable a cell is. In line with that, it has been proposed that vimentin plays a mechanical role in the cytoskeleton of living cells (Wang & Stamenovic, 2002). In my view, vimentin could be responsible for the softening of cellular structures which makes the cells more resilient against shared stresses and other external influences. In this context, vimentin could be the responsible factor for conferring the 4T1 the necessary mechanical features to better resist the mechanical stresses during the colonization of the brain tissue. However, to determine the exact role of vimentin (and other possible adhesion molecules, like integrins or E-cadherin) during colonization, these molecules should be genetically targeted and modified. For example, an upregulation of vimentin in the 410.4 cells should lead to an increase in their Colonization Index, without leading to a mesenchymal phenotype.

In this sense, it can be concluded that the plasticity and the mechanical consistence of the cells conferred by mesenchymal markers like vimentin to the tumor cells could participate in the acquisition of a more flexible or malleable cellular structure, and therefore be responsible for the better uptake and faster development of a macro-metastasis which could influence significantly the CI. However, metastatic cells may not necessarily change their fundamental epithelial nature during this process.

4.1.2.3 The reaction of the microenvironment during the colonization of the brain

We and others have shown that the microenvironment plays an important role during the colonization of the brain (Chuang, van Rossum, et al., 2013; Pukrop et al., 2010). In fact, we have identified new triggers of metastases in the framework of the MetastaSys e:Bio consortium which are mainly related to the immune response.

One of the common differentially expressed genes identified in a DEG analysis of brain and liver metastases of 410.4, was the ionized calcium-binding adapter molecule 1 (IBA1). This gene was already identified by us as playing a decisive role during metastasis in the CNS. The identification of this gene by the DEG analysis confirms the importance of activated macrophages/microglia during colonization and sustains the observations made by others regarding the role of activated macrophages during metastatic progression (Joyce & Pollard, 2009; B. Qian et al., 2009).

The TYRO protein tyrosine kinase binding protein (TYROBP), also known as DAP12, was also identified as a candidate trigger of metastases. This protein binds the T cell receptor-associated protein kinase (ZAP-70) and the spleen tyrosine kinase (SYK) and therefore plays a role in signal transduction and inflammation. Our finding confirms the observations made by others regarding the metastatic promoting role of DAP12. Studies conducted by Shabo et al. showed that the expression of DAP12 in breast cancer cells participate in the recruitment of macrophages and is associated with the development of metastases (Shabo et al., 2013).

Finally, the chemokine (C-C motif) ligand 8 (CCL8) was also identified. Tumor cells produce CCL8, a small molecule that displays chemotactic activity for monocytes, lymphocytes, basophils and eosinophils. By recruiting leukocytes to sites of inflammation this cytokine may contribute to tumor-associated leukocyte infiltration and the formation of metastasis in target organs (Barbai et al., 2015).

These data highlight once again that the activation of the microenvironment is a key process during colonization. Because of that, it could be thought that the reaction of the microenvironment in the brain parenchyma may influence the colonization potentials of 4T1 and 410.4 in vivo. To assess this question, I characterized the presence and activation of the key players in the colonization of the brain, namely: microglia, astrocytes and T cells.

In the colonization models of 4T1 and 410.4 I found activated immune cells in the brain parenchyma, especially at the metastasis/brain parenchyma interface. Activated microglia/macrophages appeared inside and around the metastatic lesion, but not in the hemisphere that had not been infiltrated by tumor cells. The activation of these tissue specific macrophages could be assessed by means of IBA1. This marker has been used to detect activated microglia in ischemic brain (Ito et al., 1998; Ito, Tanaka, Suzuki, Dembo, & Fukuuchi, 2001). However, it is not a specific marker for microglial cells in the CNS, but it also includes activated macrophages immigrated from the blood stream (Ohsawa,

Imai, Sasaki, & Kohsaka, 2004). That means that, in the brain, microglia cannot be distinguished from other macrophage populations, yet.

Iba1 has been proposed by Khirade et al. as a candidate master gene regulator of immune-modulation and a very important player in the development of distant metastases (Khirade, Lal, & Bapat, 2015). Furthermore, our group has also demonstrated the promoting role of microglia/macrophages in the colonization of the brain (Chuang, van Rossum, et al., 2013). In this work, however, I only demonstrated the activation of microglia/macrophages in the brain parenchyma of mice that developed metastases, but not a colonizing promoting role of these.

Previously, we and others have described astrocytes as part of the gliosis reaction during the colonization of the brain (Chuang, van Rossum, et al., 2013; M. Zhang & Olsson, 1997). This led me to assume that astrocytes may also be activated in the mouse metastatic tissue. As expected, I could also detect activated astrocytic cells in the hemisphere that had been infiltrated by tumor cells. Remarkably, astrocytes were found surrounding the metastatic foci but almost none infiltrating the lesions.

These observations reinforce the data published by our group a few years ago regarding human samples. In this study we found activated microglia/macrophages at the interface of the metastasis and the brain parenchyma, and inside the metastasis; whereas activated astrocytes accumulated in the adjacent brain tissue and formed a barrier at the interface to the metastatic tissue (Chuang, van Rossum, et al., 2013).

Finally, I could also detect infiltrating T cells (CD3+) in the tumor mass of 4T1 and 410.4 brain metastases. T cells are the main effector cells of the adaptive immune system and migrate into the CNS only under pathological conditions (Platten et al., 2014). Although the brain has long been considered an 'immune-privileged' organ with limited capacity for inflammatory response, brain metastases have been shown to contain tumor infiltrating lymphocytes (TIL). Dense infiltration with cytotoxic TIL (CD8+) is indeed associated with improved survival prognosis; whereas, the presence of immunosuppressive TIL (CD4+) is associated with poor prognosis (Berghoff & Preusser, 2015). In the colonization models, I characterized the presence of T cells by means of the T cell receptor-CD3 complex which is implicated in T cell differentiation, activation and proliferation. However, the CD3 complex is common to cytotoxic and regulatory T cells. Because of that, my observations regarding T cell infiltration imply both types of TIL.

According to the IHC and real time PCR analysis, it can be concluded that the microenvironment becomes activated as a consequence of the colonization of the brain by tumor cells, and may therefore actively participate in this process. Interestingly, none of the activation markers described above (IBA1, GFAP, and CD3) was differentially expressed between the 4T1 and the 410.4 colonization models. That means that the activation of the metastatic microenvironment (microglia/macrophages, astrocytes and T cells) should not differently influence the colonization potentials of both cell lines. In line with that, the theory of a significant difference in the mechanical plasticity of the cells remains a more likely explanation for the higher colonization of the 4T1.

4.2   Role of tumor-associated macrophages (TAM) in the colonization of the brain

Despite the fact that the metastatic microenvironment of the 4T1 and 410.4 seems not to be the explanation for the significant difference of the CI, the organ specific defense could actively participate in the formation of macro-metastases during CNS colonization. Our group indeed demonstrated that the colonization of the brain induces a physiological damage response of the brain tissue in vitro. The destruction of the host tissue leads to activation of damage response of the resident defense system to protect, repair, and organize the wound healing. However, these signals may be misused by tumor cells to promote brain metastases (Chuang, van Rossum, et al., 2013).

However, not only the resident macrophages can exert tumor promoting functions in the course of metastases, but also macrophages coming from the bone marrow, which are also referred to as "tumor-associated macrophages" (TAM). TAM have been shown to play different roles in the metastatic cascade. In the primary tumor, they support tumor-associated angiogenesis, promote tumor cell invasion, migration and intravasation, and suppress antitumor immune responses. In fact, macrophage infiltration usually correlates with poor prognosis (Joyce & Pollard, 2009). However, the role of TAM during metastasis is not clearly understood yet. It has been proposed that TAM participate in the seeding of tumor cells and prepare the metastatic niche in the target organ (B. Z. Qian & Pollard, 2010). In spite of this, their role in the colonization of the brain has not been investigated until now.

It has long been known that macrophages populate metastatic lesions (Joyce & Pollard, 2009). However, due to the lack of reliable markers that distinguish microglia and macrophages coming from the bone marrow, it is still unclear whether these macrophage populations consist only of tissue specific macrophages, or whether bone marrow-derived macrophages also participate in the

colonization of the brain. In line with that, unlike other tissue-specific macrophages, microglia undergo self-renewal during homeostasis, without the involvement of monocytes (Ajami, Bennett, Krieger, Tetzlaff, & Rossi, 2007). This indicates that the presence of bone marrow-derived macrophages may not be necessary in the brain, at least, in a non-pathological context.

In order to address these questions, I next studied the specific role of TAM during the colonization of the brain.

4.2.1 PI3K binding to CSF1R stimulates the tumor promoting role of macrophages

One of the mechanisms responsible for the macrophage-associated tumor promotion in the primary tumor involves the CSF1R signaling loop (see 1.2.1.1.1), in which tumor cells express the colony-stimulating factor 1 (CSF1), which acts as a potent chemoattractant and activator for CSF1R-expressing TAM; and macrophages in turn produce the epidermal growth factor (EGF) which increases the invasiveness and migration of neighboring tumor cells that express the EGF receptor (EGFR) (Garris & Pittet, 2013; Goswami et al., 2005; B. Z. Qian & Pollard, 2010).

In myeloid cells, the tumor-derived chemoattractant CSF1 can activate the catalytic subunit gamma isoform of the PI3-kinase (p110γ) (Rommel et al., 2007). Furthermore, it has been shown that the binding of the PI3K to CSF1R in TAM stimulates their tumor promoting functions (Sampaio et al., 2011). In line with that, it has also been shown that the PI3K/Akt/mTOR signaling pathway participates in the switching of microglial cells into a tumor-promoting phenotype or M2 (Ellert-Miklaszewska et al., 2013).

Based on these observations I decided to block the PI3-kinase in CNS-specific macrophages and bone marrow-derived macrophages with an oral pan PI3K-inhibitor (BKM120), in order to blunt their innate pro-tumorigenic features and reprogram the tumor microenvironment toward more effective tumor suppressing functions in brain metastases.

4.2.2 BKM120 shows a dose-dependent cytotoxic activity and efficiently inhibits the PI3K pathway in vitro

In the present work I have shown that the pan-PI3K inhibitor BKM120 (buparlisib) can effectively interfere with the viability of several murine and human breast cancer cell lines and also murine

primary stromal cells in a dose-dependent manner. I could identify a wide range of sensitivity to BKM120, starting with the 410.4 cells, which are almost not sensitive to this compound; and ending with the human breast cancer cells MCF-7, which show the higher sensitivity to BKM120, due to their PIK3CA mutation in the catalytic subunit p110α (Maira et al., 2012). My results confirm the observations made by others regarding the efficiency of BKM120 in vitro (Maira et al., 2012). Interestingly, the primary murine cells (macrophages, microglia and astrocytes) also seemed to be sensitive to buparlisib, which make this compound especially interesting for the treatment of the microenvironment in brain metastases.

Additionally, at the chosen concentration of 250 nM none of the murine breast cancer cell lines or the primary cells were affected in their proliferation skills. Moreover, I could also demonstrate that BKM120 effectively blocks the PI3K/Akt signaling pathway in a concentration dependent manner, as seen by the inhibition of the downstream targets AKT and GSK3β. The phosphorylated forms of these proteins were almost undetectable when treating the mentioned cells with BKM120 at a concentration of 250 nM. Even the breast cancer cell line 410.4, which is rather resistant to BKM120, suffered a reduction in the expression of phospho-AKT and phospho-GSK3β protein levels. This could be due to interactions with other signaling pathways.

4.2.3 BKM120 reduces macrophage-induced tumor cell invasion in vitro

The role of the tumor microenvironment in promoting tumor progression and metastasis has already been discussed (see 1.2.1). In this work I could show that the coculture of breast cancer cells together with monocyte-derived macrophages (MDM), microglia and astrocytes, significantly increases the invasion capacity of the tumor cells. However, the addition of BKM120 to the cocultures could effectively reduce the macrophage-induced tumor cell invasion almost to the control levels. Nevertheless, this effect could only be observed in the case of MDM and microglia, but not in the cocultures with astrocytes. This could be due to lower sensitivity of astrocytes to BKM120. Therefore, higher concentrations of the inhibitor may be needed to see an effect on astrocyte-induced invasion of the tumor cells.

The role of BKM120 in reducing the macrophage-induced tumor invasion could be confirmed in our organotypic brain slice coculture system. This method allows the observation of the interactions between tumor cells and parenchymal cells of the brain slice. In this case, the invasion of the breast cancer cells was reduced in a concentration dependent manner when BKM120 was added to the cocultures.

Moreover, the activation of microglia and astrocytes in the brain slice was also affected. In the normal situation, microglial cells detect the presence of foreign cells and become activated. Consequently, they migrate into the tumor plug and interact with the tumor cells. Astrocytes also become activated and display long protrusions that interact with the foreign cells in the tumor plug. This effect doesn't take place when the organotypic brain slices are cocultured with cells with a neuro-ectodermal origin. Interestingly, cells sharing a common origin with the CNS do not activate the glial defense system in the same way as the CNS-foreign epithelial cells do (Siam et al., 2015). In line with that, I could see an activation of microglial and astrocytic cells in the controls. However, when the organotypic cocultures were treated with BKM120, a decreasing tendency in the percentage of the tumor plug invaded by microglia could be measured; and the length of the astrocytic protrusions in the tumor plug was significantly reduced, in a concentration-dependent manner.

These data indicate that, on the one hand, MDM, microglia and astrocytes actively support the colonization of the brain parenchyma by the tumor cells; and, on the other hand, that BKM120 affects both the tumor cells and the brain defense, and therefore reduces the macrophage-induced tumor invasion both in vitro and ex vivo.

4.2.4 The ex vivo treatment of MDM with BKM120 prolongs survival in vivo

As explained, BKM120 can effectively block the macrophage-induced invasion of tumor cells in vitro. However, I also wanted to test this effect when a complete immune system is present. The Boyden Chamber assay has the disadvantage of being a very artificial system, since it can only model the interactions of tumor cells with one type of stromal cells. Nevertheless, this method confirmed the effectiveness of BKM120 against monocyte-derived macrophages and microglia in their invasion-promoting role of breast cancer cells. Moreover, the organotypic brain slice coculture system allows an overall view of both parenchymal cell types present in the brain slice (microglia and astrocytes) and their interactions with tumor cells. However, due to the lack of innate immune cells in the brain slice, some important aspects of the colonization are missed in this model system.

As previously discussed, it is still unclear whether the macrophage populations that populate the metastatic lesions consist only of tissue specific macrophages (microglia), or whether macrophages coming from the bone marrow (MDM) also remain in the metastatic lesion and collaborate with the local macrophages during the colonization of the CNS. Furthermore, the specific role of the TAM during the colonization step remains still unexplored.

To address these questions, I designed an in vivo experiment in which, on the one hand, the tumor-associated macrophages can be treated separately from the tumor cells; and on the other hand, the reaction of the immune system can be measured as a whole in a living animal. This experiment aimed to clarify whether the blockade of the PI3-kinase in TAM could interfere with the colonization of the brain by the tumor cells, and consequently prolong survival in mice.

The first experiments conducted in the 410.4 colonization model only revealed a cautious tendency in the overall survival of the mice when the macrophages were treated with BKM120 and injected together with 410.4 cells. However, as already commented, the low colonization index of this model and the prolonged duration of the experiment may mask the effects of the one-time administration of BKM120 before starting the in vivo experiment.

Nevertheless, a further attempt with the 4T1 colonization model provided promising results. In this case, the ex vivo one-time pre-treatment of the macrophages with BKM120 significantly prolonged the overall survival in vivo in comparison with the untreated controls. These data support my observations made in vitro regarding the potency of BKM120. Moreover, they confirm that the blockade of the PI3-kinase by a punctual ex vivo treatment of TAM with BKM120 interferes with the colonization of the brain parenchyma by breast cancer cells, which is reflected in a better overall survival in the mice.

4.2.5 The blockade of the PI3K in MDM ex vivo affects the CSF1 signaling in vivo

As already commented, in the experiment with the 410.4 breast cancer cells, the treatment of MDM with BKM120 didn't have any positive effects on the overall survival of the mice. Consistent with that, I couldn't detect any differences neither in the tumor load, nor in the activation status of microglia and macrophages, or in the expression levels of the key players of the CSF1 signaling loop.

On the contrary, the ex vivo treatment of MDM with buparlisib resulted in a prolonged overall survival in the 4T1 colonization model. In the metastatic tissue of mice injected with tumor cells and BKM120-pretreated MDM, a reduction of the tumor load could be proved. Despite that, I didn't observe any differences in the activation status of the macrophages/microglia or the astrocytes in comparison with the mice injected with untreated MDM. This observation may be due to the fact that only the MDM were treated with the PI3K inhibitor, and therefore the activation status of

microglia and astrocytes remained unaffected. Furthermore, it indicates that the positive effects in the overall survival of the mice depend exclusively on the role of the TAM.

Interestingly, the blockade of the PI3-kinase in the MDM resulted in a systemic effect on the CSF1 signaling loop. In line with that, the expression of the CSF1R itself and its ligand CSF1 was significantly decreased in the metastatic tissue of mice injected with BKM120-pretreated macrophages in comparison to the controls measured by qRT-PCR; whereas the expression of the other ligand for CSF1R in the CNS, IL34, remained unaffected.

4.2.6 The PI3K-blockade in TAM changes the infiltration pattern of tumor cells

More interestingly, I observed a different infiltration pattern between the mice injected with 4T1 and the control MDM, and those injected with BKM120-pretreated MDM. In the case of the control mice, the metastases showed more groups of infiltrating cells at the metastatic/brain parenchyma interface. On the other hand, the metastases of mice injected with 4T1 and pre-treated MDM showed a more round and well-defined metastatic edge, with less infiltration.

It has already been discussed that the infiltration pattern of the tumor cells in the brain parenchyma is characteristic of the tumor entity (see 4.1.2.1). The 4T1 colonization model usually displays a cohort infiltration pattern. However, in this experiment I detected a more displacing growth pattern with less infiltration in the majority of the mice injected with BKM120-pretreated macrophages. The brain metastases of these mice formed a round well-defined pattern, with no further infiltration zones in the brain parenchyma. This observation may imply that the treated macrophages could control the infiltration pattern and subsequently influence the time to symptomatic macro-metastasis and therefore the overall survival. Interestingly, patients without infiltration also demonstrated a much better OS compared with patients with infiltration (Siam et al., 2015).

The activation of PI3K has also been linked to EMT in many tumor entities, especially tumors of the central nervous system (Crespo et al., 2016). One of the transcription factors responsible for this process, Twist, is activated by AKT2, and contributes to the loss of E-cadherin mediated cell-cell adhesion and cell motility that leads to tumor progression and metastasis (Yang et al., 2004). Previously, I have pointed out that the 4T1 may acquire mechanical plasticity that contributes to their higher colonization potential (see 4.1.2.2). In line with that, my results regarding the infiltration pattern of the metastases in mice injected with BKM120-pretreated MDM indicate that the blockade

of the PI3K/Akt signaling pathway in TAM may also influence their contribution to tumor cell invasion. However, the mechanisms underlying this process need to be further investigated.

4.2.7 The blockade of the CSF1 signaling leads to a phenotypic switch in TAM

These data point to a correction in the tumor promoting role of TAM. Interestingly, it has been indicated that the PI3K/Akt/mTOR signaling pathway is involved in the switching of microglial cells into a tumor promoting phenotype or M2 (Ellert-Miklaszewska et al., 2013). For this reason, I finally wanted to find out whether the inhibition of the PI3-kinase with BKM120 could indeed provoke a macrophage-switch from a tumor-promoting into a tumor-suppressing phenotype.

This could be proved by the downregulation of the transcriptional regulator of myeloid cells PU.1 in the metastatic tissue of mice where the PI3-kinase had been blocked with BKM120 in MDM. As has been already explained, this hematopoietic transcription factor plays a key role in macrophage differentiation (Celada et al., 1996; Jego et al., 2014). Additionally, Bowman et al. recently identified PU.1 as one of the motifs enriched in TAM, interestingly both in TAM-MDM as well as TAM-microglia (Bowman et al., 2016). Consequently, the downregulation of PU.1 in the metastatic tissue of mice injected with breast cancer cells and BKM120-pretreated macrophages, may underline the change of the activation status of tumor-associated macrophages, into a tumor-suppressing phenotype.

These data could be confirmed by a pathway analysis performed in the context of the MetastaSys e:Bio consortium, which revealed the presence of PU1 in the untreated MDM samples but not in the BKM120-treated counterparts. Additionally, other transcription factors like LEF1 and TCF4 were also identified in the untreated samples. An essential function of the transcription factors LEF1/TCF4 has been demonstrated in cerebral metastases of lung adenocarcinomas (Bleckmann et al., 2013) and in CRC (Kriegl et al., 2010), where the nuclear LEF1/TCF4 expression correlates with poor prognosis. Therefore, the results of the pathway analysis reinforce the theory of a macrophage switch after treatment with BKM120 into a tumor-suppressing phenotype.

Additionally, I also detected the downregulation of PD-L1 in the metastatic tissue of mice injected with breast cancer cells and BKM120-pretreated macrophages. PD-L1 is expressed in the tumor microenvironment by tumor cells and tumor-infiltrating immune cells, like TAM (Loke & Allison, 2003). The binding of PD-L1 to its receptor (PD-1) in T cells results in the inhibition of the anti-tumor immune response (D. S. Chen, Irving, & Hodi, 2012; D. S. Chen & Mellman, 2013). According to that, the downregulation of PD-L1 in the metastatic tissue as a result of the ex vivo one-time pre-

treatment of MDM with BKM120 also points to a change in the tumor promoting role of the macrophages.

4.3   Future perspectives in the treatment of brain metastasis

Taken together, my data indicate that the treatment of TAM with BKM120 provokes a macrophage switch from a tumor-promoting into a tumor-suppressing phenotype. This phenotypic switch leads to a reduced infiltration of the tumor cells into the brain parenchyma and results in prolonged overall survival of the mice.

Interestingly, the prolonged survival of the mice resulted from a single pre-treatment of TAM ex vivo. In line with that, I would expect that a systemic therapy with BKM120 would lead to a much better prognosis. However, BKM120 has shown off-target effects (Maira et al., 2012), and its implementation in vivo must therefore be further investigated.

Additionally, in order to improve the effects of BKM120 in brain metastases, other agents could be used in combination. For example, agents targeting PD-L1 in tumor cells or PD-1 in T cells have shown promising results in primary tumors (Quezada & Peggs, 2013; Sznol & Chen, 2013). The effectiveness of such treatments in brain metastases needs to be further investigated. However, my results indicate that agents targeting PD-L1 may foster the already demonstrated positive effects of BKM120. The presence of cytotoxic T cells was not assessed in this study. Nevertheless, it could be expected that the treatment with anti-PD-1 agents would re-activate the adaptive immune defense and therefore support their role in controlling the metastatic disease. Both our models would be ideal candidates to study the BKM120 effect in combination with anti-PD-1 agents.

To sum up, I have shown that the pharmacological re-education of TAM with the PI3K inhibitor BKM120 can re-activate the tumor suppressing role of the macrophages. In this context, when the CSF1 signaling is blocked, macrophages don't promote tumor progression anymore, but display tumor suppressing functions. Although it has not been investigated in this study, one of these functions could be the recruitment of cytotoxic T cells to the metastatic lesion. In order to support and improve this immune-stimulating function of the macrophages, other agents that impede tumor mediated immune suppression, like anti-PD-L1 or anti-PD-1, could be the perfect partners in a combination therapy with BKM120. In this context, re-establishing the link between innate and adaptive immunity seems to be a promising therapeutic option in the treatment of brain metastases.

5   Summary and conclusions

This study investigated triggers of colonization during brain metastases. The colonization of the target organ is the most inefficient but also the most life-threatening step in the metastatic cascade. From a clinical point of view, colonization is the most relevant event and, more importantly, the only targetable step during metastases progression. However, while the first steps of the metastatic cascade have been characterized in detail, the colonization of the target organ remains unexplored. In order to investigate the mechanisms underlying this process, brain colonization in vivo models were developed in this study. With this aim, two related breast cancer cell lines were stereotactically injected in syngeneic mice. By means of a new quantification tool, the Colonization Index, I could demonstrate the different colonization potentials of the 4T1 and the parental 410.4.

Even though both cell lines displayed an epithelial phenotype and a cohort infiltration pattern in the brain parenchyma, the 4T1 showed a higher colonization potential compared to the 410.4. Although we and others have demonstrated the tumor-promoting role of stromal cells during brain metastases, in this study I showed that the microenvironment doesn't influence the different colonization potential of the cell lines. On the contrary, I propose that the plasticity conferred to the cells by mesenchymal markers like vimentin, could be responsible for the better colonization of the 4T1, whereas the epithelial nature of the tumor cells remains unchanged. However, this needs to be further investigated.

Furthermore, I have shown that tumor-associated macrophages (TAM) coming from the bone marrow actively participate in the colonization of the brain by tumor cells. Several studies have pointed out the manipulation of the tumor-associated stromal cells as a meaningful therapeutic option for the treatment of metastases. The re-education of the innate immunity (especially TAM) is of special interest in order to re-activate their tumor suppressing roles and recruit cells from the adaptive immunity, like cytotoxic T cells, which play an important role in tumor elimination. In the present study, I could blunt the pro-tumorigenic features of monocyte-derived macrophages (MDM), and therefore impede the macrophage-assisted invasion of breast cancer tumor cells by blocking the PI3-kinase, a downstream effector of CSF1R, with BKM120.

More interestingly, I showed that the treatment of MDM with the PI3K-inhibitor provokes a macrophage switch from a tumor-promoting to a tumor-suppressing phenotype, which results in prolonged overall survival (OS). The mechanism underlying this process involves the downregulation of the myeloid transcription factor PU.1 in the metastatic tissue (see Figure 40). Interestingly, this TF

has recently been demonstrated to be enriched in both tumor-associated MDM and microglia. Therefore, my results point out PU.1 as a key player in the tumor promoting functions of macrophages.

Additionally, the immune-suppressing factor PD-L1 was also found to be downregulated after treatment of MDM with BKM120. Agents targeting the PD-L1/PD-1 pathway have shown promising clinical success as cancer immunotherapy. For this reason, I propose that agents like BKM120, that re-establish the immune-stimulating function of macrophages, in combination with agents that impede tumor-mediated immune-suppression, may be a feasible and meaningful therapeutic option in the treatment of brain metastases.
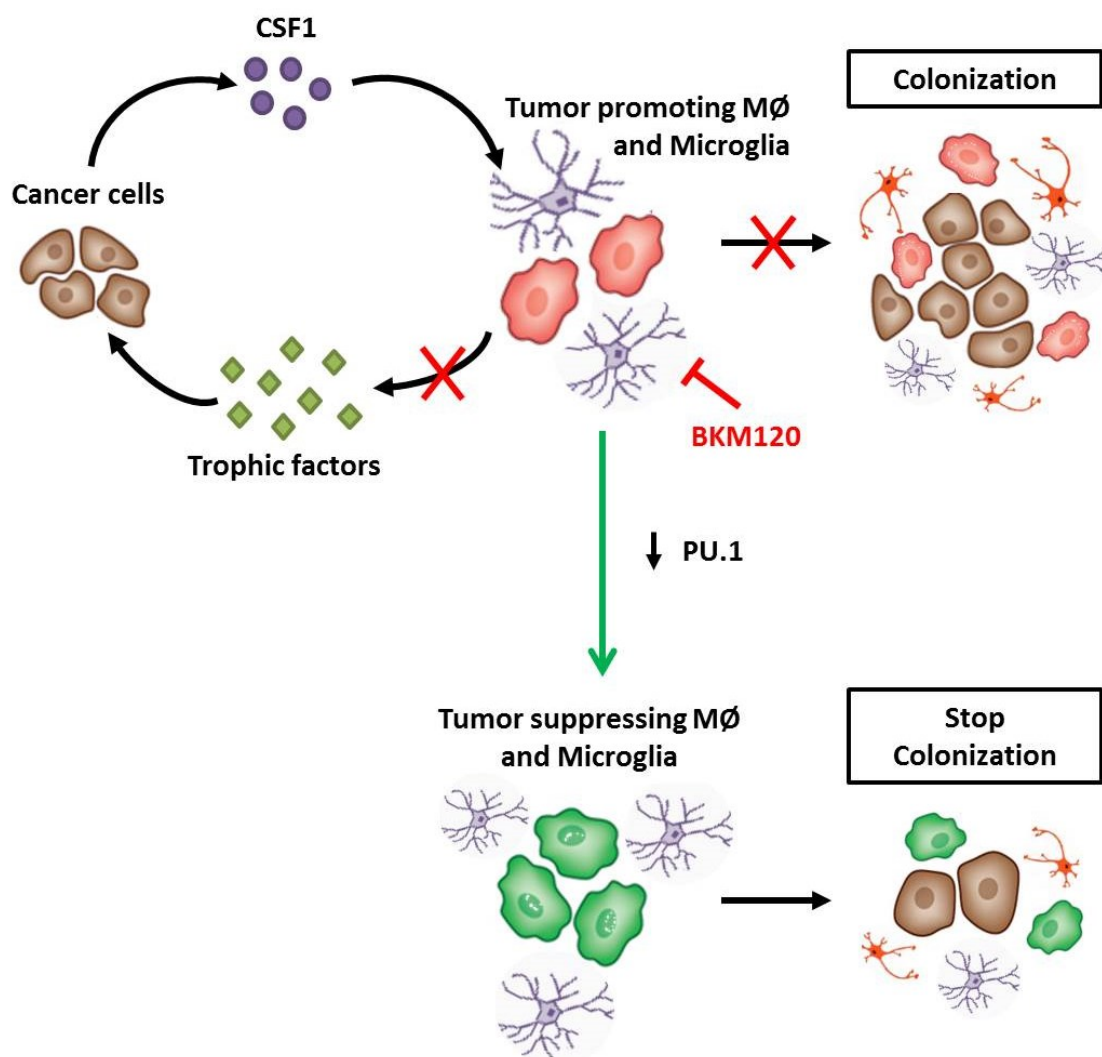
Figure 40: Schematic representation of the macrophage phenotypic switch after PI3K-inhibition
The blockade of the PI3-kinase with BKM120 provokes a macrophage switch into a tumor-suppressing phenotype, represented by the downregulation of the myeloid transcription factor PU.1. The re-education of the macrophages leads to a reduction of the CNS-colonization and a prolonged OS in vivo.

Taken together, I have identified triggers of colonization associated both with tumor cells and with the tumor microenvironment. On the one hand, the particular expression profile of adhesion molecules like vimentin may provide tumor cells with mesenchymal features that favor colonization without altering their epithelial nature. On the other hand, the stromal cells in the tumor microenvironment may undergo a malignant change prompted by the tumor cells that promotes the colonization of the brain during brain metastasis. Fortunately, the tumor promoting role of macrophages can be pharmacologically reverted to their intrinsic tumor-suppressing function with agents targeting the innate immunity like BKM120.

6   Bibliography

Ajami, B., Bennett, J. L., Krieger, C., Tetzlaff, W., & Rossi, F. M. (2007). Local self-renewal can sustain CNS microglia maintenance and function throughout adult life. *Nat Neurosci, 10*(12), 1538-1543. doi:10.1038/nn2014

Alessi, D. R., James, S. R., Downes, C. P., Holmes, A. B., Gaffney, P. R., Reese, C. B., & Cohen, P. (1997). Characterization of a 3-phosphoinositide-dependent protein kinase which phosphorylates and activates protein kinase Balpha. *Curr Biol, 7*(4), 261-269.

Aslakson, C. J., & Miller, F. R. (1992). Selective events in the metastatic process defined by analysis of the sequential dissemination of subpopulations of a mouse mammary tumor. *Cancer Res, 52*(6), 1399-1405.

Bahrami, A., Truong, L. D., & Ro, J. Y. (2008). Undifferentiated tumor: true identity by immunohistochemistry. *Arch Pathol Lab Med, 132*(3), 326-348. doi:10.1043/1543-2165(2008)132[326:UTTIBI]2.0.CO;2

Barbai, T., Fejos, Z., Puskas, L. G., Timar, J., & Raso, E. (2015). The importance of microenvironment: the role of CCL8 in metastasis formation of melanoma. *Oncotarget, 6*(30), 29111-29128. doi:10.18632/oncotarget.5059

Berghoff, A. S., & Preusser, M. (2015). The inflammatory microenvironment in brain metastases: potential treatment target? *Chin Clin Oncol, 4*(2), 21. doi:10.3978/j.issn.2304-3865.2015.06.03

Berx, G., & Van Roy, F. (2001). The E-cadherin/catenin complex: an important gatekeeper in breast cancer tumorigenesis and malignant progression. *Breast Cancer Res, 3*(5), 289-293.

Bindal, R. K., Sawaya, R., Leavens, M. E., & Lee, J. J. (1993). Surgical treatment of multiple brain metastases. *J Neurosurg, 79*(2), 210-216. doi:10.3171/jns.1993.79.2.0210

Bingle, L., Brown, N. J., & Lewis, C. E. (2002). The role of tumour-associated macrophages in tumour progression: implications for new anticancer therapies. *J Pathol, 196*(3), 254-265. doi:10.1002/path.1027

Bleckmann, A., Siam, L., Klemm, F., Rietkotter, E., Wegner, C., Kramer, F., . . . Pukrop, T. (2013). Nuclear LEF1/TCF4 correlate with poor prognosis but not with nuclear beta-catenin in cerebral metastasis of lung adenocarcinomas. *Clin Exp Metastasis, 30*(4), 471-482. doi:10.1007/s10585-012-9552-7

Bos, P. D., Nguyen, D. X., & Massague, J. (2010). Modeling metastasis in the mouse. *Curr Opin Pharmacol, 10*(5), 571-577. doi:10.1016/j.coph.2010.06.003

Bowman, R. L., Klemm, F., Akkari, L., Pyonteck, S. M., Sevenich, L., Quail, D. F., . . . Joyce, J. A. (2016). Macrophage Ontogeny Underlies Differences in Tumor-Specific Education in Brain Malignancies. *Cell Rep*. doi:10.1016/j.celrep.2016.10.052

Brastianos, P. K., Carter, S. L., Santagata, S., Cahill, D. P., Taylor-Weiner, A., Jones, R. T., . . . Hahn, W. C. (2015). Genomic Characterization of Brain Metastases Reveals Branched Evolution and Potential Therapeutic Targets. *Cancer Discov, 5*(11), 1164-1177. doi:10.1158/2159-8290.CD-15-0369

Cailleau, R., Young, R., Olive, M., & Reeves, W. J., Jr. (1974). Breast tumor cell lines from pleural effusions. *J Natl Cancer Inst, 53*(3), 661-674.

Campbell, P. J., Yachida, S., Mudie, L. J., Stephens, P. J., Pleasance, E. D., Stebbings, L. A., . . . Futreal, P. A. (2010). The patterns and dynamics of genomic instability in metastatic pancreatic cancer. *Nature, 467*(7319), 1109-1113. doi:10.1038/nature09460

Cardiff, R. D., Miller, C. H., & Munn, R. J. (2014). Manual hematoxylin and eosin staining of mouse tissue sections. *Cold Spring Harb Protoc, 2014*(6), 655-658. doi:10.1101/pdb.prot073411

Carpenter, C. L., Auger, K. R., Chanudhuri, M., Yoakim, M., Schaffhausen, B., Shoelson, S., & Cantley, L. C. (1993). Phosphoinositide 3-kinase is activated by phosphopeptides that bind to the SH2 domains of the 85-kDa subunit. *J Biol Chem, 268*(13), 9478-9483.

Carracedo, A., & Pandolfi, P. P. (2008). The PTEN-PI3K pathway: of feedbacks and cross-talks. *Oncogene, 27*(41), 5527-5541. doi:10.1038/onc.2008.247

Celada, A., Borras, F. E., Soler, C., Lloberas, J., Klemsz, M., van Beveren, C., . . . Maki, R. A. (1996). The transcription factor PU.1 is involved in macrophage proliferation. *J Exp Med, 184*(1), 61-69.

Charles, N. A., Holland, E. C., Gilbertson, R., Glass, R., & Kettenmann, H. (2012). The brain tumor microenvironment. *Glia, 60*(3), 502-514.

Chen, D. S., Irving, B. A., & Hodi, F. S. (2012). Molecular pathways: next-generation immunotherapy-- inhibiting programmed death-ligand 1 and programmed death-1. *Clin Cancer Res, 18*(24), 6580-6587. doi:10.1158/1078-0432.CCR-12-1362

Chen, D. S., & Mellman, I. (2013). Oncology meets immunology: the cancer-immunity cycle. *Immunity, 39*(1), 1-10. doi:10.1016/j.immuni.2013.07.012

Chen, E. I., Hewel, J., Krueger, J. S., Tiraby, C., Weber, M. R., Kralli, A., . . . Felding-Habermann, B. (2007). Adaptation of energy metabolism in breast cancer brain metastases. *Cancer Res, 67*(4), 1472-1486. doi:10.1158/0008-5472.CAN-06-3137

Chuang, H. N., Lohaus, R., Hanisch, U. K., Binder, C., Dehghani, F., & Pukrop, T. (2013). Coculture system with an organotypic brain slice and 3D spheroid of carcinoma cells. *J Vis Exp*(80). doi:10.3791/50881

Chuang, H. N., van Rossum, D., Sieger, D., Siam, L., Klemm, F., Bleckmann, A., . . . Pukrop, T. (2013). Carcinoma cells misuse the host tissue damage response to invade the brain. *Glia, 61*(8), 1331-1346. doi:10.1002/glia.22518

Clarke, P. A., & Workman, P. (2012). Phosphatidylinositide-3-kinase inhibitors: addressing questions of isoform selectivity and pharmacodynamic/predictive biomarkers in early clinical trials. *J Clin Oncol, 30*(3), 331-333. doi:10.1200/JCO.2011.38.7167

Conley, F. K. (1979). Development of a metastatic brain tumor model in mice. *Cancer Res, 39*(3), 1001-1007.

Crespo, S., Kind, M., & Arcaro, A. (2016). The role of the PI3K/AKT/mTOR pathway in brain tumor metastasis. *Journal of Cancer Metastasis and Treatment, 2*(3), 80-89.

Currie, R. A., Walker, K. S., Gray, A., Deak, M., Casamayor, A., Downes, C. P., . . . Lucocq, J. (1999). Role of phosphatidylinositol 3,4,5-trisphosphate in regulating the activity and localization of 3-phosphoinositide-dependent protein kinase-1. *Biochem J, 337 (Pt 3)*, 575-583.

Damiens, K., Ayoub, J. P., Lemieux, B., Aubin, F., Saliba, W., Campeau, M. P., & Tehfe, M. (2012). Clinical features and course of brain metastases in colorectal cancer: an experience from a single institution. *Curr Oncol, 19*(5), 254-258. doi:10.3747/co.19.1048

De Simoni, A., & Yu, L. M. (2006). Preparation of organotypic hippocampal slice cultures: interface method. *Nat Protoc, 1*(3), 1439-1445. doi:10.1038/nprot.2006.228

Dibble, C. C., & Manning, B. D. (2009). A molecular link between AKT regulation and chemotherapeutic response. *Cancer Cell, 16*(3), 178-180. doi:10.1016/j.ccr.2009.08.011

Dienstmann, R., Rodon, J., Serra, V., & Tabernero, J. (2014). Picking the point of inhibition: a comparative review of PI3K/AKT/mTOR pathway inhibitors. *Mol Cancer Ther, 13*(5), 1021-1031. doi:10.1158/1535-7163.MCT-13-0639

Ellert-Miklaszewska, A., Dabrowski, M., Lipko, M., Sliwa, M., Maleszewska, M., & Kaminska, B. (2013). Molecular definition of the pro-tumorigenic phenotype of glioma-activated microglia. *Glia, 61*(7), 1178-1190. doi:10.1002/glia.22510

Engelman, J. A., Luo, J., & Cantley, L. C. (2006). The evolution of phosphatidylinositol 3-kinases as regulators of growth and metabolism. *Nat Rev Genet, 7*(8), 606-619. doi:10.1038/nrg1879

Faltas, B. (2012). Cornering metastases: therapeutic targeting of circulating tumor cells and stem cells. *Front Oncol, 2*, 68. doi:10.3389/fonc.2012.00068

Fidler, I. J. (1970). Metastasis: quantitative analysis of distribution and fate of tumor emboli labeled with 125 I-5-iodo-2'-deoxyuridine. *J Natl Cancer Inst, 45*(4), 773-782.

Fidler, I. J. (2002). Critical determinants of metastasis. *Semin Cancer Biol, 12*(2), 89-96. doi:10.1006/scbi.2001.0416

Fuller, L., & Dailey, M. E. (2007). Preparation of rodent hippocampal slice cultures. *CSH Protoc, 2007*, pdb prot4848. doi:10.1101/pdb.prot4848

Galon, J., Costes, A., Sanchez-Cabo, F., Kirilovsky, A., Mlecnik, B., Lagorce-Pages, C., . . . Pages, F. (2006). Type, density, and location of immune cells within human colorectal tumors predict clinical outcome. *Science, 313*(5795), 1960-1964. doi:10.1126/science.1129139

Galon, J., Fridman, W. H., & Pages, F. (2007). The adaptive immunologic microenvironment in colorectal cancer: a novel perspective. *Cancer Res, 67*(5), 1883-1886. doi:10.1158/0008-5472.CAN-06-4806

Garris, C., & Pittet, M. J. (2013). Therapeutically reeducating macrophages to treat GBM. *Nat Med, 19*(10), 1207-1208. doi:10.1038/nm.3355

Gewinner, C., Wang, Z. C., Richardson, A., Teruya-Feldstein, J., Etemadmoghadam, D., Bowtell, D., . . . Cantley, L. C. (2009). Evidence that inositol polyphosphate 4-phosphatase type II is a tumor suppressor that inhibits PI3K signaling. *Cancer Cell, 16*(2), 115-125. doi:10.1016/j.ccr.2009.06.006

Gjoen, T., Seljelid, R., & Kolset, S. O. (1989). Binding of metastatic colon carcinoma cells to liver macrophages. *J Leukoc Biol, 45*(4), 362-369.

Goswami, S., Sahai, E., Wyckoff, J. B., Cammer, M., Cox, D., Pixley, F. J., . . . Condeelis, J. S. (2005). Macrophages promote the invasion of breast carcinoma cells via a colony-stimulating factor-1/epidermal growth factor paracrine loop. *Cancer Res, 65*(12), 5278-5283. doi:10.1158/0008-5472.CAN-04-1853

Gupta, P. B., Chaffer, C. L., & Weinberg, R. A. (2009). Cancer stem cells: mirage or reality? *Nat Med, 15*(9), 1010-1012. doi:10.1038/nm0909-1010

Guy, C. T., Webster, M. A., Schaller, M., Parsons, T. J., Cardiff, R. D., & Muller, W. J. (1992). Expression of the neu protooncogene in the mammary epithelium of transgenic mice induces metastatic disease. *Proc Natl Acad Sci U S A, 89*(22), 10578-10582.

Hagemann, T., Robinson, S. C., Schulz, M., Trumper, L., Balkwill, F. R., & Binder, C. (2004). Enhanced invasiveness of breast cancer cell lines upon co-cultivation with macrophages is due to TNF-alpha dependent up-regulation of matrix metalloproteases. *Carcinogenesis, 25*(8), 1543-1549. doi:10.1093/carcin/bgh146

Hanisch, U. K., & Kettenmann, H. (2007). Microglia: active sensor and versatile effector cells in the normal and pathologic brain. *Nat Neurosci, 10*(11), 1387-1394. doi:10.1038/nn1997

Hanisch, U. K., van Rossum, D., Xie, Y., Gast, K., Misselwitz, R., Auriola, S., . . . Moller, T. (2004). The microglia-activating potential of thrombin: the protease is not involved in the induction of proinflammatory cytokines and chemokines. *J Biol Chem, 279*(50), 51880-51887. doi:10.1074/jbc.M408318200

Hart, I. R., & Fidler, I. J. (1980a). Cancer invasion and metastasis. *Q Rev Biol, 55*(2), 121-142.

Hart, I. R., & Fidler, I. J. (1980b). Role of organ selectivity in the determination of metastatic patterns of B16 melanoma. *Cancer Res, 40*(7), 2281-2287.

Hassan, N. F., Rifat, S., Campbell, D. E., McCawley, L. J., & Douglas, S. D. (1991). Isolation and flow cytometric characterization of newborn mouse brain-derived microglia maintained in vitro. *J Leukoc Biol, 50*(1), 86-92.

Heyn, C., Ronald, J. A., Ramadan, S. S., Snir, J. A., Barry, A. M., MacKenzie, L. T., . . . Foster, P. J. (2006). In vivo MRI of cancer cell fate at the single-cell level in a mouse model of breast cancer metastasis to the brain. *Magn Reson Med, 56*(5), 1001-1010. doi:10.1002/mrm.21029

Hiraoka, K., Zenmyo, M., Watari, K., Iguchi, H., Fotovati, A., Kimura, Y. N., . . . Kuwano, M. (2008). Inhibition of bone and muscle metastases of lung cancer cells by a decrease in the number of monocytes/macrophages. *Cancer Sci, 99*(8), 1595-1602. doi:10.1111/j.1349-7006.2008.00880.x

Ito, D., Imai, Y., Ohsawa, K., Nakajima, K., Fukuuchi, Y., & Kohsaka, S. (1998). Microglia-specific localisation of a novel calcium binding protein, Iba1. *Brain Res Mol Brain Res, 57*(1), 1-9.

Ito, D., Tanaka, K., Suzuki, S., Dembo, T., & Fukuuchi, Y. (2001). Enhanced expression of Iba1, ionized calcium-binding adapter molecule 1, after transient focal cerebral ischemia in rat brain. *Stroke, 32*(5), 1208-1215.

Jeanes, A., Gottardi, C. J., & Yap, A. S. (2008). Cadherins and cancer: how does cadherin dysfunction promote tumor progression? *Oncogene, 27*(55), 6920-6929. doi:10.1038/onc.2008.343

Jego, G., Lanneau, D., De Thonel, A., Berthenet, K., Hazoume, A., Droin, N., . . . Garrido, C. (2014). Dual regulation of SPI1/PU.1 transcription factor by heat shock factor 1 (HSF1) during macrophage differentiation of monocytes. *Leukemia, 28*(8), 1676-1686. doi:10.1038/leu.2014.63

Joyce, J. A., & Pollard, J. W. (2009). Microenvironmental regulation of metastasis. *Nat Rev Cancer, 9*(4), 239-252. doi:10.1038/nrc2618

Kaplan, R. N., Riba, R. D., Zacharoulis, S., Bramley, A. H., Vincent, L., Costa, C., . . . Lyden, D. (2005). VEGFR1-positive haematopoietic bone marrow progenitors initiate the pre-metastatic niche. *Nature, 438*(7069), 820-827. doi:10.1038/nature04186

Katso, R., Okkenhaug, K., Ahmadi, K., White, S., Timms, J., & Waterfield, M. D. (2001). Cellular function of phosphoinositide 3-kinases: implications for development, homeostasis, and cancer. *Annu Rev Cell Dev Biol, 17*, 615-675. doi:10.1146/annurev.cellbio.17.1.615

Kessenbrock, K., Plaks, V., & Werb, Z. (2010). Matrix metalloproteinases: regulators of the tumor microenvironment. *Cell, 141*(1), 52-67. doi:10.1016/j.cell.2010.03.015

Khirade, M. F., Lal, G., & Bapat, S. A. (2015). Derivation of a fifteen gene prognostic panel for six cancers. *Sci Rep, 5*, 13248. doi:10.1038/srep13248

Kitamura, T., Qian, B. Z., Soong, D., Cassetta, L., Noy, R., Sugano, G., . . . Pollard, J. W. (2015). CCL2-induced chemokine cascade promotes breast cancer metastasis by enhancing retention of metastasis-associated macrophages. *J Exp Med, 212*(7), 1043-1059. doi:10.1084/jem.20141836

Kowalski, P. J., Rubin, M. A., & Kleer, C. G. (2003). E-cadherin expression in primary carcinomas of the breast and its distant metastases. *Breast Cancer Res, 5*(6), R217-222. doi:10.1186/bcr651

Kreutz, S., Koch, M., Ghadban, C., Korf, H. W., & Dehghani, F. (2007). Cannabinoids and neuronal damage: differential effects of THC, AEA and 2-AG on activated microglial cells and degenerating neurons in excitotoxically lesioned rat organotypic hippocampal slice cultures. *Exp Neurol, 203*(1), 246-257. doi:10.1016/j.expneurol.2006.08.010

Kriegl, L., Horst, D., Reiche, J. A., Engel, J., Kirchner, T., & Jung, A. (2010). LEF-1 and TCF4 expression correlate inversely with survival in colorectal cancer. *J Transl Med, 8*, 123. doi:10.1186/1479-5876-8-123

Kripke, M. L. (1979). Speculations on the role of ultraviolet radiation in the development of malignant melanoma. *J Natl Cancer Inst, 63*(3), 541-548.

Laemmli, U. K. (1970). Cleavage of structural proteins during the assembly of the head of bacteriophage T4. *Nature, 227*(5259), 680-685.

Lanier, L. L. (2009). DAP10- and DAP12-associated receptors in innate immunity. *Immunol Rev, 227*(1), 150-160. doi:10.1111/j.1600-065X.2008.00720.x

Lin, E. Y., Nguyen, A. V., Russell, R. G., & Pollard, J. W. (2001). Colony-stimulating factor 1 promotes progression of mammary tumors to malignancy. *J Exp Med, 193*(6), 727-740.

Liu, T. J., Koul, D., LaFortune, T., Tiao, N., Shen, R. J., Maira, S. M., . . . Yung, W. K. (2009). NVP-BEZ235, a novel dual phosphatidylinositol 3-kinase/mammalian target of rapamycin inhibitor, elicits multifaceted antitumor activities in human gliomas. *Mol Cancer Ther, 8*(8), 2204-2210. doi:10.1158/1535-7163.MCT-09-0160

Lockman, P. R., Mittapalli, R. K., Taskar, K. S., Rudraraju, V., Gril, B., Bohn, K. A., . . . Smith, Q. R. (2010). Heterogeneous blood-tumor barrier permeability determines drug efficacy in experimental brain metastases of breast cancer. *Clin Cancer Res, 16*(23), 5664-5678. doi:10.1158/1078-0432.CCR-10-1564

Loke, P., & Allison, J. P. (2003). PD-L1 and PD-L2 are differentially regulated by Th1 and Th2 cells. *Proc Natl Acad Sci U S A, 100*(9), 5336-5341. doi:10.1073/pnas.0931259100

Lokman, N. A., Elder, A. S., Ricciardelli, C., & Oehler, M. K. (2012). Chick chorioallantoic membrane (CAM) assay as an in vivo model to study the effect of newly identified molecules on ovarian cancer invasion and metastasis. *Int J Mol Sci, 13*(8), 9959-9970. doi:10.3390/ijms13089959

Lorger, M., & Felding-Habermann, B. (2010). Capturing changes in the brain microenvironment during initial steps of breast cancer brain metastasis. *Am J Pathol, 176*(6), 2958-2971. doi:10.2353/ajpath.2010.090838

Louveau, A., Smirnov, I., Keyes, T. J., Eccles, J. D., Rouhani, S. J., Peske, J. D., . . . Kipnis, J. (2015). Structural and functional features of central nervous system lymphatic vessels. *Nature, 523*(7560), 337-341. doi:10.1038/nature14432

Lowry, O. H., Rosebrough, N. J., Farr, A. L., & Randall, R. J. (1951). Protein measurement with the Folin phenol reagent. *J Biol Chem, 193*(1), 265-275.

Maira, S. M., Pecchi, S., Huang, A., Burger, M., Knapp, M., Sterker, D., . . . Voliva, C. F. (2012). Identification and characterization of NVP-BKM120, an orally available pan-class I PI3-kinase inhibitor. *Mol Cancer Ther, 11*(2), 317-328. doi:10.1158/1535-7163.MCT-11-0474

Mantovani, A., Sozzani, S., Locati, M., Allavena, P., & Sica, A. (2002). Macrophage polarization: tumor-associated macrophages as a paradigm for polarized M2 mononuclear phagocytes. *Trends Immunol, 23*(11), 549-555.

Marshall, O. J. (2004). PerlPrimer: cross-platform, graphical primer design for standard, bisulphite and real-time PCR. *Bioinformatics, 20*(15), 2471-2472. doi:10.1093/bioinformatics/bth254

Mathieu, A., Remmelink, M., D'Haene, N., Penant, S., Gaussin, J. F., Van Ginckel, R., . . . Salmon, I. (2004). Development of a chemoresistant orthotopic human nonsmall cell lung carcinoma model in nude mice: analyses of tumor heterogenity in relation to the immunohistochemical levels of expression of cyclooxygenase-2, ornithine decarboxylase, lung-related resistance protein, prostaglandin E synthetase, and glutathione-S-transferase-alpha (GST)-alpha, GST-mu, and GST-pi. *Cancer, 101*(8), 1908-1918. doi:10.1002/cncr.20571

Merkler, D., Ernsting, T., Kerschensteiner, M., Bruck, W., & Stadelmann, C. (2006). A new focal EAE model of cortical demyelination: multiple sclerosis-like lesions with rapid resolution of inflammation and extensive remyelination. *Brain, 129*(Pt 8), 1972-1983. doi:10.1093/brain/awl135

Miller, F. R., Miller, B. E., & Heppner, G. H. (1983). Characterization of metastatic heterogeneity among subpopulations of a single mouse mammary tumor: heterogeneity in phenotypic stability. *Invasion Metastasis, 3*(1), 22-31.

Minniti, G., Clarke, E., Lanzetta, G., Osti, M. F., Trasimeni, G., Bozzao, A., . . . Enrici, R. M. (2011). Stereotactic radiosurgery for brain metastases: analysis of outcome and risk of brain radionecrosis. *Radiat Oncol, 6*, 48. doi:10.1186/1748-717X-6-48

Mosmann, T. (1983). Rapid colorimetric assay for cellular growth and survival: application to proliferation and cytotoxicity assays. *J Immunol Methods, 65*(1-2), 55-63.

Nanni, P., Nicoletti, G., Palladini, A., Croci, S., Murgo, A., Ianzano, M. L., . . . Lollini, P. L. (2012). Multiorgan metastasis of human HER-2+ breast cancer in Rag2-/-;Il2rg-/- mice and treatment with PI3K inhibitor. *PLoS One, 7*(6), e39626. doi:10.1371/journal.pone.0039626

Nicolson, G. L., Brunson, K. W., & Fidler, I. J. (1978). Specificity of arrest, survival, and growth of selected metastatic variant cell lines. *Cancer Res, 38*(11 Pt 2), 4105-4111.

Niessner, H., Schmitz, J., Tabatabai, G., Schmid, A. M., Calaminus, C., Sinnberg, T., . . . Meier, F. (2016). PI3K Pathway Inhibition Achieves Potent Antitumor Activity in Melanoma Brain Metastases In Vitro and In Vivo. *Clin Cancer Res*. doi:10.1158/1078-0432.CCR-16-0064

Nussbaum, E. S., Djalilian, H. R., Cho, K. H., & Hall, W. A. (1996). Brain metastases. Histology, multiplicity, surgery, and survival. *Cancer, 78*(8), 1781-1788.

Ohsawa, K., Imai, Y., Sasaki, Y., & Kohsaka, S. (2004). Microglia/macrophage-specific protein Iba1 binds to fimbrin and enhances its actin-bundling activity. *J Neurochem, 88*(4), 844-856.

Pages, F., Berger, A., Camus, M., Sanchez-Cabo, F., Costes, A., Molidor, R., . . . Galon, J. (2005). Effector memory T cells, early metastasis, and survival in colorectal cancer. *N Engl J Med, 353*(25), 2654-2666. doi:10.1056/NEJMoa051424

Paget, S. (1889). The distribution of secondary growths in cancer of the breast. *Lancet, 1*, 571-573.

Painter, J. T., Clayton, N. P., & Herbert, R. A. (2010). Useful immunohistochemical markers of tumor differentiation. *Toxicol Pathol, 38*(1), 131-141. doi:10.1177/0192623309356449

Parcesepe, P., Giordano, G., Laudanna, C., Febbraro, A., & Pancione, M. (2016). Cancer-Associated Immune Resistance and Evasion of Immune Surveillance in Colorectal Cancer. *Gastroenterol Res Pract, 2016*, 6261721. doi:10.1155/2016/6261721

Park, S. J., Kim, H. T., Lee, D. H., Kim, K. P., Kim, S. W., Suh, C., & Lee, J. S. (2012). Efficacy of epidermal growth factor receptor tyrosine kinase inhibitors for brain metastasis in non-small cell lung cancer patients harboring either exon 19 or 21 mutation. *Lung Cancer, 77*(3), 556-560. doi:10.1016/j.lungcan.2012.05.092

Peterson, G. L. (1979). Review of the Folin phenol protein quantitation method of Lowry, Rosebrough, Farr and Randall. *Anal Biochem, 100*(2), 201-220.

Pfannes, S. D., Muller, B., Korner, S., Bessler, W. G., & Hoffmann, P. (2001). Induction of soluble antitumoral mediators by synthetic analogues of bacterial lipoprotein in bone marrow-derived macrophages from LPS-responder and -nonresponder mice. *J Leukoc Biol, 69*(4), 590-597.

Platten, M., Ochs, K., Lemke, D., Opitz, C., & Wick, W. (2014). Microenvironmental clues for glioma immunotherapy. *Curr Neurol Neurosci Rep, 14*(4), 440. doi:10.1007/s11910-014-0440-1

Politi, K., & Pao, W. (2011). How genetically engineered mouse tumor models provide insights into human cancers. *J Clin Oncol, 29*(16), 2273-2281. doi:10.1200/JCO.2010.30.8304

Poste, G., & Fidler, I. J. (1980). The pathogenesis of cancer metastasis. *Nature, 283*(5743), 139-146.

Pukrop, T., Dehghani, F., Chuang, H. N., Lohaus, R., Bayanga, K., Heermann, S., . . . Binder, C. (2010). Microglia promote colonization of brain tissue by breast cancer cells in a Wnt-dependent way. *Glia, 58*(12), 1477-1489. doi:10.1002/glia.21022

Pukrop, T., Klemm, F., Hagemann, T., Gradl, D., Schulz, M., Siemes, S., . . . Binder, C. (2006). Wnt 5a signaling is critical for macrophage-induced invasion of breast cancer cell lines. *Proc Natl Acad Sci U S A, 103*(14), 5454-5459. doi:10.1073/pnas.0509703103

Pulaski, B. A., & Ostrand-Rosenberg, S. (2001). Mouse 4T1 breast tumor model. *Curr Protoc Immunol, Chapter 20*, Unit 20 22. doi:10.1002/0471142735.im2002s39

Qian, B., Deng, Y., Im, J. H., Muschel, R. J., Zou, Y., Li, J., . . . Pollard, J. W. (2009). A distinct macrophage population mediates metastatic breast cancer cell extravasation, establishment and growth. *PLoS One, 4*(8), e6562. doi:10.1371/journal.pone.0006562

Qian, B. Z., & Pollard, J. W. (2010). Macrophage diversity enhances tumor progression and metastasis. *Cell, 141*(1), 39-51. doi:10.1016/j.cell.2010.03.014

Quail, D. F., & Joyce, J. A. (2013). Microenvironmental regulation of tumor progression and metastasis. *Nat Med, 19*(11), 1423-1437. doi:10.1038/nm.3394

Quezada, S. A., & Peggs, K. S. (2013). Exploiting CTLA-4, PD-1 and PD-L1 to reactivate the host immune response against cancer. *Br J Cancer, 108*(8), 1560-1565. doi:10.1038/bjc.2013.117

Rapaport, F., Khanin, R., Liang, Y., Pirun, M., Krek, A., Zumbo, P., . . . Betel, D. (2013). Comprehensive evaluation of differential gene expression analysis methods for RNA-seq data. *Genome Biol, 14*(9), R95. doi:10.1186/gb-2013-14-9-r95

Raz, A., Hanna, N., & Fidler, I. J. (1981). In vivo isolation of a metastatic tumor cell variant involving selective and nonadaptive processes. *J Natl Cancer Inst, 66*(1), 183-189.

Reiling, N., Klug, K., Krallmann-Wenzel, U., Laves, R., Goyert, S., Taylor, M. E., . . . Ehlers, S. (2001). Complex encounters at the macrophage-mycobacterium interface: studies on the role of the mannose receptor and CD14 in experimental infection models with Mycobacterium avium. *Immunobiology, 204*(5), 558-571. doi:10.1078/0171-2985-00093

Reymond, N., d'Agua, B. B., & Ridley, A. J. (2013). Crossing the endothelial barrier during metastasis. *Nat Rev Cancer, 13*(12), 858-870. doi:10.1038/nrc3628

Rietkotter, E., Bleckmann, A., Bayerlova, M., Menck, K., Chuang, H. N., Wenske, B., . . . Pukrop, T. (2015). Anti-CSF-1 treatment is effective to prevent carcinoma invasion induced by

monocyte-derived cells but scarcely by microglia. *Oncotarget, 6*(17), 15482-15493. doi:10.18632/oncotarget.3855

Robinson, B. D., Sica, G. L., Liu, Y. F., Rohan, T. E., Gertler, F. B., Condeelis, J. S., & Jones, J. G. (2009). Tumor microenvironment of metastasis in human breast carcinoma: a potential prognostic marker linked to hematogenous dissemination. *Clin Cancer Res, 15*(7), 2433-2441. doi:10.1158/1078-0432.CCR-08-2179

Rohan, T. E., Xue, X., Lin, H. M., D'Alfonso, T. M., Ginter, P. S., Oktay, M. H., . . . Jones, J. G. (2014). Tumor microenvironment of metastasis and risk of distant metastasis of breast cancer. *J Natl Cancer Inst, 106*(8). doi:10.1093/jnci/dju136

Rommel, C., Camps, M., & Ji, H. (2007). PI3K delta and PI3K gamma: partners in crime in inflammation in rheumatoid arthritis and beyond? *Nat Rev Immunol, 7*(3), 191-201. doi:10.1038/nri2036

Roussos, E. T., Condeelis, J. S., & Patsialou, A. (2011). Chemotaxis in cancer. *Nat Rev Cancer, 11*(8), 573-587. doi:10.1038/nrc3078

Sampaio, N. G., Yu, W., Cox, D., Wyckoff, J., Condeelis, J., Stanley, E. R., & Pixley, F. J. (2011). Phosphorylation of CSF-1R Y721 mediates its association with PI3K to regulate macrophage motility and enhancement of tumor cell invasion. *J Cell Sci, 124*(Pt 12), 2021-2031. doi:10.1242/jcs.075309

Sanford, K. K., Hobbs, G. L., & Earle, W. R. (1956). The tumor-producing capacity of strain L mouse cells after 10 years in vitro. *Cancer Res, 16*(2), 162-166.

Schackert, G., & Fidler, I. J. (1988). Site-specific metastasis of mouse melanomas and a fibrosarcoma in the brain or meninges of syngeneic animals. *Cancer Res, 48*(12), 3478-3484.

Shabo, I., Olsson, H., Stal, O., & Svanvik, J. (2013). Breast cancer expression of DAP12 is associated with skeletal and liver metastases and poor survival. *Clin Breast Cancer, 13*(5), 371-377. doi:10.1016/j.clbc.2013.05.003

Shaw, R. J., & Cantley, L. C. (2006). Ras, PI(3)K and mTOR signalling controls tumour cell growth. *Nature, 441*(7092), 424-430. doi:10.1038/nature04869

Siam, L., Bleckmann, A., Chaung, H. N., Mohr, A., Klemm, F., Barrantes-Freer, A., . . . Pukrop, T. (2015). The metastatic infiltration at the metastasis/brain parenchyma-interface is very heterogeneous and has a significant impact on survival in a prospective study. *Oncotarget, 6*(30), 29254-29267. doi:10.18632/oncotarget.4201

Soffietti, R., Trevisan, E., & Ruda, R. (2012). Targeted therapy in brain metastasis. *Curr Opin Oncol, 24*(6), 679-686. doi:10.1097/CCO.0b013e3283571a1c

Soule, H. D., Vazguez, J., Long, A., Albert, S., & Brennan, M. (1973). A human cell line from a pleural effusion derived from a breast carcinoma. *J Natl Cancer Inst, 51*(5), 1409-1416.

Spill, F., Reynolds, D. S., Kamm, R. D., & Zaman, M. H. (2016). Impact of the physical microenvironment on tumor progression and metastasis. *Curr Opin Biotechnol, 40*, 41-48. doi:10.1016/j.copbio.2016.02.007

Stanley, E. R. (1985). The macrophage colony-stimulating factor, CSF-1. *Methods Enzymol, 116*, 564-587.

Stevens, A. R., & Ewing, J. (1928). Adenocarcinoma of the Testis in the Adult. *Ann Surg, 88*(6), 1074-1078.

Stoppini, L., Buchs, P. A., & Muller, D. (1991). A simple method for organotypic cultures of nervous tissue. *J Neurosci Methods, 37*(2), 173-182.

Sznol, M., & Chen, L. (2013). Antagonist antibodies to PD-1 and B7-H1 (PD-L1) in the treatment of advanced human cancer. *Clin Cancer Res, 19*(5), 1021-1034. doi:10.1158/1078-0432.CCR-12-2063

Talmadge, J. E., Donkor, M., & Scholar, E. (2007). Inflammatory cell infiltration of tumors: Jekyll or Hyde. *Cancer Metastasis Rev, 26*(3-4), 373-400. doi:10.1007/s10555-007-9072-0

Tao, K., Fang, M., Alroy, J., & Sahagian, G. G. (2008). Imagable 4T1 model for the study of late stage breast cancer. *BMC Cancer, 8*, 228. doi:10.1186/1471-2407-8-228

Tarin, D., Price, J. E., Kettlewell, M. G., Souter, R. G., Vass, A. C., & Crossley, B. (1984). Mechanisms of human tumor metastasis studied in patients with peritoneovenous shunts. *Cancer Res, 44*(8), 3584-3592.

Thompson, R. H., Gillett, M. D., Cheville, J. C., Lohse, C. M., Dong, H., Webster, W. S., . . . Kwon, E. D. (2004). Costimulatory B7-H1 in renal cell carcinoma patients: Indicator of tumor aggressiveness and potential therapeutic target. *Proc Natl Acad Sci U S A, 101*(49), 17174-17179. doi:10.1073/pnas.0406351101

Trempe, G. L. (1976). Human breast cancer in culture. *Recent Results Cancer Res*(57), 33-41.

Tsai, J. H., & Yang, J. (2013). Epithelial-mesenchymal plasticity in carcinoma metastasis. *Genes Dev, 27*(20), 2192-2206. doi:10.1101/gad.225334.113

Vanharanta, S., & Massague, J. (2013). Origins of metastatic traits. *Cancer Cell, 24*(4), 410-421. doi:10.1016/j.ccr.2013.09.007

Wang, N., & Stamenovic, D. (2002). Mechanics of vimentin intermediate filaments. *J Muscle Res Cell Motil, 23*(5-6), 535-540.

Weber, C. E., & Kuo, P. C. (2012). The tumor microenvironment. *Surg Oncol, 21*(3), 172-177. doi:10.1016/j.suronc.2011.09.001

Weber, G. F. (2008). Molecular mechanisms of metastasis. *Cancer Lett, 270*(2), 181-190. doi:10.1016/j.canlet.2008.04.030

Winkler, F. (2015). The brain metastatic niche. *J Mol Med (Berl), 93*(11), 1213-1220. doi:10.1007/s00109-015-1357-0

Wu, C., Orozco, C., Boyer, J., Leglise, M., Goodale, J., Batalov, S., . . . Su, A. I. (2009). BioGPS: an extensible and customizable portal for querying and organizing gene annotation resources. *Genome Biol, 10*(11), R130. doi:10.1186/gb-2009-10-11-r130

Wyckoff, J. B., Wang, Y., Lin, E. Y., Li, J. F., Goswami, S., Stanley, E. R., . . . Condeelis, J. (2007). Direct visualization of macrophage-assisted tumor cell intravasation in mammary tumors. *Cancer Res, 67*(6), 2649-2656. doi:10.1158/0008-5472.CAN-06-1823

Xing, F., Kobayashi, A., Okuda, H., Watabe, M., Pai, S. K., Pandey, P. R., . . . Watabe, K. (2013). Reactive astrocytes promote the metastatic growth of breast cancer stem-like cells by activating Notch signalling in brain. *EMBO Mol Med, 5*(3), 384-396. doi:10.1002/emmm.201201623

Yang, J., Mani, S. A., Donaher, J. L., Ramaswamy, S., Itzykson, R. A., Come, C., . . . Weinberg, R. A. (2004). Twist, a master regulator of morphogenesis, plays an essential role in tumor metastasis. *Cell, 117*(7), 927-939. doi:10.1016/j.cell.2004.06.006

Yona, S., Kim, K. W., Wolf, Y., Mildner, A., Varol, D., Breker, M., . . . Jung, S. (2013). Fate mapping reveals origins and dynamics of monocytes and tissue macrophages under homeostasis. *Immunity, 38*(1), 79-91. doi:10.1016/j.immuni.2012.12.001

Zhang, C., & Yu, D. (2011). Microenvironment determinants of brain metastasis. *Cell Biosci, 1*(1), 8. doi:10.1186/2045-3701-1-8

Zhang, M., & Olsson, Y. (1997). Hematogenous metastases of the human brain--characteristics of peritumoral brain changes: a review. *J Neurooncol, 35*(1), 81-89.

Zhang, R. D., Fidler, I. J., & Price, J. E. (1991). Relative malignant potential of human breast carcinoma cell lines established from pleural effusions and a brain metastasis. *Invasion Metastasis, 11*(4), 204-215.

Curriculum vitae

Raquel Blazquez

Born on 7th February 1987 in Madrid, Spain

Paarstraße 36, 93059 Regensburg, Germany

Phone: +49 (0) 152 14672014

E-mail: r.blazquez.gonzalez@gmail.com

EDUCATION AND RESEARCH EXPERIENCE

03/2013 – present	Georg-August University of Göttingen, Germany
	Doctoral thesis: "Uncovering triggers of colonization in brain metastasis"
10/2010 – 10/2011	Autonomous University of Madrid, Spain
	M.Sc. Molecular Biomedicine
10/2005 – 06/2010	Francisco de Vitoria University, Madrid, Spain
	B. Sc. Biotechnology
09/2003 – 06/2005	Pureza de Maria School, Madrid, Spain
	Abitur degree
09/1998 – 06/2003	Pureza de Maria School, Madrid, Spain
	High school

AWARDS AND SCHOLARSHIPS

2010	Scholarship for Academic Excellence from the Autonomous University of Madrid
2005 – 2010	Scholarship for Academic Excellence from the Francisco de Vitoria University

PUBLICATIONS

Blazquez, R., Pukrop, T. 3D co-culture model of the brain parenchyma/metastasis interface of brain metastasis. 3D Cell Culture: Methods and Protocols, Methods in Molecular Biology, Springer, *accepted*.

Schwartz, H., Blacher, E., Amer, M., Livneh, N., Abramovitz, L., Klein, A., Ben-Shushan, D., Soffer, S., **Blazquez, R.**, Barrantes-Freer, A., Müller, M., Müller-Decker, K., Stein, R., Tsarfaty, G., Satchi-Fainaro, R., Umansky, V., Pukrop, T., Erez, N. Incipient melanoma brain metastases instigate astrogliosis and neuroinflammation (2016), Cancer Research 76(15):4359-71.

Siam, L., Bleckmann, A., Chaung, HN., Mohr, A., Klemm, F., Barrantes-Freer, A., **Blazquez, R.**, Wolff, HA., Lüke, F., Rohde, V., Stadelmann, C., Pukrop, T. The metastatic infiltration at the metastasis/brain parenchyma-interface is very heterogeneous and has a significant impact on survival in a prospective study (2015), Oncotarget 6(30):29254-67.

PRESENTATIONS

Blazquez, R., Seitz, S., Pukrop, T. PI3K-inhibition blocks CSF1 signaling in tumor-associated macrophages and their tumor-promoting function (2016). Oral presentation at the FOR 2127 Symposium "Selection and adaptation during metastatic cancer progression", Herzogssaal, Regensburg, Germany, June 01-03.

Blazquez, R., Renner-Sattler, K., Lüke, F., Pukrop T. Influence of metabolism of colon cancer cells in the development of distant brain metastasis (2016). Poster presentation at the DFG Symposium "Tumor metabolism meets Immunology", Thon-Dittmer Palais, Regensburg, Germany, April 28-30.

Chuang, HN., **Blazquez, R.**, Hanisch, UK., Pukrop T. Microglia, the organ macrophage-like cells, significantly impact brain colonization of carcinoma cells (2014). Poster presentation at the EMBO|EMBL Symposium "Tumour microenvironment and signaling", German Cancer Center, Heidelberg, Germany, May 07-10.